NUCLEAR SCIENCE AND ENGINEERING: **81**, 213-271 (1982)

New Calculation of Prompt Fission Neutron Spectra and Average Prompt Neutron Multiplicities

David G. Madland and J. Rayford Nix

Los Alamos National Laboratory, Theoretical Division
P.O. Box 1663, Los Alamos, New Mexico 87545

Received October 14, 1981
Accepted January 8, 1982

On the basis of standard nuclear evaporation theory, we calculate the prompt fission neutron spectrum N(E) as a function of both the fissioning nucleus and its excitation energy. To simulate the initial distribution of fission-fragment excitation energy and the subsequent cooling of the fragments as neutrons are emitted, we take the distribution of fission-fragment residual nuclear temperature to be triangular in shape, extending linearly from zero to a maximum value T_m. This maximum temperature is determined from the average energy release, the separation energy and kinetic energy of the neutron inducing fission, the total average fission-fragment kinetic energy, and the level density parameter of the Fermi gas model. The neutron energy spectrum for fixed residual nuclear temperature is integrated over this triangular distribution to obtain the neutron energy spectrum in the center-of-mass system of a given fission fragment, which is then transformed to the laboratory system. When the cross section σ_c for the inverse process of compound nucleus formation is assumed constant, N(E) is the sum of a four-term closed expression involving the exponential integral and the incomplete gamma function for the light fragment and an analogous result for the heavy fragment. We also calculate N(E) by numerical integration for an energy-dependent cross section σ_c that is obtained from an optical model; this shifts the peak in N(E) to somewhat lower neutron energy and changes the overall shape slightly. The spectra calculated for both a constant cross section and an energy-dependent cross section reproduce recent experimental data for several fissioning nuclei and excitation energies for a single choice of the nuclear level density parameter and without the use of any further adjustable parameters. However, the spectra calculated with an energy-dependent cross section agree somewhat better with the experimental data than do those calculated with a constant cross section. Our approach is also used to calculate $\bar{\nu}_p$, the average number of prompt neutrons per fission, as a function of excitation energy for several fissioning nuclei. At high excitation energy, where fission following the emission of one or more neutrons is possible, we take into account the effects of and competition between first-, second-, and third-chance fission when calculating both N(E) and $\bar{\nu}_p$. For ease of computation, we present finally an approximate way to simulate the energy dependence of the compound nucleus cross section through a slight readjustment of the value of the level density parameter.

I. INTRODUCTION

For the design of nuclear reactors and other applications, it is important to know the prompt fission neutron spectrum $N(E)$ as a function of both the fissioning nucleus and its excitation energy. The prompt fission neutron spectrum has been considered theoretically since the early days of fission by Feather,[1] Watt,[2] Terrell,[3] and many others.[4-15] (References appear on p. 269.) However, most calculations of $N(E)$ for practical applications are still based on either a Watt or a Maxwellian spectrum,[2,4-6]

with parameters that are adjusted to optimally reproduce experimental data for a given fissioning nucleus at a given excitation energy. Such an approach cannot be used to predict $N(E)$ for a different fissioning nucleus or a different excitation energy from what has been measured experimentally.

Furthermore, both the Watt and Maxwellian spectra neglect two important physical effects:

1. the distribution of fission-fragment residual nuclear temperature that results from the initial distribution of fission-fragment excitation energy and the subsequent cooling of the fragments as neutrons are emitted
2. the energy dependence of the cross section for the inverse process of compound nucleus formation.

The Maxwellian spectrum also neglects the center-of-mass motion of the fission fragments from which the neutrons are emitted! Because of these omissions, the agreement that is obtained in practice between these spectra and experimental data is achieved by adjusting parameters to values that are somewhat unphysical.

The distribution of fission-fragment residual nuclear temperature has been considered in several previous studies.[3-5,7-11,14,15] Terrell[3] showed that this distribution is approximately triangular in shape, with a moderately broad high-temperature cutoff. By superimposing evaporation spectra for seven different temperatures weighted according to this distribution, he demonstrated numerically that the resulting prompt fission neutron spectrum is similar to a Maxwellian spectrum over an intermediate range of neutron energy. However, at both low and high neutron energies, the resulting spectrum is somewhat smaller than the Maxwellian spectrum.

In other studies of the temperature distribution, the center-of-mass neutron energy spectrum has been calculated as a superposition of evaporation spectra corresponding to either two or three different residual nuclear temperatures.[7,8,11] It has also been approximated in terms of an assumed simple functional form.[9,10] Finally, Kapoor et al.[8] considered a triangular distribution of temperature, extending linearly from zero to a maximum value T_m, and showed that the resulting center-of-mass neutron energy spectrum is given in terms of an exponential integral.

More recently, a Hauser-Feshbach calculation of the prompt spontaneous-fission neutron spectrum for ^{252}Cf has been performed by Browne and Dietrich.[14,15] This approach removes both of the deficiencies inherent in the Watt and Maxwellian spectra, but is sufficiently complicated that it is difficult to apply it to a variety of fissioning nuclei and excitation energies.

In our approach, we incorporate in a simple way the two dominant physical effects that are usually neglected. In particular, we take the distribution of fission-fragment residual nuclear temperature to be triangular in shape, extending linearly from zero to a maximum value T_m, and we calculate the energy-dependent compound nucleus cross section σ_c for representative average fission fragments by use of an optical model. Our formulation permits $N(E)$ to be calculated easily for any fissioning nucleus at any excitation energy. The same approach can also be used to calculate $\bar{\nu}_p$, the average number of prompt neutrons per fission, as a function of the fissioning nucleus and its excitation energy. Preliminary accounts of this work have been given in Refs. 16 through 19.

Our work is intended to serve two basic purposes. First, it provides a theoretical description of $N(E)$ and $\bar{\nu}_p$ that incorporates several previously neglected physical effects. Second, it provides a practical method to calculate these quantities for applied purposes, especially where experimental measurements do not exist. Whereas our present comparisons with experimental data provide a test of our theory, it should be stressed that, in cases where experimental data exist, higher accuracy could be achieved by parameter adjustment within our formalism.

Proceeding in two steps, we derive in Sec. II a closed expression for $N(E)$ that takes into account the distribution of fission-fragment residual nuclear temperature, but that still retains a constant compound nucleus cross section. Then, in Sec. III, we also include the energy dependence of the cross section, at which point $N(E)$ must be calculated by numerical integration. From comparisons in Sec. IV with experimental data for several fissioning nuclei and excitation energies, we find that both physical effects are important. In Sec. V we apply our approach to the calculation of the average prompt neutron multiplicity $\bar{\nu}_p$ for several cases where experimental data exist. To describe $N(E)$ and $\bar{\nu}_p$ at high excitation energy, where fission following the emission of one or more neutrons is possible, we take into account in Sec. VI the effects of and competition between first-, second-, and third-chance fission. For ease of computation, we discuss in Sec. VII an approximate way to simulate the energy dependence of the compound nucleus cross section through a slight readjustment of the value of the level density parameter. Our conclusions are presented in Sec. VIII. An expression for the integral of the closed form of $N(E)$ is given in Appendix A, and some technical details concerning the treatment of experimental prompt fission neutron spectra are given in Appendix B. Calculations of $N(E)$ and $\bar{\nu}_p$ for the ^{239}Pu + n system, in addition to those given in the text, are presented in Appendix C.

II. CONSTANT COMPOUND NUCLEUS CROSS SECTION

We use standard nuclear evaporation theory to calculate the neutron energy spectrum in the center-of-mass system of a given fission fragment, and then transform to the laboratory system, taking into account that the average velocity of the light fragment is higher than that of the heavy fragment.

When the cross section σ_c for the inverse process of compound nucleus formation is assumed constant, the center-of-mass neutron energy spectrum corresponding to a fixed residual nuclear temperature T is given approximately by[20,21]

$$\phi(\epsilon) = \frac{\epsilon}{T^2} \exp(-\epsilon/T) \ , \qquad (1)$$

where ϵ is the center-of-mass neutron energy. In accordance with usual practice in nuclear physics, we absorb the Boltzmann constant into the definition of temperature so that it has units of energy. This spectrum, along with all other distributions in this paper unless otherwise noted, is normalized to unity when integrated from zero to infinity.

As stressed by Weisskopf,[20] T is not the temperature of the evaporating compound nucleus at excitation energy E^*, but is instead the temperature of the residual nucleus at an excitation energy $E^* - B_n$ that is diminished by the neutron separation energy B_n. In the derivation of Eq. (1), it is assumed that the neutron energy ϵ is small compared to $E^* - B_n$. When this condition is not satisfied, the probability of emitting a neutron is less than that predicted by Eq. (1). In particular, it is exactly zero for $\epsilon > E^* - B_n$, where neutron emission is energetically forbidden.

II.A. Distribution of Fission-Fragment Residual Nuclear Temperature

The prompt fission neutron spectrum depends strongly on the distribution of fission-fragment excitation energy and only weakly on the distributions of fission-fragment mass and kinetic energy. We therefore take into account the former distribution, but use average values for the last two distributions.

The initial distribution of total fission-fragment excitation energy is approximately Gaussian in shape, with a total average value that is given by

$$\langle E^* \rangle = \langle E_r \rangle + B_n + E_n - \langle E_f^{\rm tot} \rangle \ . \qquad (2)$$

Here, $\langle E_r \rangle$ is the average energy release, B_n and E_n are the separation and kinetic energies of the neutron inducing fission, and $\langle E_f^{\rm tot} \rangle$ is the total average fission-fragment kinetic energy. For spontaneous fission, both B_n and E_n in Eq. (2) are zero.

The energy release for division into a given pair of fission fragments is the difference between the ground-state mass of the fissioning compound nucleus and the ground-state masses of the two fission fragments. We use units in which the speed of light is unity, so that mass and energy are measured in the same energy units. The average energy release $\langle E_r \rangle$ is then given by the integral of the product of this energy difference and the fission-fragment mass and charge distributions, taken over all possible mass and charge divisions. Because the energy difference is a slowly varying function of mass and charge division, and because the mass and charge distributions are strongly correlated and relatively narrow, we approximate the integral by using energy differences appropriate to seven mass and charge divisions that are centered about the average values of the distributions rounded to the nearest integers. This particular method of fragment choice, including a relative weighting of two for the central fragment compared to the other fragments, eliminates spurious odd-particle fluctuations by accounting for two each of the four possible odd-particle configurations. However, in applying the method it is important to note that the average energy release is not independent of excitation energy due to the slight dependence of the mass and charge distributions on excitation energy.

For the cases studied here, we take the average fission-fragment masses and charges from the experimental measurements of Unik et al.[22] Additional measurements of these quantities are included in the review by Hoffman and Hoffman.[23] We show in Fig. 1 the seven heavy fission fragments that are used in calculating the energy release for the fission of either the compound nucleus ^{236}U or ^{240}Pu, for

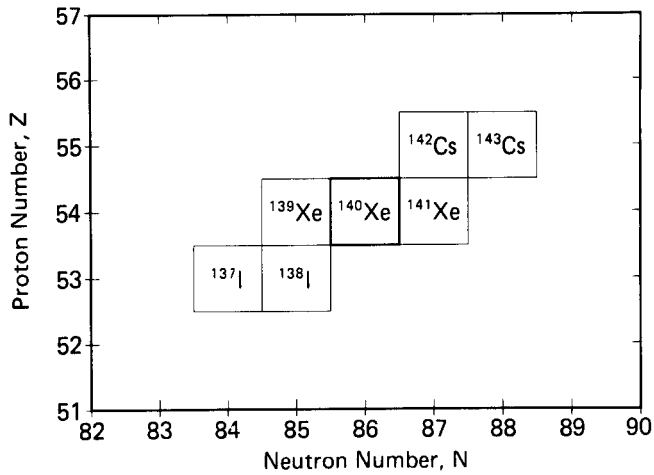

Fig. 1. Heavy fission fragments used in calculating the average energy release for the fission of either the compound nucleus ^{236}U or ^{240}Pu. The average or central heavy fragment in each case is ^{140}Xe.

which the average or central heavy fragment is in each case ^{140}Xe. For calculating the energy differences, we use the experimental or derived systematic masses of Wapstra and Bos[24] when they exist, and otherwise the mass formula of Myers.[25] The average energy release $\langle E_r \rangle$ calculated in this way should be accurate to within ~1 MeV. Values of the neutron separation energy B_n are also taken from the work of Wapstra and Bos.[24] Table I contains the values of the mass and charge numbers of the average light and heavy fission fragments, the average energy release $\langle E_r \rangle$, and the neutron separation energy B_n used in all of the cases studied here.

For the total average fission-fragment kinetic energy $\langle E_f^{\text{tot}} \rangle$, we use the experimental results of Unik et al.,[22] which are appropriate to thermal-neutron-induced fission or spontaneous fission, and neglect any small dependence on excitation energy. Hoffman and Hoffman[23] include additional measurements of $\langle E_f^{\text{tot}} \rangle$ in their review. For actinide nuclei at low excitation energy that are not included in this compilation, one could either interpolate between the values for nearby nuclei or use the results of a least-squares adjustment by Unik et al.[22] For nuclei lighter than actinide nuclei, or for nuclei at either high angular momentum or high excitation energy, the results of a least-squares adjustment by Viola[26] would be more appropriate. Table I contains the values of the total average fission-fragment kinetic energy $\langle E_f^{\text{tot}} \rangle$ used in all of the cases studied here.

Starting with an initial distribution of fission-fragment excitation energy obtained from experimental distributions of fission-fragment kinetic energy and neutron number, Terrell[3] summed the residual distributions following the emission of successive neutrons to obtain the distribution of excitation energy that governs neutron emission. This distribution was then transformed into the distribution $P(T)$ of fission-fragment residual nuclear temperature by use of the Fermi gas model, where the excitation energy E^* is related to the nuclear temperature T and the nuclear level density parameter a by

$$E^* = aT^2 \ .$$

The resulting temperature distribution is approximately triangular in shape, with a moderately broad high-temperature cutoff.

Terrell observed that if this diffuse cutoff is replaced by a sharp cutoff, so that $P(T)$ is approximated by the triangular distribution

$$P(T) = \begin{cases} 2T/T_m^2 \ , & T \leqq T_m \\ 0 \ , & T > T_m \ , \end{cases} \tag{3}$$

then the maximum temperature T_m is related to the initial total average fission-fragment excitation energy

TABLE I

Quantities Used in Calculating the Prompt Fission Neutron Spectra and Average Prompt Neutron Multiplicities for the Fission Reactions Studied in the Present Work*

Fission Reaction	Average Light Fragment	Average Heavy Fragment	$\langle E_r \rangle$ (MeV)	B_n (MeV)	$\langle E_f^{\text{tot}} \rangle$ (MeV)
^{229}Th + n	^{90}Kr	^{140}Xe	177.252	6.791	163.6
^{233}U + n	^{95}Sr	^{139}Xe	188.971	6.844	172.1
^{235}U + n	^{96}Sr	^{140}Xe	186.980	6.546	171.8
^{235}U*[a]	^{96}Sr[b]	^{139}Xe[b]	188.946	5.298	171.95[c]
^{234}U*[d]	^{95}Sr	^{139}Xe	188.971	6.844	172.1
^{238}U + n	^{98}Sr[b]	^{141}Xe[b]	186.436[e]	4.806	170.070[f]
^{239}Pu + n	^{100}Zr	^{140}Xe	198.154	6.534	177.1
^{240}Pu + n	^{101}Zr[b]	^{140}Xe[b]	199.179[e]	5.241	177.530[f]
^{249}Cf + n	^{108}Tc	^{142}Cs	221.138[e]	6.623	189.1
^{252}Cf(sf)[g]	^{108}Mo	^{144}Ba	219.408[e]	---	185.9

*Unless otherwise noted, the average light and heavy fragments as well as $\langle E_f^{\text{tot}} \rangle$ are obtained directly from Table I and Figs. 1 and 2 of Ref. 22. Similarly, $\langle E_r \rangle$ and B_n are obtained using Ref. 24 unless otherwise noted.

[a]Compound fissioning nucleus in the neutron-induced, second-chance fission of ^{235}U.

[b]Obtained by interpolation of data contained in Table I and Fig. 1 of Ref. 22.

[c]Obtained by interpolation of the experimental values contained in this table for ^{233}U + n and ^{235}U + n.

[d]Compound fissioning nucleus in the neutron-induced, third-chance fission of ^{235}U.

[e]Calculated using masses from both Refs. 24 and 25.

[f]Calculated using the least-squares adjustment of Ref. 22.

[g]sf = spontaneous fission.

approximately by

$$T_m = (\langle E^* \rangle / a)^{1/2} \quad . \tag{4}$$

The approximate validity of this expression is based on a specific relationship between the fission-fragment neutron separation energy and the width of the initial distribution of fission-fragment excitation energy.

Kapoor et al.[8] found that such a triangular temperature distribution accounts satisfactorily for the center-of-mass energy spectrum for neutrons emitted in the thermal-neutron-induced fission of ^{235}U, except at high energy, where the experimental spectrum is slightly larger than the calculated spectrum. This small discrepancy could arise because a triangular temperature distribution eliminates the high-energy contributions to the spectrum that would otherwise be present from temperatures larger than T_m. However, this omission is compensated to some extent by use of Eq. (1) for $\phi(\epsilon)$, which overestimates somewhat the spectrum at high energy.

In our studies here we use a triangular temperature distribution and assume that the same distribution $P(T)$ applies to both the light and heavy fragments. This would be the case, for example, if the system were in statistical equilibrium at the scission point, with the excitation energy and level density parameter of each fragment proportional to its mass number. Then, the maximum temperature T_m can be calculated from Eqs. (2) and (4). For the level density parameter a, we use the relationship

$$a = A/(11 \text{ MeV}) \ , \tag{5}$$

where A is the mass number of the fissioning nucleus. This result is given by the dashed curve in Fig. 2, where it is compared with experimental values for nuclei throughout the periodic table.[27,28] Although these points are best represented on the

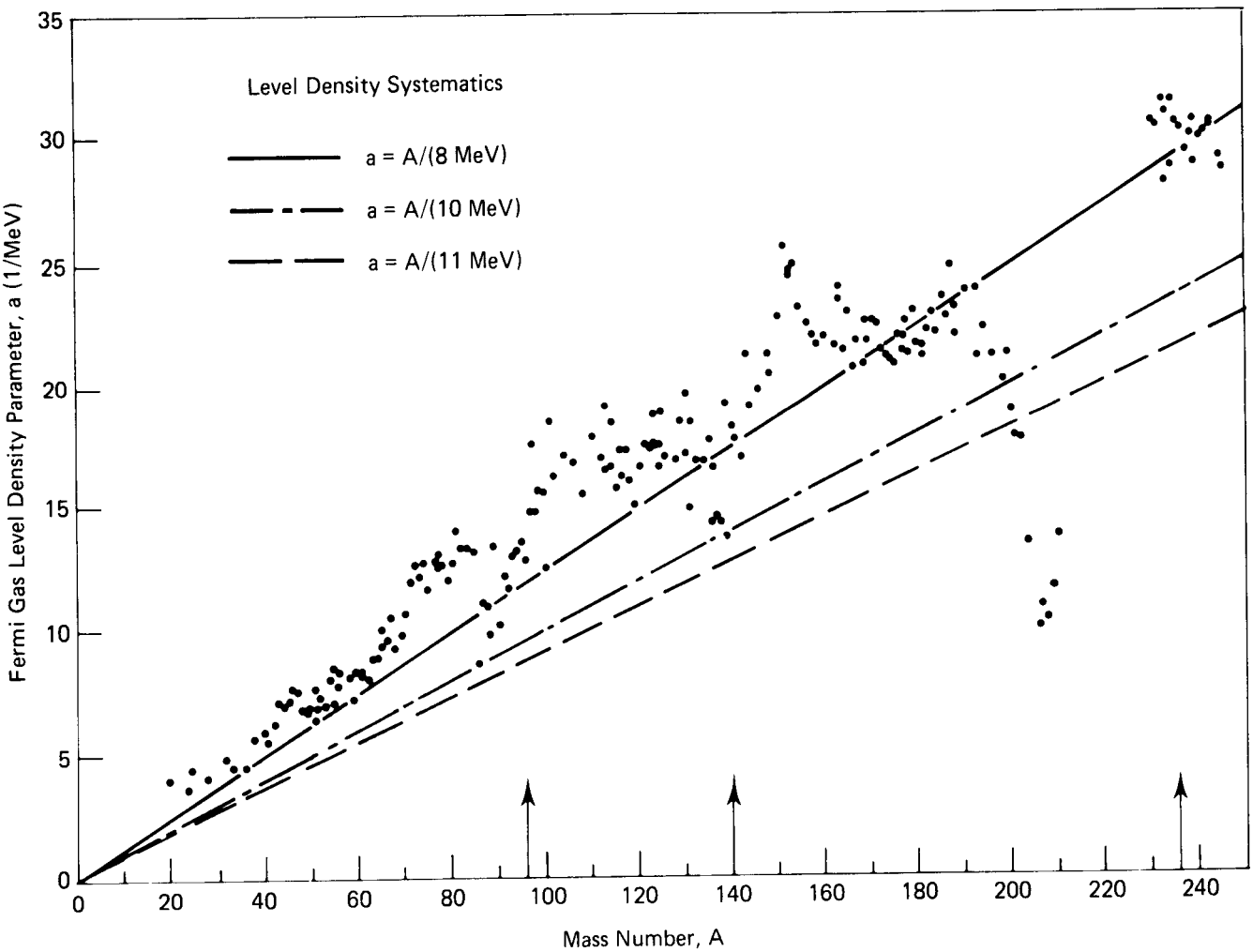

Fig. 2. Comparison of experimentally deduced values of the Fermi gas level density parameter a for nuclei throughout the periodic table (solid circles, Refs. 27 and 28) with three linear relationships. The arrows indicate the regions corresponding to the average light and heavy fragment masses as well as the fissioning mass for the case of the compound nucleus ^{236}U. The present calculations are performed using the result $a = A/(11 \text{ MeV})$, depicted by the dashed line, for reasons stated in the text.

average by the solid line corresponding to $a = A/(8\ \text{MeV})$, values for nuclei near closed shells lie somewhat below the line. As indicated by the arrows in Fig. 2, for the fission of the compound nucleus ^{236}U, the average light and heavy fission fragments are near closed shells. Therefore, the values of a that are appropriate for fission fragments are somewhat smaller than those given by $a = A/(8\ \text{MeV})$. On the basis of Fig. 2 alone, it would appear that the result $a = A/(10\ \text{MeV})$ would be optimum for fission fragments. However, when this result is used in a calculation of the prompt fission neutron spectrum that includes an energy-dependent cross section, the experimental spectrum is reproduced slightly less well than when Eq. (5) is used. This is presumably because the slightly higher value of T_m that results from the use of Eq. (5) compensates for our neglect of high-energy contributions to the spectrum from temperatures larger than T_m. We therefore tolerate a slight readjustment in the value of the level density parameter and use Eq. (5).

II.B. Center-of-Mass Neutron Energy Spectrum

The neutron energy spectrum in the center-of-mass system of a fission fragment is obtained by integrating Eq. (1) over the triangular temperature distribution given by Eq. (3). This yields

$$\Phi(\epsilon) = \int_0^\infty \phi(\epsilon)P(T)dT = \frac{2\epsilon}{T_m^2}\int_0^{T_m} \frac{\exp(-\epsilon/T)}{T}dT$$

$$= \frac{2\epsilon}{T_m^2}E_1(\epsilon/T_m)\ , \qquad (6)$$

where

$$E_1(x) = \int_x^\infty \frac{\exp(-u)}{u}du$$

is the exponential integral.[29] This result has been obtained previously by Kapoor et al.[8]

Although $\Phi(\epsilon)$ itself is given in terms of an exponential integral, the moments $\langle\epsilon^n\rangle$ of this distribution can all be evaluated simply by interchanging the order of integration, which leads to

$$\langle\epsilon^n\rangle = \int_0^\infty \epsilon^n\Phi(\epsilon)d\epsilon = \frac{2(n+1)!}{n+2}T_m^n\ . \qquad (7)$$

In particular, the mean energy and mean-square energy are given by

$$\langle\epsilon\rangle = \frac{4}{3}T_m \qquad (8)$$

and

$$\langle\epsilon^2\rangle = 3T_m^2\ . \qquad (9)$$

The center-of-mass neutron energy spectrum calculated from Eq. (6) is shown by the solid curve in Fig. 3 for the fission of ^{235}U induced by 0.53-MeV neutrons, and the mean and mean-square energies of this spectrum, calculated using Eqs. (8) and (9), are given in the first entry of Table II. This reaction is chosen because of the existence of recent experimental data on the prompt fission neutron spectrum.[31]

We also show in Fig. 3 two approximations to $\Phi(\epsilon)$ that are obtained by assuming the functional form

$$\Phi(\epsilon) = k\epsilon^\alpha \exp(-\epsilon/T_{\text{eff}})\ .$$

The effective temperature T_{eff} and the exponent α of the pre-exponential factor can be determined by equating the first and second moments of this approximate spectrum to those given by Eqs. (8) and (9). This yields the Le Couteur spectrum,[32]

$$\Phi(\epsilon) = \frac{\epsilon^{5/11}\exp\left[-\epsilon\Big/\left(\frac{11}{12}T_m\right)\right]}{\Gamma\left(\frac{16}{11}\right)\left(\frac{11}{12}T_m\right)^{16/11}}\ , \qquad (10)$$

which is shown by the dashed curve in Fig. 3. The gamma function appearing as a normalization factor is defined by[33]

$$\Gamma(a) = \int_0^\infty u^{a-1}\exp(-u)du\ .$$

The third and higher moments of the Le Couteur spectrum are slightly smaller than those given by Eq. (7).

Because the exponent 5/11 of the pre-exponential factor is very close to $\frac{1}{2}$, the simpler approximation that is obtained by setting $\alpha = \frac{1}{2}$ is almost as good. The effective temperature is then determined by equating the first moment of this approximate spectrum to that given by Eq. (8). This yields the center-of-mass Maxwellian spectrum,

$$\Phi(\epsilon) = \frac{2\sqrt{\epsilon}\exp\left[-\epsilon\Big/\left(\frac{8}{9}T_m\right)\right]}{\sqrt{\pi}\left(\frac{8}{9}T_m\right)^{3/2}}\ , \qquad (11)$$

which is shown by the dot-dashed curve in Fig. 3. The second and higher moments of this spectrum are slightly smaller than those for either the present spectrum or the Le Couteur spectrum.

As can be seen more clearly in Fig. 4, where we plot the ratio of these two approximations to the present spectrum, both are accurate to within a few percent for center-of-mass neutron energies between ~0.2 and 4 MeV. However, for energies below ~0.2 MeV, both approximations are larger than the present spectrum, whereas for energies above ~4 MeV, they are smaller.

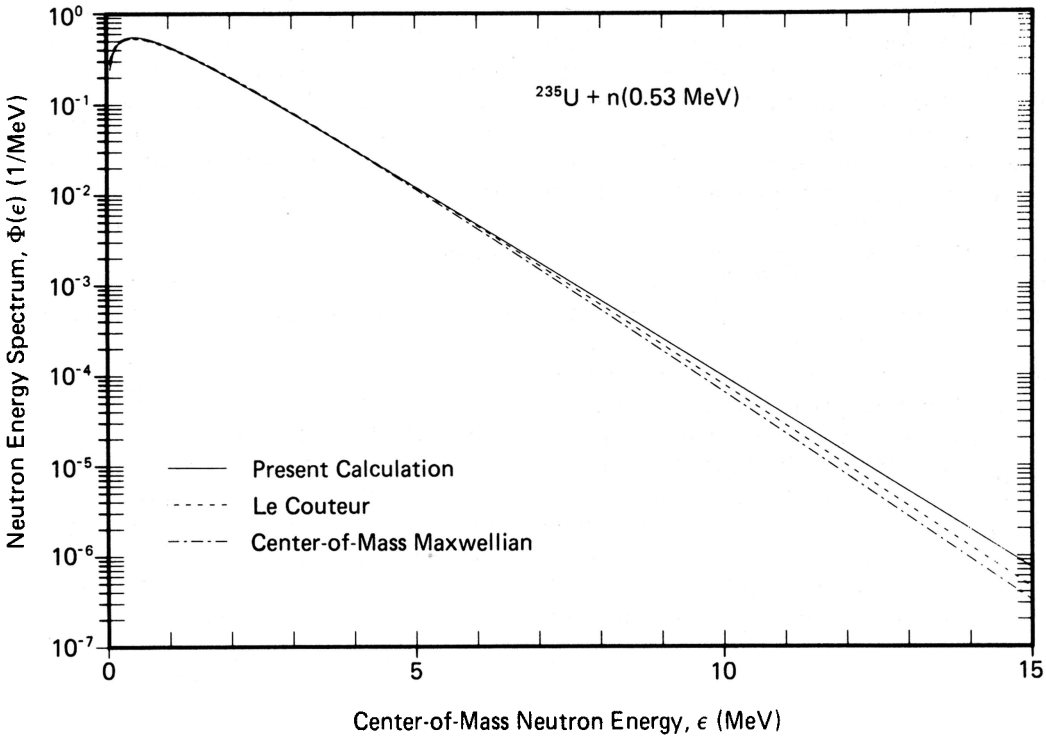

Fig. 3. Neutron energy spectrum in the fission-fragment center-of-mass system for the fission of ^{235}U induced by 0.53-MeV neutrons. The solid curve gives the present spectrum calculated from Eq. (6); the dashed curve gives the Le Couteur spectrum calculated from Eq. (10); and the dot-dashed curve gives the center-of-mass Maxwellian spectrum calculated from Eq. (11). The value of the constant appearing in each spectrum is T_m = 1.019 MeV.

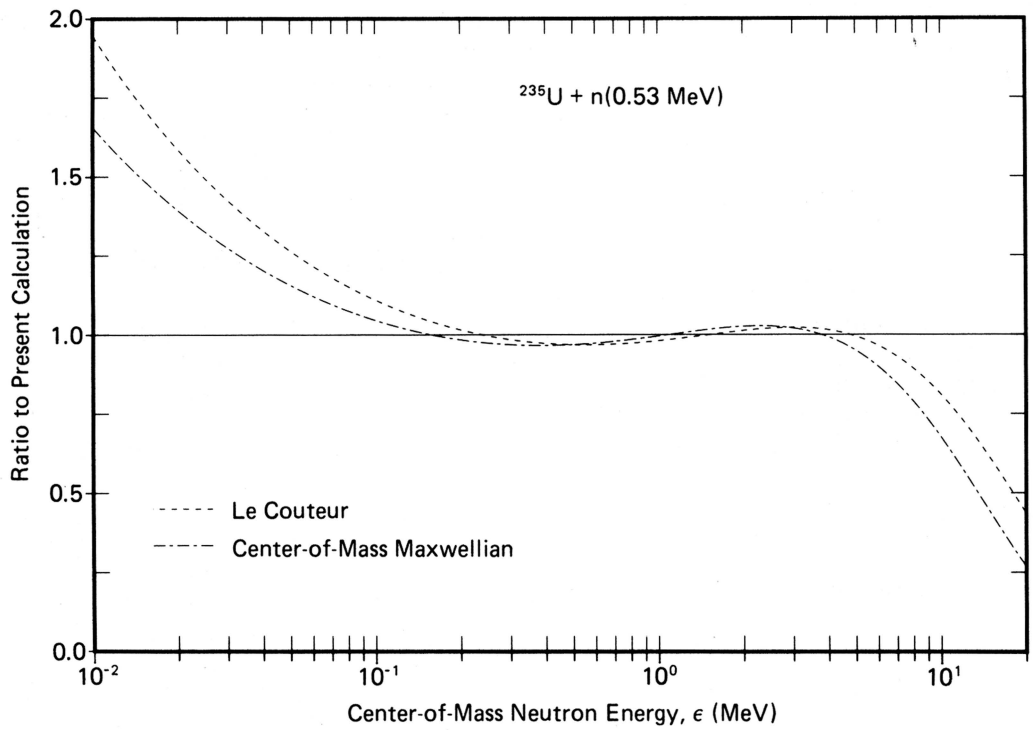

Fig. 4. Ratio of the Le Couteur spectrum and the center-of-mass Maxwellian spectrum to the present spectrum, corresponding to the curves shown in Fig. 3.

TABLE II

Mean and Mean-Square Energies of Calculated Prompt Fission Neutron Spectra

Fission Reaction	$\sigma_c(\epsilon)$	Center-of-Mass System		Laboratory System	
		$\langle\epsilon\rangle$ (MeV)	$\langle\epsilon^2\rangle$ (MeV^2)	$\langle E\rangle$ (MeV)	$\langle E^2\rangle$ (MeV^2)
^{235}U + n(0.53 MeV)	Constant	1.358	3.112	2.138	7.333
^{235}U + n(0.53 MeV)	B-G potential[a]	1.265	2.780	2.046	6.739
^{235}U + n(0.60 MeV)	Constant	1.360	3.122	2.141	7.348
^{235}U + n(0.60 MeV)	B-G potential	1.267	2.789	2.048	6.753
^{239}Pu + n(0.53 MeV)	Constant	1.514	3.866	2.294	8.475
^{239}Pu + n(0.53 MeV)	B-G potential	1.414	3.469	2.194	7.802
^{252}Cf(sf)	Constant	1.613	4.388	2.381	9.155
^{252}Cf(sf)	B-G potential	1.511	3.956	2.279	8.455
^{235}U + n(7.0 MeV)[b]	Constant	1.543	4.017	2.323	8.718
^{235}U + n(7.0 MeV)[b]	B-G potential	1.439	3.590	2.219	7.999
^{235}U + n(7.0 MeV)[c]	B-G potential	1.382	3.303	2.098	7.265
^{235}U + n(14.0 MeV)[b]	Constant	1.721	4.996	2.501	10.159
^{235}U + n(14.0 MeV)[b]	B-G potential	1.606	4.465	2.386	9.307
^{235}U + n(14.0 MeV)[d]	B-G potential	1.477	3.686	2.081	7.164

[a]Optical model potential of Becchetti and Greenlees (Ref. 30).
[b]Calculated assuming first-chance fission only.
[c]Calculated assuming first- and second-chance fission.
[d]Calculated assuming first-, second-, and third-chance fission.

II.C. Transformation to Laboratory System

We now transform the spectrum given by Eq. (6) from the center-of-mass system of a fission fragment to the laboratory system, under the assumption that the neutrons are emitted isotropically from a fission fragment moving with average kinetic energy per nucleon E_f. This is accomplished by use of the general result[1,3]

$$N(E,E_f) = \frac{1}{4\sqrt{E_f}} \int_{(\sqrt{E}-\sqrt{E_f})^2}^{(\sqrt{E}+\sqrt{E_f})^2} \frac{\Phi(\epsilon)}{\sqrt{\epsilon}}\, d\epsilon \ , \qquad (12)$$

where E is the laboratory neutron energy. Upon inserting Eq. (6) and interchanging the order of integration, we obtain for the laboratory prompt fission neutron energy spectrum of one of the fragments

$$N(E,E_f) = \frac{1}{3(E_f T_m)^{1/2}} \left[u_2^{3/2} E_1(u_2) - u_1^{3/2} E_1(u_1) + \gamma\left(\frac{3}{2},u_2\right) - \gamma\left(\frac{3}{2},u_1\right) \right] , \qquad (13)$$

where

$$u_1 = (\sqrt{E} - \sqrt{E_f})^2/T_m \ ,$$
$$u_2 = (\sqrt{E} + \sqrt{E_f})^2/T_m \ ,$$

and

$$\gamma(a,x) = \int_0^x u^{a-1} \exp(-u)du$$

is the incomplete gamma function.[33] This spectrum can be calculated readily on a modern computer, as both the exponential integral and the incomplete gamma function are usually standard library functions. For applied purposes we present in Appendix A a closed-form expression for the integral of Eq. (13) over an arbitrary energy interval.

From conservation of momentum it follows that the average kinetic energy per nucleon of the light fragment is given by

$$E_f^L = \frac{A_H}{A_L} \frac{\langle E_f^{\rm tot}\rangle}{A} \ , \qquad (14)$$

where

$\langle E_f^{\rm tot}\rangle$ = total average fission-fragment kinetic energy

A = mass number of the compound nucleus undergoing fission

A_L and A_H = average mass numbers of the light and heavy fragments, respectively.

Similarly, the average kinetic energy per nucleon of the heavy fragment is

$$E_f^H = \frac{A_L}{A_H} \frac{\langle E_f^{\rm tot}\rangle}{A} \ . \qquad (15)$$

For the fission of ^{235}U induced by 0.53-MeV neutrons, we show in Fig. 5 the laboratory neutron energy spectra $N(E,E_f^L)$ and $N(E,E_f^H)$ corresponding to neutrons emitted from the light and heavy fragments, respectively. Because of the higher velocity of the light fragment, $N(E,E_f^L)$ is significantly larger than $N(E,E_f^H)$ at high laboratory neutron energy E. Similarly, the lower velocity of the heavy fragment makes $N(E,E_f^H)$ larger than $N(E,E_f^L)$ at low laboratory neutron energy.

For the fission of actinide nuclei, the average number of neutrons emitted from a given fragment depends strongly on fragment mass in accordance with the familiar sawtooth curve.[6,34] However, in the vicinity of the average fragments, the average numbers of neutrons emitted from the light and heavy fragments are approximately equal.[6,34] Accordingly, we equate the prompt fission neutron spectrum to the average of the spectra calculated for the light and heavy fragments. The laboratory prompt fission neutron energy spectrum $N(E)$ is therefore written as

$$N(E) = \frac{1}{2}\,[N(E,E_f^L) + N(E,E_f^H)] \ . \tag{16}$$

The mean and mean-square energies for this spectrum are given by

$$\langle E\rangle = \frac{1}{2}\,(E_f^L + E_f^H) + \frac{4}{3}\,T_m \tag{17}$$

and

$$\langle E^2\rangle = \frac{1}{2}\,[(E_f^L)^2 + (E_f^H)^2] + \frac{20}{9}\,(E_f^L + E_f^H)T_m + 3T_m^2 \ . \tag{18}$$

The spectrum calculated from Eq. (16) is shown by the solid curve in Fig. 6 for the fission of ^{235}U induced by 0.53-MeV neutrons and the mean and mean-square energies of this spectrum, calculated using Eqs. (17) and (18), are given in the first entry of Table II. For comparison, the dashed curve shows the result $N(E,E_f)$ corresponding to use of the same average kinetic energy per nucleon:

$$E_f = \frac{1}{2}\,(E_f^L + E_f^H) \tag{19}$$

for both the light and heavy fragments. This approximation leads to Eq. (17) for the mean laboratory neutron energy and is excellent for laboratory neutron energies below ~6 MeV. However, for higher neutron energies the approximate result lies somewhat below the exact result, which leads to a mean-square laboratory neutron energy that is somewhat smaller than that given by Eq. (18).

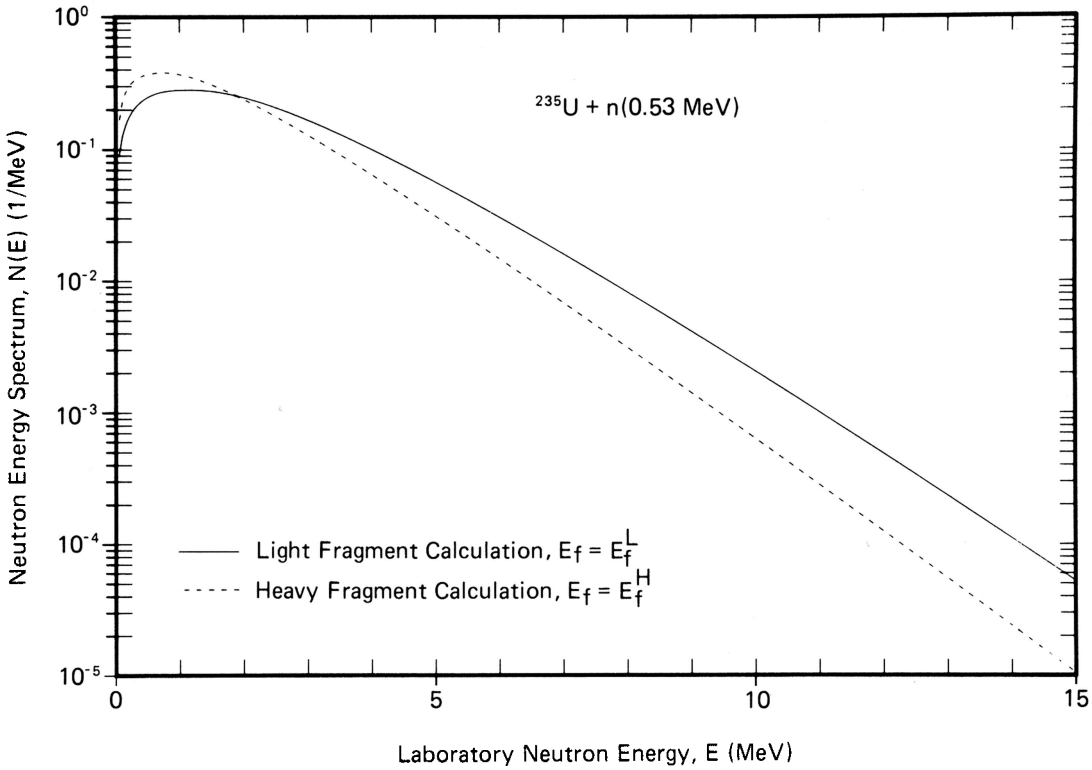

Fig. 5. Prompt fission neutron spectra in the laboratory system calculated for the light and heavy fragments separately, in the fission of ^{235}U induced by 0.53-MeV neutrons. The values of the constants for the light fragment calculation are E_f^L = 1.062 MeV and T_m = 1.019 MeV, whereas for the heavy fragment calculation they are E_f^H = 0.499 MeV and T_m = 1.019 MeV.

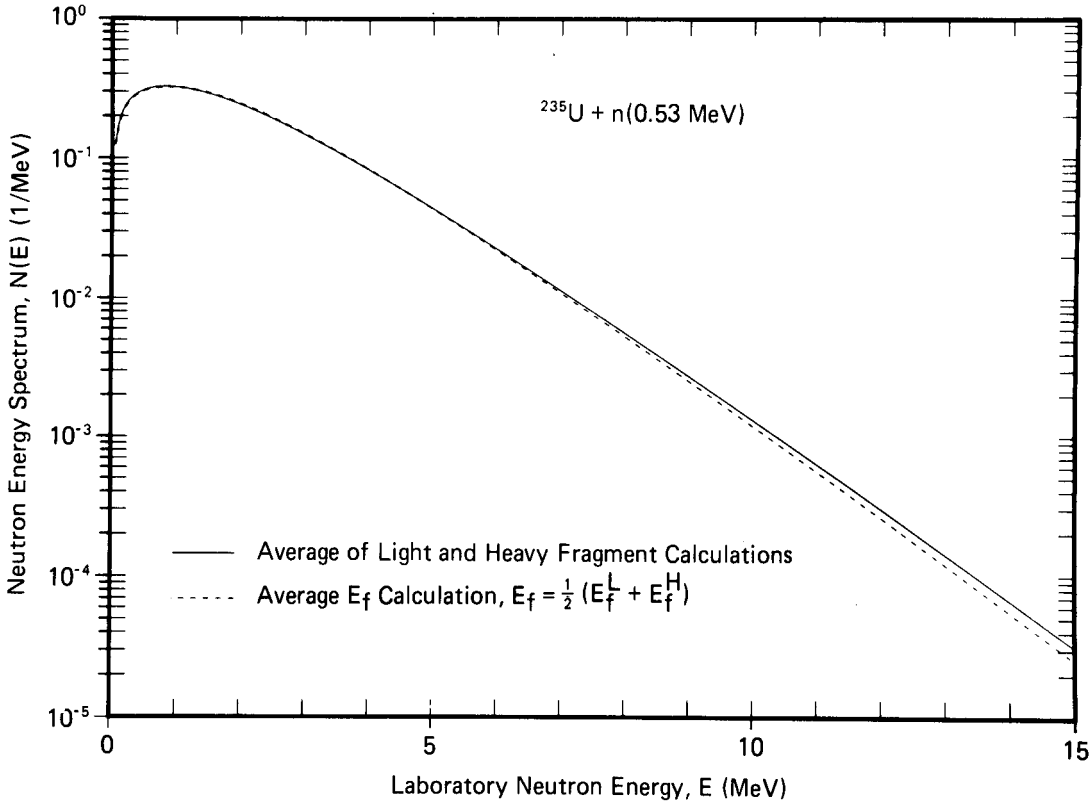

Fig. 6. Prompt fission neutron spectra in the laboratory system for the fission of ^{235}U induced by 0.53-MeV neutrons. The spectrum shown by the solid curve is calculated from Eq. (16) with the values of the three constants appearing given by E_f^L = 1.062 MeV, E_f^H = 0.499 MeV, and T_m = 1.019 MeV. The spectrum shown by the dashed curve is calculated with the same average kinetic energy per nucleon in both fragments. The values of the two constants appearing in this spectrum are E_f = 0.780 MeV and T_m = 1.019 MeV.

The spectrum calculated from Eq. (16) is shown again by the solid curve in Fig. 7 for the fission of ^{235}U induced by 0.53-MeV neutrons. The dashed curve in Fig. 7 shows the Watt spectrum that is obtained by approximating the center-of-mass spectrum $\Phi(\epsilon)$ by the Maxwellian spectrum given by Eq. (11) and by using the same average kinetic energy per nucleon E_f from Eq. (19) for both the light and heavy fragments. Transformation to the laboratory system by use of Eq. (12) yields

$$N(E) = \frac{\exp(-E_f/T_W)}{(\pi E_f T_W)^{1/2}} \times \sinh[2(E_f E)^{1/2}/T_W] \exp(-E/T_W) \ , \quad (20)$$

where the effective Watt temperature T_W is given by

$$T_W = \frac{8}{9} T_m \ .$$

By construction, the mean laboratory neutron energy for this spectrum is equal to that given by Eq. (17) for the exact spectrum.

The dot-dashed curve in Fig. 7 shows the laboratory Maxwellian spectrum

$$N(E) = \frac{2\sqrt{E} \exp(-E/T_M)}{\sqrt{\pi}\, T_M^{3/2}} \ , \quad (21)$$

where the effective Maxwellian temperature

$$T_M = \frac{1}{3}(E_f^L + E_f^H) + \frac{8}{9} T_m$$

is determined by requiring that the mean laboratory neutron energy of this spectrum be equal to that given by Eq. (17) for the exact spectrum.

As can be seen more clearly in Fig. 8, where we plot the ratio of these two approximations to the exact spectrum, the Watt spectrum is accurate to within a few percent for laboratory neutron energies between 0 and ~7 MeV. For higher energies, the Watt spectrum is smaller than the exact spectrum because the Watt temperature T_W is smaller than the maximum temperature T_m. In practice, the Watt spectrum is usually increased at high energies to better reproduce experimental data there by increasing T_W and decreasing E_f to values that are somewhat unphysical.

The Maxwellian spectrum, which neglects the

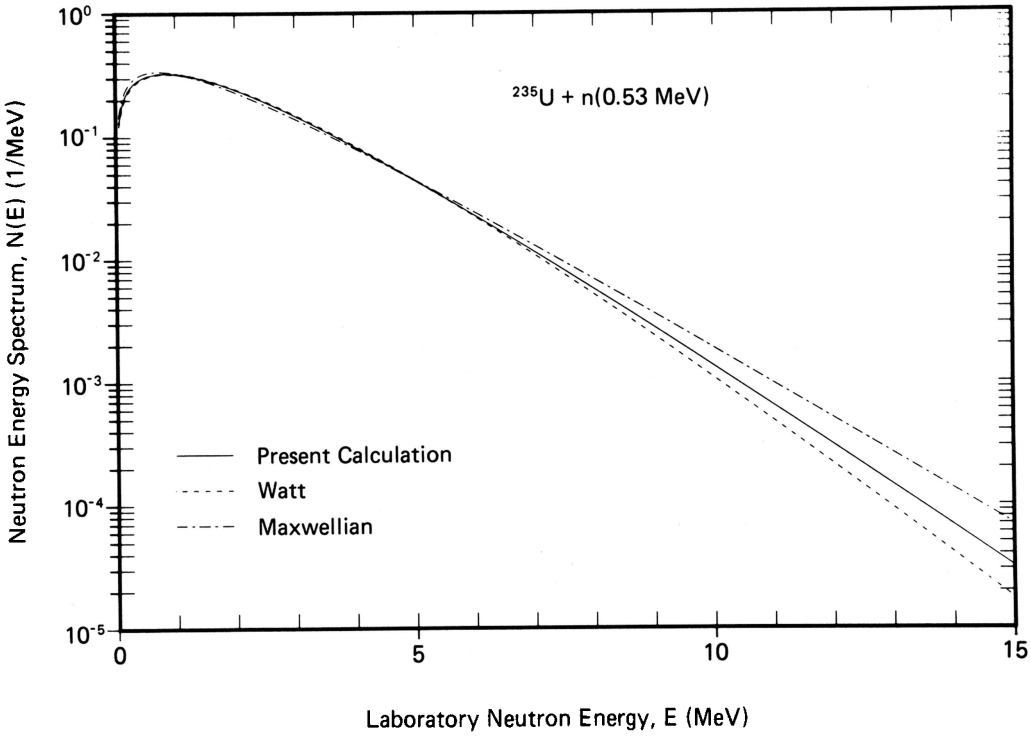

Fig. 7. Prompt fission neutron spectrum in the laboratory system for the fission of ^{235}U induced by 0.53-MeV neutrons. The solid curve gives the present spectrum calculated from Eq. (16); the dashed curve gives the Watt spectrum calculated from Eq. (20); and the dot-dashed curve gives the Maxwellian spectrum calculated from Eq. (21). The values of the three constants appearing in the present spectrum are E_f^L = 1.062 MeV, E_f^H = 0.499 MeV, and T_m = 1.019 MeV, whereas those in the Watt spectrum are E_f = 0.780 MeV and T_W = 0.905 MeV. The value of the single constant appearing in the Maxwellian spectrum is T_M = 1.426 MeV. The mean laboratory neutron energies of the three spectra are identical.

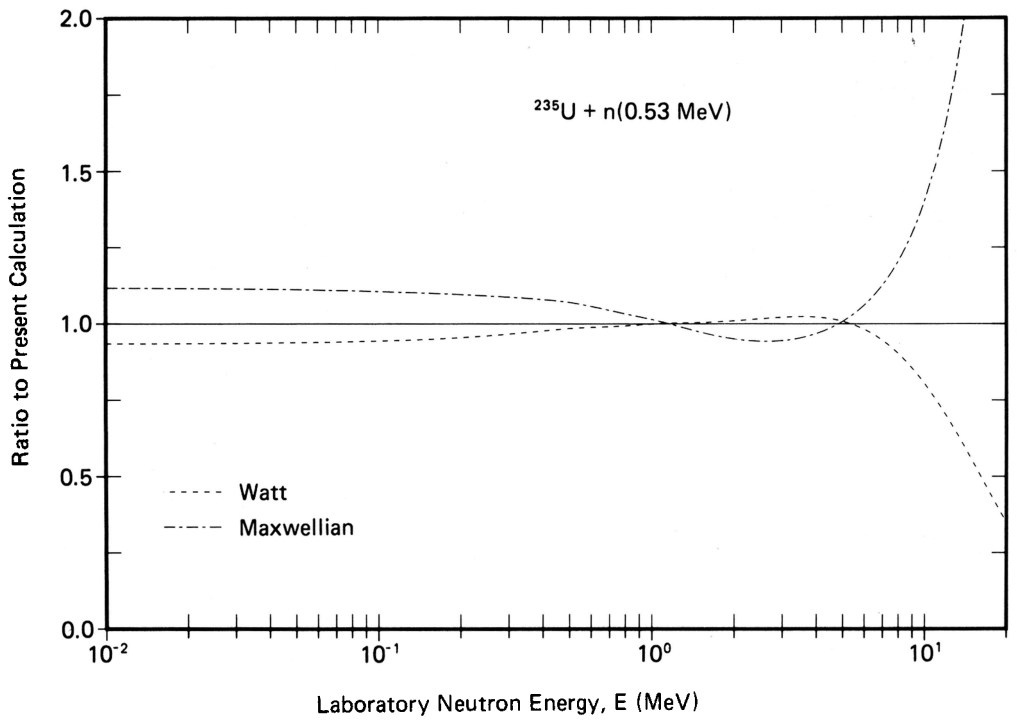

Fig. 8. Ratio of the Watt spectrum and the Maxwellian spectrum to the present spectrum, corresponding to the curves shown in Fig. 7.

motion of the fission fragments from which the neutrons are emitted, is a less accurate approximation. The Maxwellian spectrum is larger than the exact spectrum for laboratory neutron energies between 0 and ~1 MeV, whereas it is smaller for energies between ~1 and 5 MeV. For higher energies it is larger than the exact spectrum because the Maxwellian temperature T_M, which must account for the motion of the fission fragments as well as the center-of-mass motion of the neutrons, is larger than the maximum temperature T_m. In practice, the Maxwellian spectrum is usually decreased at high energies to better reproduce experimental data there by decreasing T_M. To preserve the normalization, this simultaneously increases the spectrum somewhat at lower energies.

The spurious enhancement of the Maxwellian spectrum for energies below ~1 MeV ironically accounts for part of its popularity in practice. As shown in Sec. III, the energy dependence of the compound nucleus cross section σ_c increases the spectrum at low energies relative to that calculated for a constant cross section. For the wrong physical reason, the Maxwellian spectrum reproduces this increase at low neutron energies somewhat better than do other spectra calculated for a constant cross section.

II.D. Sensitivity to Average Excitation Energy and Level Density Parameter

The prompt fission neutron spectrum calculated from Eq. (16) depends on the average fission-fragment kinetic energies per nucleon E_f^L and E_f^H and the maximum temperature T_m in the triangular distribution of fission-fragment residual nuclear temperature. The spectrum is less sensitive to E_f^L and E_f^H than to T_m. Furthermore, E_f^L and E_f^H can be calculated fairly accurately by use of Eqs. (14) and (15). We therefore explore the sensitivity of the spectrum to T_m, which is calculated by use of Eqs. (2), (4), and (5).

A major uncertainty in T_m arises from an uncertainty in the average excitation energy $\langle E^* \rangle$, which in turn arises from uncertainties in the average energy release $\langle E_r \rangle$ and the total average fission-fragment kinetic energy $\langle E_f^{\text{tot}} \rangle$. As shown in Fig. 9, increasing $\langle E^* \rangle$ relative to the value calculated from Eq. (2) increases the spectrum at high laboratory neutron energy, whereas decreasing $\langle E^* \rangle$ has the opposite effect.

Another major uncertainty in T_m arises from our use of the specific value 11 MeV in the denominator of Eq. (5) for calculating the nuclear level density parameter. As illustrated in Fig. 10, increasing

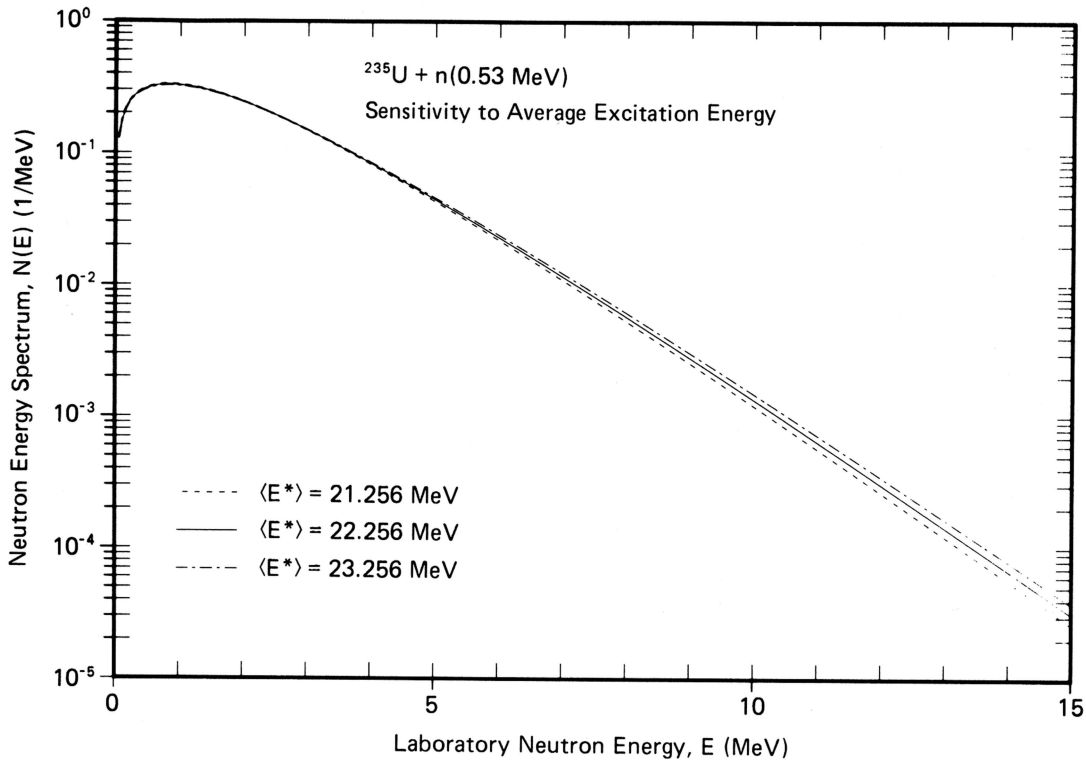

Fig. 9. Sensitivity of the prompt fission neutron spectrum to the average excitation energy $\langle E^* \rangle$. For the dashed curve T_m = 0.995 MeV, for the solid curve T_m = 1.019 MeV, and for the dot-dashed curve T_m = 1.041 MeV. The values of the average kinetic energy per nucleon are for each case held fixed at E_f^L = 1.062 MeV and E_f^H = 0.499 MeV.

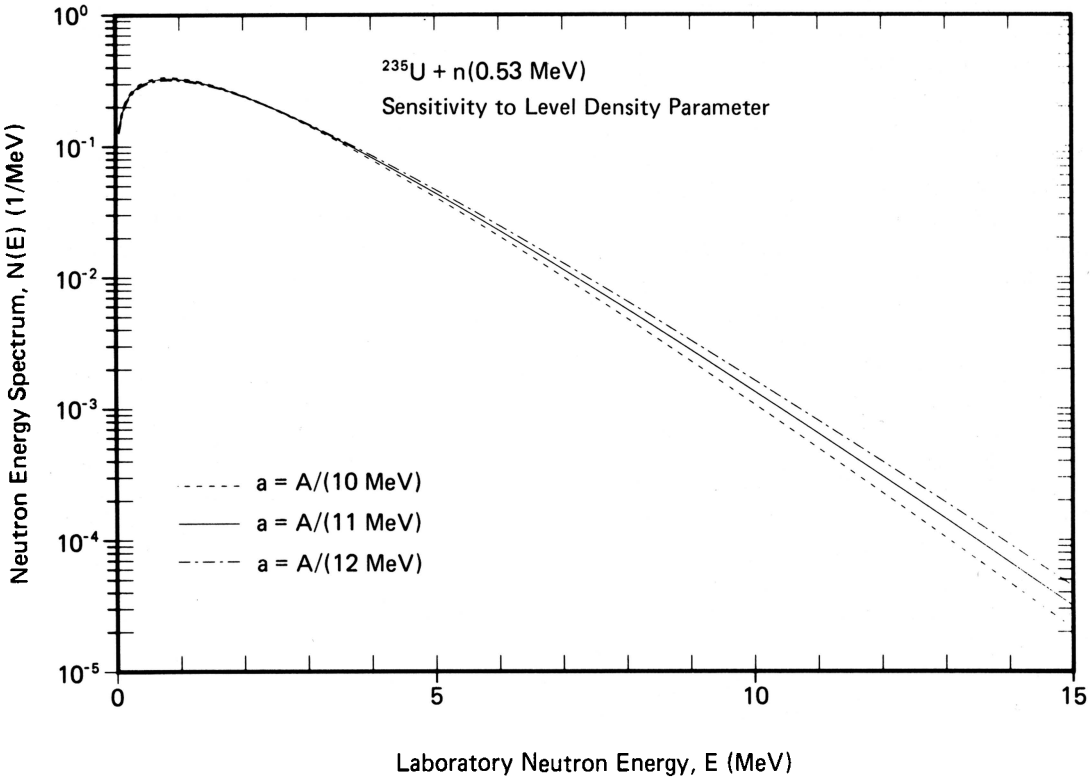

Fig. 10. Sensitivity of the prompt fission neutron spectrum to the level density parameter a. For the dashed curve T_m = 0.971 MeV, for the solid curve T_m = 1.019 MeV, and for the dot-dashed curve T_m = 1.064 MeV. The values of the average kinetic energy per nucleon are for each case held fixed at E_f^L = 1.062 MeV and E_f^H = 0.499 MeV.

the denominator increases the spectrum at high energy, whereas decreasing the denominator has the opposite effect.

II.E. Dependence on Fissioning Nucleus and Excitation Energy

Our approach provides definite predictions concerning the dependence of the spectrum on both the fissioning nucleus and the kinetic energy of the neutron inducing fission. Figure 11 shows how the spectrum increases at high energy and decreases at low energy as the charge of the fissioning nucleus increases, for thermal-neutron-induced fission. Figure 12 shows how the spectrum increases at high energy and decreases at low energy as the kinetic energy of the incident neutron increases, for the first-chance fission of ^{235}U. As discussed in Sec. VI, the inclusion of multiple-chance fission processes at high incident neutron energy decreases the spectrum at high energy relative to that calculated for first-chance fission.

III. ENERGY-DEPENDENT COMPOUND NUCLEUS CROSS SECTION

When the energy dependence of the cross section $\sigma_c(\epsilon)$ for the inverse process of compound nucleus formation is taken into account, the center-of-mass neutron energy spectrum corresponding to a fixed residual nuclear temperature T is given approximately by[20,21]

$$\phi(\epsilon,\sigma_c) = k(T)\sigma_c(\epsilon)\epsilon \exp(-\epsilon/T) \ , \qquad (22)$$

where the temperature-dependent normalization constant $k(T)$ is

$$k(T) = \left[\int_0^\infty \sigma_c(\epsilon)\epsilon \exp(-\epsilon/T)d\epsilon\right]^{-1} .$$

Upon integrating this spectrum over the triangular temperature distribution given by Eq. (3), we find for the neutron energy spectrum in the center-of-mass system of a fission fragment

$$\Phi(\epsilon,\sigma_c) = \frac{2\sigma_c(\epsilon)\epsilon}{T_m^2} \int_0^{T_m} k(T)T \exp(-\epsilon/T)dT \ . \qquad (23)$$

The neutron energy spectrum $N(E,E_f)$ in the laboratory system for a fission fragment moving with average kinetic energy per nucleon E_f is obtained by inserting this result into Eq. (12). This yields

$$N(E,E_f,\sigma_c) = \frac{1}{2\sqrt{E_f}\,T_m^2} \int_{(\sqrt{E}-\sqrt{E_f})^2}^{(\sqrt{E}+\sqrt{E_f})^2} \sigma_c(\epsilon)\sqrt{\epsilon}\,d\epsilon$$

$$\times \int_0^{T_m} k(T)T \exp(-\epsilon/T)dT \ . \qquad (24)$$

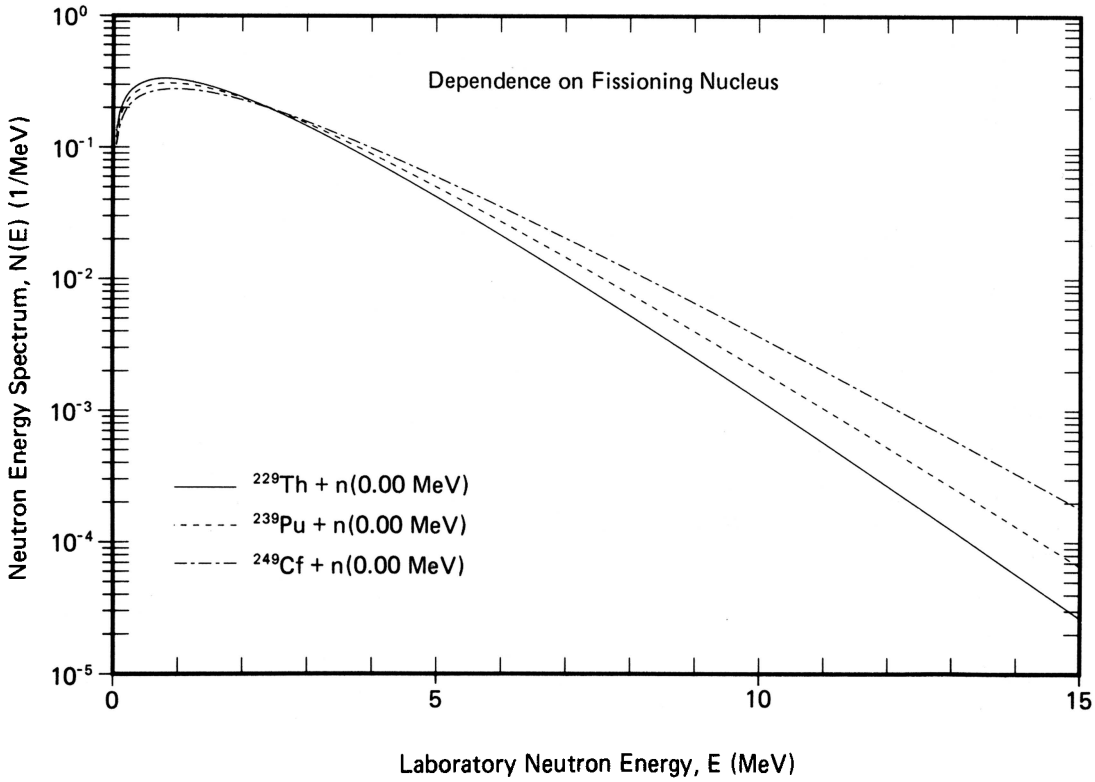

Fig. 11. Dependence of the prompt fission neutron spectrum on the fissioning nucleus, for thermal-neutron-induced fission. The values of the constants are E_f^L = 1.106 MeV, E_f^H = 0.457 MeV, and T_m = 0.989 MeV for ^{229}Th + n; E_f^L = 1.033 MeV, E_f^H = 0.527 MeV, and T_m = 1.124 MeV for ^{239}Pu + n; and E_f^L = 0.995 MeV, E_f^H = 0.575 MeV, and T_m = 1.304 MeV for ^{249}Cf + n.

The center-of-mass neutron energy spectrum $\Phi(\epsilon)$ is obtained by evaluating Eq. (23) for both light and heavy fission fragments and averaging the results in accordance with the discussion of Eq. (16). Similarly, the laboratory prompt fission neutron energy spectrum $N(E)$ is obtained by evaluating Eq. (24) for both light and heavy fission fragments and averaging the results. Compound nucleus formation cross sections for neutrons incident on light and heavy fission fragments are required as a function of the neutron energy to perform these evaluations.

III.A. Compound Nucleus Cross Section

We require the cross section for the inverse process of compound nucleus formation for a fission fragment that has undergone neutron emission. The compound nucleus cross section $\sigma_c(\epsilon)$ is required as a function of neutron energy ϵ in the fission-fragment center-of-mass system, for both light and heavy fragments of the fragment mass distribution. For example, in the case of the fissioning nucleus ^{236}U, $\sigma_c(\epsilon)$ is needed for neutrons incident on each fragment of Fig. 1 less one neutron and each complementary fragment less one neutron. These cross sections should, in principle, be averaged for the light and heavy fragment groups separately using the same weighting procedure as that discussed in Sec. II.A for determining the average energy release $\langle E_r \rangle$. However, for reasons that become apparent later in this section, we do not perform the two averages explicitly, but instead approximate them by using the compound nucleus cross sections for neutrons incident on the central fragment and the complementary central fragment. These two cross sections are then used in Eqs. (22), (23), and (24) to obtain the prompt fission neutron energy spectrum.

Ideally, $\sigma_c(\epsilon)$ would be obtained by analysis of a complete set of experimental neutron scattering cross-section measurements performed on the desired nuclei at the desired neutron energies. However, such experiments are clearly not possible because nuclei with neutron excesses as large as those encountered in fission fragments are unstable against particle emission. Therefore, the compound nucleus cross sections must be calculated.

We use phenomenological global optical potentials for this calculation. Phenomenological potentials are used because they generally best represent the experimental data upon which they are based. Global potentials are used because they describe the scattering in a specified target mass range and projectile energy range by a parameterization of the constants

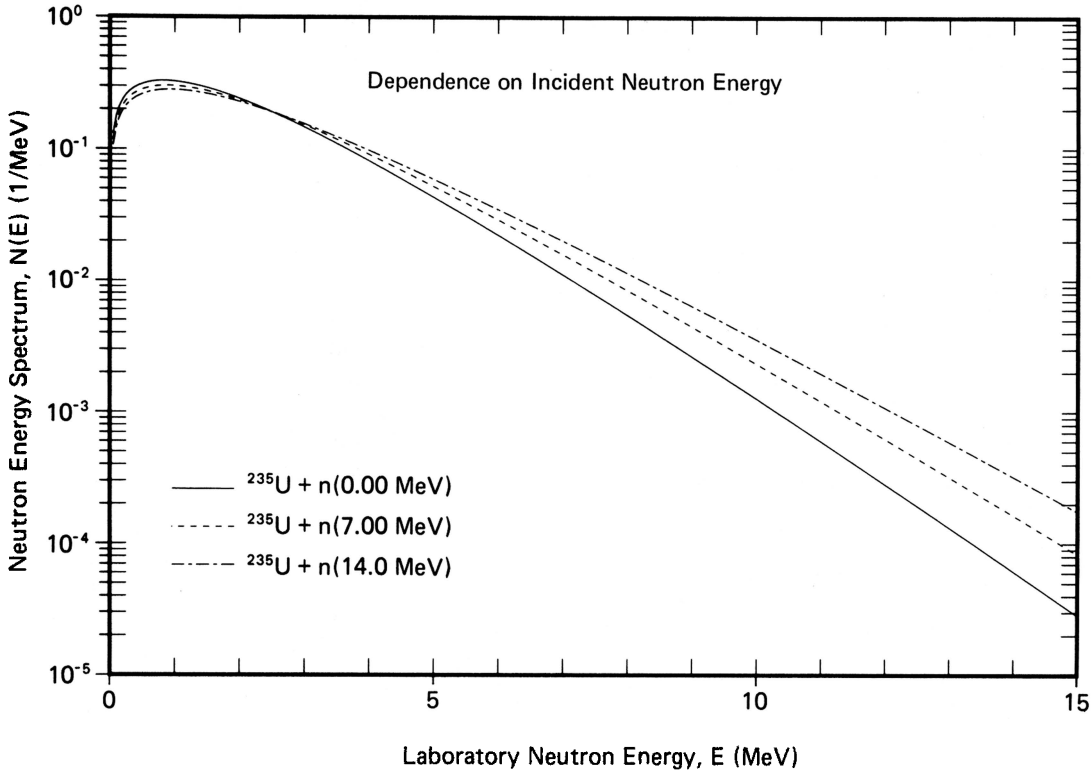

Fig. 12. Dependence of the prompt fission neutron spectrum on the kinetic energy of the incident neutron for the fission of ^{235}U. The maximum temperature T_m is 1.006 MeV when the incident neutron energy is 0, 1.157 MeV when the incident neutron energy is 7 MeV, and 1.290 MeV when the incident neutron energy is 14 MeV. The values of the average kinetic energy per nucleon are for each case held fixed at E_f^L = 1.062 MeV and E_f^H = 0.499 MeV. For the last two cases, the spectra are calculated for first-chance fission only.

of the potential in terms of gross properties of the target nucleus such as mass number, charge number, and radius, as well as the projectile energy. Using such potentials, we generate the neutron-nucleus total and shape-elastic cross sections and take their difference, the total absorption cross section, as the compound nucleus cross section. This overestimates the compound nucleus cross section by an amount equal to the direct reaction component of the total absorption cross section. It is difficult to calculate the competition between the direct reaction and compound nucleus reaction components of the total absorption cross section over a wide range of neutron bombarding energy.[35] However, in the fission-fragment mass range, direct reaction contributions are usually negligible for neutron energies below ~1 MeV. For higher neutron energies, cross sections for direct transitions to specific final states in inelastic scattering, as well as nucleon transfer reactions, are usually smaller than ~10 mb (Ref. 36). Since the neutron-nucleus total absorption cross section in the region of interest above 1 MeV is typically several barns, our overestimate of the compound nucleus cross section is not serious.

A second source of error arises because the phenomenological global potentials are based on experimental data on stable nuclei, whereas fission fragments generally lie outside the valley of stability. Use of such a potential in our calculation is clearly an extrapolation outside the target mass region from which the potential was determined, even though the mass numbers may be identical in the two cases. An important difference, of course, is in the magnitude of the relative neutron excess, given by the nuclear asymmetry

$$I = (N - Z)/A \ ,$$

where in this context N, Z, and A are the neutron number, proton number, and mass number of the target nucleus, respectively. The quantity I, moreover, is proportional to the target ground-state isospin, normalized by the target volume, and thus the isospin-dependent terms of the potential depend on I (Ref. 37).

The strengths of the isospin-dependent terms become less well known as the relative neutron excess increases, and although they are relatively small compared to the total strength of the potential, the calculated total absorption cross section nevertheless depends on them to some extent. For this reason the calculated total absorption cross sections for

average fission fragments are not sufficiently accurate to justify the use of the previously outlined averaging procedure. Instead, as stated earlier, we calculate the total absorption cross section for neutrons incident on the central fragment of both the light and heavy average fragment groups. For example, in the neutron-induced fission of ^{235}U, we perform calculations for neutrons incident on ^{96}Sr and its complement ^{140}Xe, shown in Fig. 1. We choose the central fragment instead of the central fragment minus one neutron simply for convenience.

We show in Figs. 13 and 14 the calculated compound nucleus cross section for ^{96}Sr + n and ^{140}Xe + n, respectively, corresponding to three different phenomenological global optical model potentials. These potentials, which have been widely used in neutron scattering calculations, are due to Becchetti and Greenlees,[30] Wilmore and Hodgson,[38] and Moldauer.[39] The Becchetti-Greenlees potential is based on neutron and proton scattering data, including differential elastic, reaction, and total cross-section data, as well as polarization data, for targets in the range $40 \leqq A \leqq 208$ and projectile energies in the range 1 MeV $\leqq E_n, E_p \leqq 50$ MeV. Isospin-dependent terms are present in both the real and imaginary parts of the potential. The Wilmore-Hodgson potential is based on neutron scattering differential elastic and total cross-section data for targets in the range $28 \leqq A \leqq 235$ and neutron energies in the range 1 MeV $\leqq E_n \leqq 15$ MeV. No explicit isospin-dependent terms are contained in this potential. The Moldauer potential is based on neutron scattering s-wave strength-function data and differential elastic and total cross-section data for targets in the range $40 \leqq A \leqq 150$ and neutron energies in the range $E_n \leqq 1$ MeV. This potential also does not contain any explicit isospin-dependent terms.

Clearly, none of the three potentials is based on a scattering data set that totally represents the center-of-mass neutron energy range of Figs. 13 and 14, that is, 1 keV to 40 MeV. Despite the existence of gaps in the data sets, however, the compound nucleus cross sections resulting from the three potentials are similar both in absolute magnitude and shape, for each target nucleus shown. The similarity in energy-dependent shape is significant because the calculated prompt fission neutron spectrum is influenced only by the shape behavior of the compound nucleus cross section with respect to center-of-mass neutron energy and is strictly independent of the absolute magnitude of the cross section. This is easily seen by inspection of Eq. (24), keeping in mind the expression for the temperature-dependent

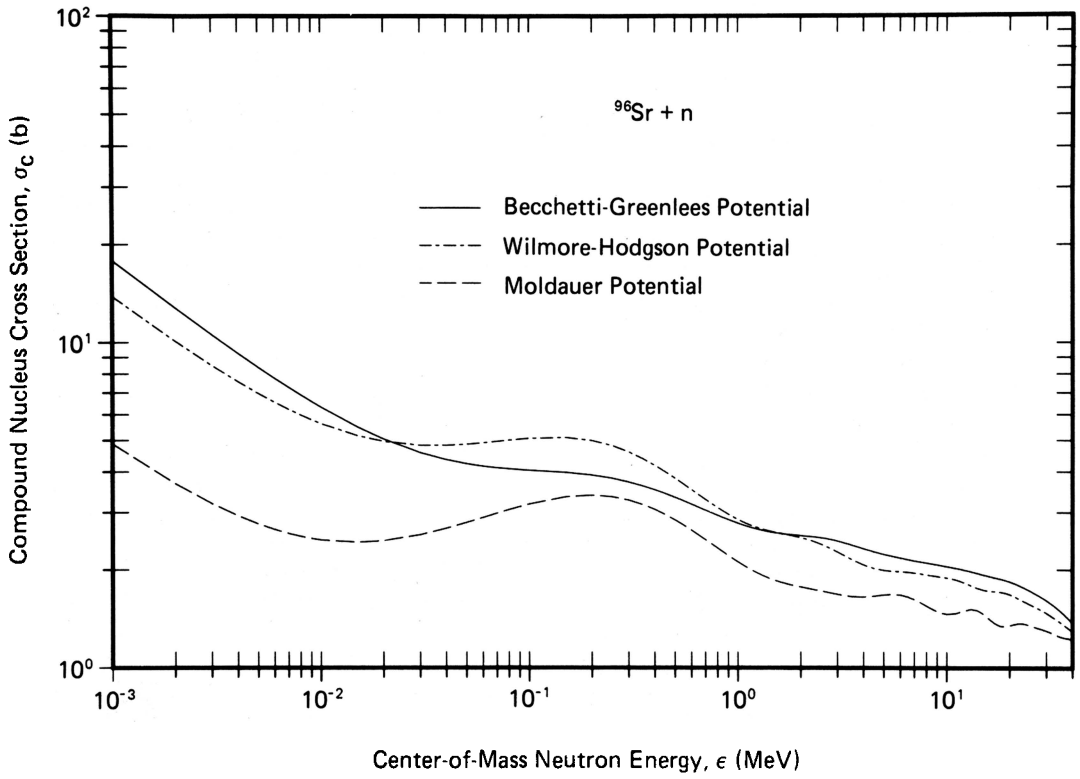

Fig. 13. Comparison of compound nucleus formation cross sections as a function of center-of-mass neutron energy for the reaction ^{96}Sr + n calculated using three different phenomenological global optical model potentials (Becchetti-Greenlees, Ref. 30; Wilmore-Hodgson, Ref. 38; Moldauer, Ref. 39).

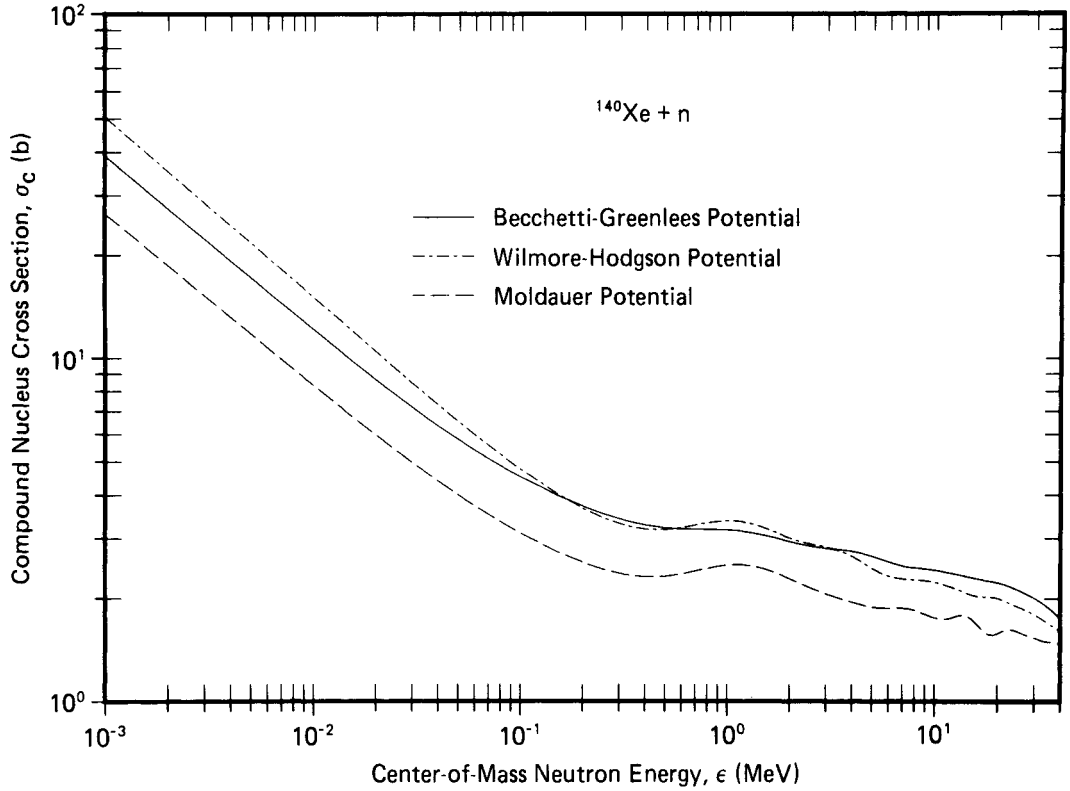

Fig. 14. Comparison of compound nucleus formation cross sections as a function of center-of-mass neutron energy calculated for the reaction ^{140}Xe + n using the same optical model potentials as for the reaction ^{96}Sr + n shown in Fig. 13.

normalization $k(T)$. Thus, differences in the absolute magnitudes of compound nucleus cross sections calculated with different optical potentials are of no concern here, where we are interested only in differences in the energy-dependent shapes of these cross sections, which are slight for the three potentials considered.

At sufficiently low neutron energy, the compound nucleus cross section is proportional to $1/v$, where v is the neutron velocity.[40] Accordingly, for neutron energies below a specified value, we represent the optical model compound nucleus cross section by

$$\sigma_c(\epsilon) = \alpha + \frac{\beta}{\sqrt{\epsilon}} , \qquad (25)$$

to simplify the numerical integrations described in the remainder of Sec. III. The constants α and β are determined from the value and slope of the calculated compound nucleus cross section $\sigma_c(\epsilon)$ at the specified energy, which is chosen to be 1 keV in the present work.

III.B. Center-of-Mass Neutron Energy Spectrum

Given an energy-dependent compound nucleus cross section $\sigma_c(\epsilon)$ for an average fission fragment, we obtain the neutron energy spectrum in the center-of-mass system of the fragment by numerical integration of Eq. (23). The upper limit of this integral is the maximum temperature T_m of the fission-fragment residual nuclear temperature distribution given by Eq. (3). The value of T_m is determined from Eqs. (2), (4), and (5), as in the case of the center-of-mass spectrum calculated for a constant cross section discussed in Sec. II.B.

The center-of-mass neutron energy spectrum $\Phi(\epsilon)$ is then given by the average of the spectra calculated for neutron emission from the light L and heavy H average fission fragments, namely,

$$\Phi(\epsilon) = \frac{1}{2} [\Phi(\epsilon,\sigma_c^L) + \Phi(\epsilon,\sigma_c^H)] , \qquad (26)$$

and the center-of-mass energy moments of this spectrum $\langle\epsilon^n\rangle$ are given by

$$\langle\epsilon^n\rangle = \int_0^\infty \epsilon^n \Phi(\epsilon) d\epsilon . \qquad (27)$$

We perform the numerical integration of Eq. (23) for the central fission fragment of each peak of the fragment mass distribution by Gauss-Legendre quadrature. The factor $k(T)$ of the integrand is itself evaluated by Gauss-Laguerre quadrature for each value of the temperature T required. We represent the compound nucleus cross section $\sigma_c(\epsilon)$ of each central fragment by a cubic-spline fit to an array of 100 values of $\sigma_c(\epsilon)$ that have been calculated using an optical model potential as discussed in Sec. III.A. For center-of-mass neutron energies below 1 keV, we

represent $\sigma_c(\epsilon)$ by Eq. (25), whereas for neutron energies above 40 MeV $\sigma_c(\epsilon)$ is assumed to remain constant at the value appropriate to 40 MeV.

Using the earlier example of the fission of ^{235}U induced by 0.53-MeV neutrons, we illustrate in Figs. 15 and 16 the composition of the center-of-mass neutron energy spectrum when the energy dependence of the compound nucleus cross section is taken into account. The contributions to the spectrum due to neutron emission from the average light and heavy fission fragments, calculated with Eq. (23), are shown together with the average center-of-mass spectrum calculated with Eq. (26). The compound nucleus cross sections used in the equations are calculated using the Becchetti-Greenlees optical model potential[30] for neutrons incident on the average light fragment ^{96}Sr and on the average heavy fragment ^{140}Xe. For comparison purposes we show the center-of-mass neutron energy spectrum calculated with Eq. (6), which is based on the assumption of constant compound nucleus cross sections for all fission fragments. As Fig. 15 illustrates, the main effect of the energy-dependent cross sections is to soften the average center-of-mass spectrum above ~1 MeV and to harden it below, relative to that calculated for a constant cross section. In addition, the average spectrum peak position is shifted downward in energy from 450 keV for the constant cross-section calculation to 350 keV for the energy-dependent cross-section calculation.

The shape effects can be seen more clearly in Fig. 16 where the ratio to the constant cross-section calculation is plotted for each of the energy-dependent cross-section calculations. At 10 keV the average energy-dependent cross-section spectrum is over a factor of 2 harder than the constant cross-section spectrum, whereas at 20 MeV it is ~30% softer, with the crossover point occurring at ~800 keV. Thus, according to the energy-dependent cross-section calculation, it is more probable to emit low- than high-energy neutrons, relative to the constant cross-section calculation. A consequence is that the energy moments of the center-of-mass spectrum calculated with Eq. (27) are smaller than those for a constant cross section calculated with Eq. (7). In the case of ^{235}U fission induced by 0.53-MeV neutrons, the first and second moments $\langle\epsilon\rangle$ and $\langle\epsilon^2\rangle$ of the energy-dependent cross-section calculation are 1.265 MeV and 2.780 MeV^2, respectively, from Table II, whereas they are 1.358 MeV and 3.112 MeV^2 for the constant cross-section calculation. The energy-dependent cross sections therefore introduce corrections of ~7 and 11% to the mean and mean-square center-of-mass neutron energies, respectively.

The differences between the average light fragment spectrum and average heavy fragment spectrum reflect the differences between the energy-dependent cross sections for the average light and heavy fragments as shown in the solid curves of Figs. 13 and 14. These cross sections enter Eq. (23) linearly, and also integrally in the factor $k(T)$, as can be seen by inspection. Referring back to Fig. 16, for center-of-mass energies ϵ below ~100 keV and above ~800 keV, one observes a greater probability of neutron emission from the average heavy fragment than from the average light fragment while the converse is true for center-of-mass energies between ~100 and 800 keV. Similar behavior is found by using the Wilmore-Hodgson[38] or Moldauer[39] optical model potential.

III.C. Transformation to Laboratory System

Given the center-of-mass neutron energy spectra $\Phi(\epsilon,\sigma_c^L)$ and $\Phi(\epsilon,\sigma_c^H)$ due to neutron emission from the average light and heavy fission fragments, we obtain the corresponding neutron energy spectra in the laboratory system by numerical integration of Eq. (24). The additional constant required in the evaluation of this expression is the average kinetic energy per nucleon E_f of the moving fragment. The value of E_f^L for the average light fragment is determined from Eq. (14) while E_f^H for the average heavy fragment is determined from Eq. (15), as in the case of the laboratory spectrum calculated for a constant cross section discussed in Sec. II.C.

The laboratory prompt fission neutron energy spectrum is then given by the average of the spectra calculated for neutron emission from the light L and heavy H average fission fragments, namely,

$$N(E) = \frac{1}{2}\left[N(E,E_f^L,\sigma_c^L) + N(E,E_f^H,\sigma_c^H)\right] , \qquad (28)$$

and the laboratory energy moments of this spectrum $\langle E^n\rangle$ are given by

$$\langle E^n\rangle = \int_0^\infty E^n N(E)dE . \qquad (29)$$

The temperature integration of Eq. (24) has already been described. We perform the integration over center-of-mass energy by Gauss-Legendre quadrature using the representation of $\sigma_c(\epsilon)$ described earlier. The evaluation of Eq. (24) thus involves three Gaussian quadrature integrations, namely, Gauss-Laguerre quadrature for the normalization integral $k(T)$ and Gauss-Legendre quadrature for the integration over temperature T and center-of-mass energy ϵ. The convergence properties of the three integrations have been tested[41] as a function of the quadrature order used by constructing an array of constant values of $\sigma_c(\epsilon)$ and comparing the numerical integration of Eq. (24) to the closed expression given by Eq. (13). The exercise shows that 32 order quadrature provides agreement to six significant figures

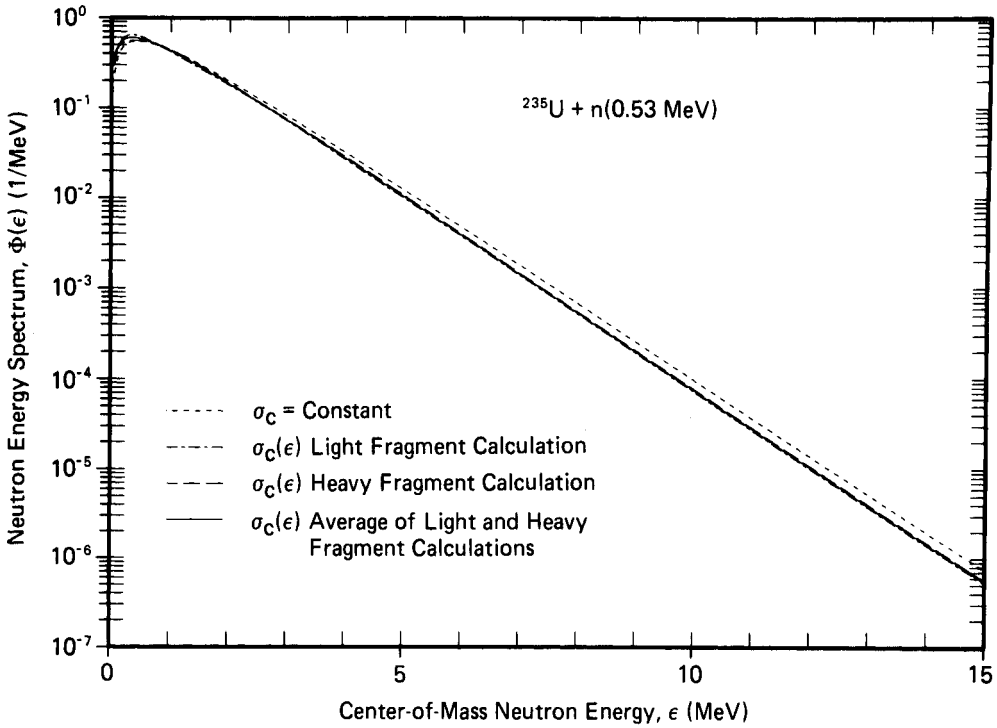

Fig. 15. Neutron energy spectra in the fission-fragment center-of-mass system for the fission of ^{235}U induced by 0.53-MeV neutrons. The short-dashed curve gives the spectrum for σ_c = constant calculated with Eq. (6) and is identical to the solid curve of Fig. 3. The dot-dashed and long-dashed curves give the spectra calculated for neutron emission from the average light and heavy fragments, respectively, using Eq. (23). The solid curve gives the spectrum calculated with Eq. (26), which averages the contributions from both peaks of the fragment mass distribution. The optical model potential of Becchetti and Greenlees (Ref. 30) is used to calculate $\sigma_c(\epsilon)$ for the average fragment of each mass peak. The value of the constant appearing in each spectrum is T_m = 1.019 MeV.

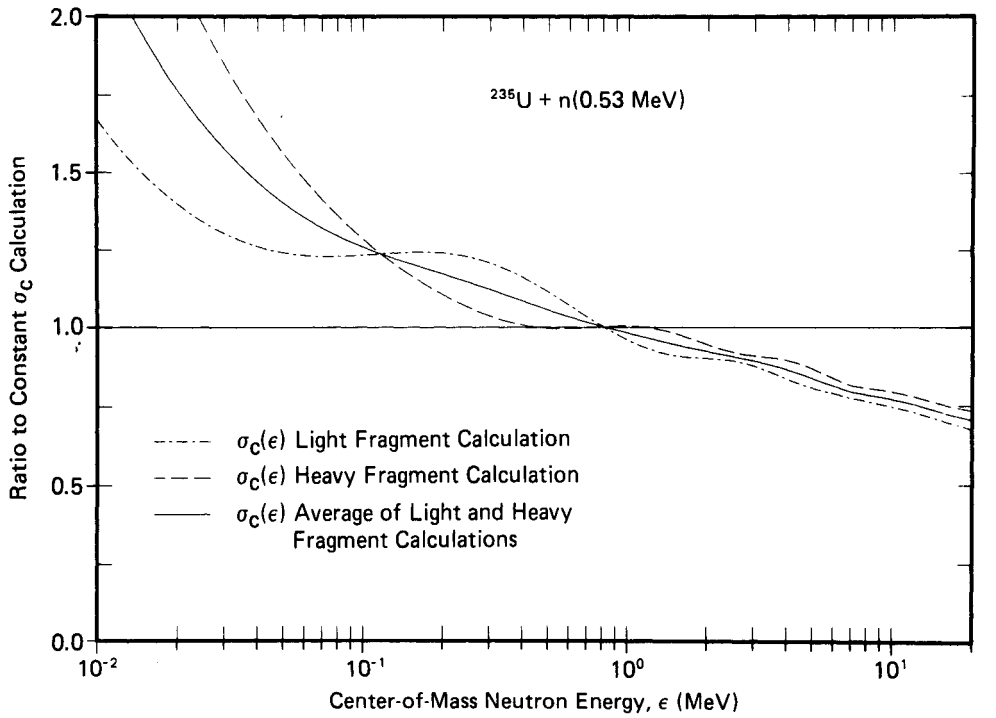

Fig. 16. Ratio of the average light fragment spectrum, the average heavy fragment spectrum, and the average spectrum to the spectrum calculated with σ_c = constant, corresponding to the curves shown in Fig. 15.

and, consequently, we use this order quadrature in the present work.

Considering again the fission of ^{235}U induced by 0.53-MeV neutrons, we illustrate in Figs. 17 and 18 the composition of the laboratory prompt neutron energy spectrum when the energy dependence of the compound nucleus cross section is taken into account. The contributions to the spectrum due to neutron emission from the average light and heavy fission fragments, calculated with Eq. (24), are shown together with the average laboratory spectrum calculated with Eq. (28). The compound nucleus cross sections used in the equations are calculated with the Becchetti-Greenlees optical model potential[30] for neutrons incident on the average light fragment ^{96}Sr and on the average heavy fragment ^{140}Xe. For comparison purposes we show the laboratory prompt neutron energy spectrum calculated with Eq. (16), which is based on the assumption of constant compound nucleus cross sections for all fission fragments. Figure 17 shows that the effect of the energy-dependent cross sections on the laboratory spectrum is similar to their effect on the center-of-mass spectrum, namely, the average laboratory spectrum is softer above ~2 MeV and harder below, relative to that calculated for a constant cross section. Also, there is a downward shift in the peak position of the average spectrum from 850 keV for the constant cross-section calculation to 740 keV.

The shape effects can be seen more clearly in Fig. 18 where the ratio to the constant cross-section calculation is plotted for each of the energy-dependent cross-section calculations. In the region below ~2 MeV there is a broad peak in the average energy-dependent cross-section spectrum relative to the constant cross-section spectrum extending from ~100 keV to 2 MeV with an 8% maximum enhancement occurring at 500 keV. Above 2 MeV the average spectrum softens with increasing energy relative to the constant cross-section calculation up to a 27% effect at 20 MeV. Thus, as would be expected from the center-of-mass result, the influence of the energy-dependent cross sections is to increase the probability for emission of low-energy neutrons and to decrease the probability for emission of high-energy neutrons. Consequently, the energy moments of the laboratory spectrum calculated with Eq. (29) are smaller than those for a constant cross section calculated with Eqs. (17) and (18). For ^{235}U fission induced by 0.53-MeV neutrons, the first and second moments $\langle E \rangle$ and $\langle E^2 \rangle$ of the energy-dependent cross-section calculation are 2.046 MeV and 6.739 MeV^2, respectively, from Table II, whereas they are 2.138 MeV and 7.333 MeV^2 for the constant cross-section calculation. The energy-dependent cross sections therefore introduce corrections of ~4 and 8% to the mean and mean-square laboratory neutron energies, respectively.

In the laboratory system the differences between the average light fragment spectrum and average heavy fragment spectrum reflect the difference between the average kinetic energy per nucleon E_f^L and E_f^H of each average fragment as well as the differences between their energy-dependent cross sections. The dominant effect due to the difference between E_f^L and E_f^H has already been discussed following Eq. (15) and is illustrated in Fig. 5 for the constant cross-section calculation and in Fig. 17 for the energy-dependent cross-section calculation. The lesser effect due to cross-section differences consists mainly of the different degree of spectrum softening between the average light and average heavy fragment spectra above ~2 MeV. Without the energy-dependent cross sections, the light and heavy fragment spectrum ratios of Fig. 18 would be somewhat higher in this energy region. A similar result is obtained by using the Wilmore-Hodgson[38] or Moldauer[39] optical model potential.

III.D. Dependence on Optical Model Potential

We now illustrate the dependence of the prompt fission neutron spectrum on the optical model potential used to calculate the compound nucleus formation cross section $\sigma_c(\epsilon)$. The decision to employ global optical model potentials and the properties of three such potentials that are widely used in neutron scattering calculations have already been discussed in Sec. III.A. In addition, compound nucleus cross sections calculated using the three potentials have been discussed and compared in Figs. 13 and 14 where the cross sections illustrated are for neutrons incident on central average fragments appropriate to the neutron-induced fission of ^{235}U.

Using again the example of the fission of ^{235}U induced by 0.53-MeV neutrons, we show in Figs. 19 and 20 the laboratory prompt fission neutron spectra obtained using the three potentials to generate $\sigma_c(\epsilon)$ as well as that calculated for σ_c = constant. Inspection of Fig. 19 shows that the spectra calculated using optical model cross sections are all generally softer in the high-energy region and harder in the low-energy region than that calculated for σ_c = constant. Second, these spectra are more similar to each other than they are to the constant cross-section spectrum. The similarity is a consequence of the similar energy dependence exhibited by the three sets of $\sigma_c(\epsilon)$ used as can be seen in Figs. 13 and 14. This point was discussed in Sec. III.A where it was noted that the spectrum is only sensitive to the energy-dependent shape of $\sigma_c(\epsilon)$ and not to the absolute magnitude of $\sigma_c(\epsilon)$. Thus, in applications to the fission spectrum, optical model potentials possessing a realistic energy dependence should be used; that is, if a global potential is employed, it should be based on experimental

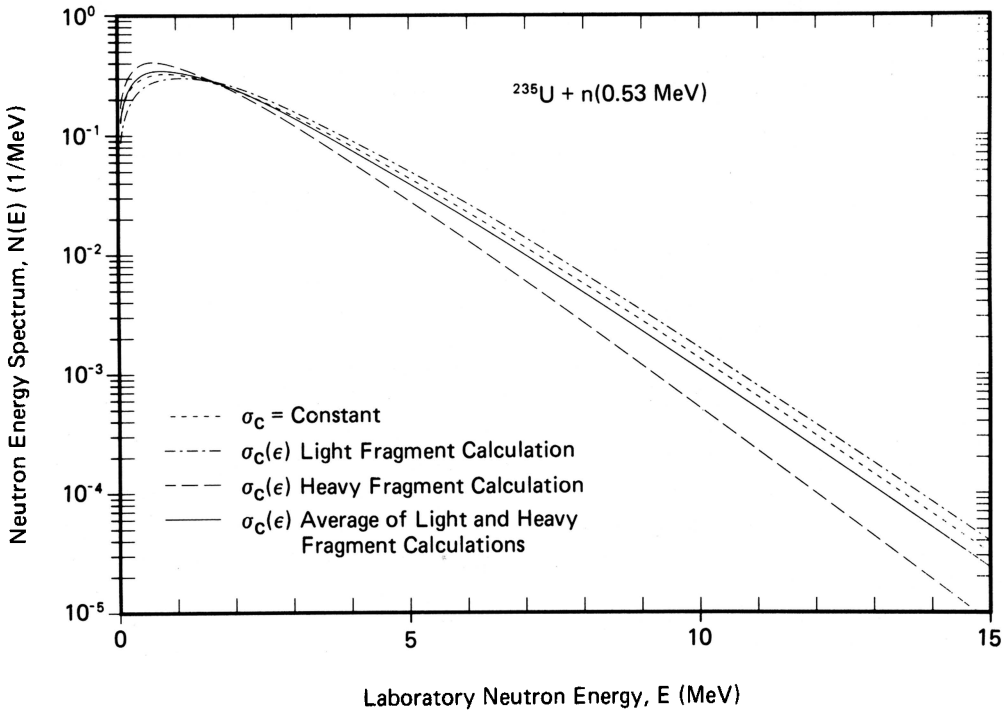

Fig. 17. Prompt fission neutron spectra in the laboratory system for the fission of ^{235}U induced by 0.53-MeV neutrons. The short-dashed curve gives the spectrum for σ_c = constant calculated with Eq. (16) and is identical to the solid curve in Figs. 6 and 7. The dot-dashed and long-dashed curves give the spectra calculated for neutron emission from the average light and heavy fragments, respectively, using Eq. (24). The solid curve gives the spectrum calculated with Eq. (28), which averages the contributions from both peaks of the fragment mass distribution. The optical model potential of Becchetti and Greenlees (Ref. 30) is used to calculate $\sigma_c(\epsilon)$ for the average fragment of each mass peak. The values of the constants appearing in the spectra are E_f^L = 1.062 MeV and T_m = 1.019 MeV for the light fragment calculation, E_f^H = 0.499 MeV and T_m = 1.019 MeV for the heavy fragment calculation, and E_f^L = 1.062 MeV, E_f^H = 0.499 MeV, and T_m = 1.019 MeV for the remaining spectra.

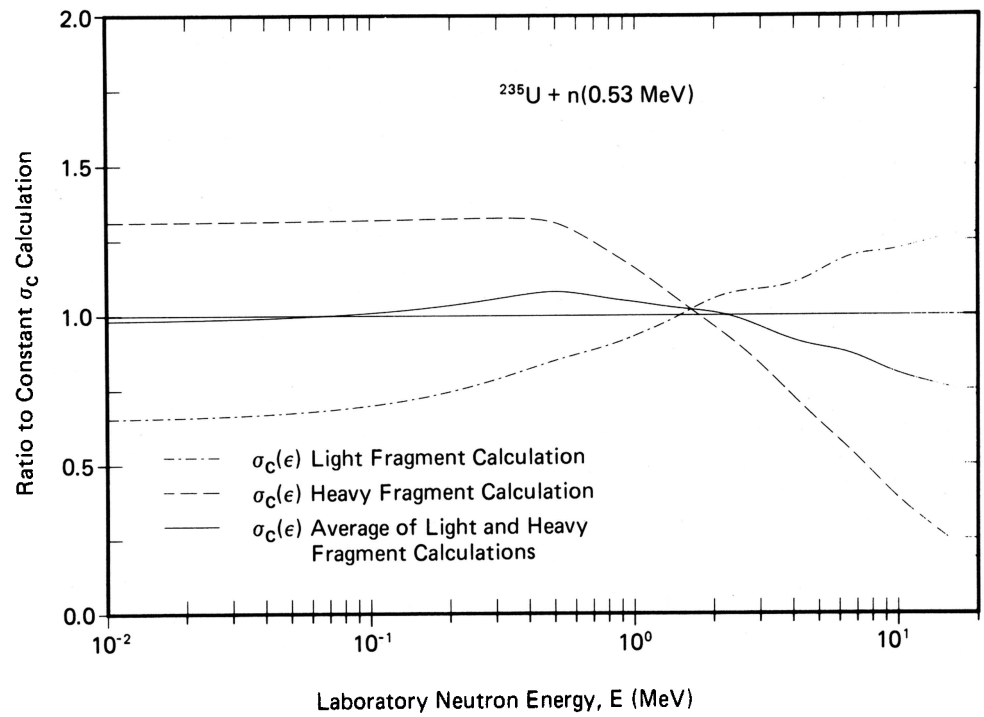

Fig. 18. Ratio of the average light fragment spectrum, the average heavy fragment spectrum, and the average spectrum to the spectrum calculated with σ_c = constant, corresponding to the curves shown in Fig. 17.

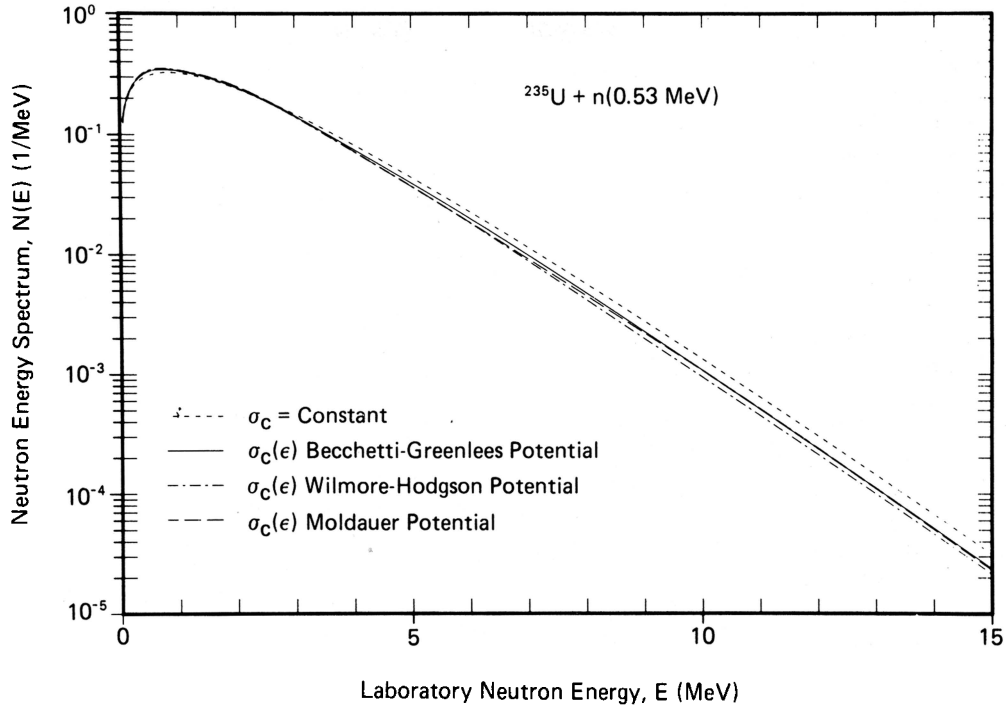

Fig. 19. Prompt fission neutron spectra in the laboratory system for the fission of ^{235}U induced by 0.53-MeV neutrons. The short-dashed curve gives the spectrum for σ_c = constant calculated with Eq. (16) and is identical to the short-dashed curve in Fig. 17. The remaining curves are calculated with Eq. (28), but differ by the choice of optical model potential used to calculate $\sigma_c(\epsilon)$ for the average fragment of each mass peak, as depicted in Figs. 13 and 14. The solid curve gives the spectrum calculated using the potential of Becchetti and Greenlees (Ref. 30) and is identical to the solid curve of Fig. 17. The dot-dashed curve gives the spectrum calculated using the potential of Wilmore and Hodgson (Ref. 38), and the long-dashed curve gives the spectrum calculated using the potential of Moldauer (Ref. 39). The values of the constants appearing in the spectra are E_f^L = 1.062 MeV, E_f^H = 0.499 MeV, and T_m = 1.019 MeV.

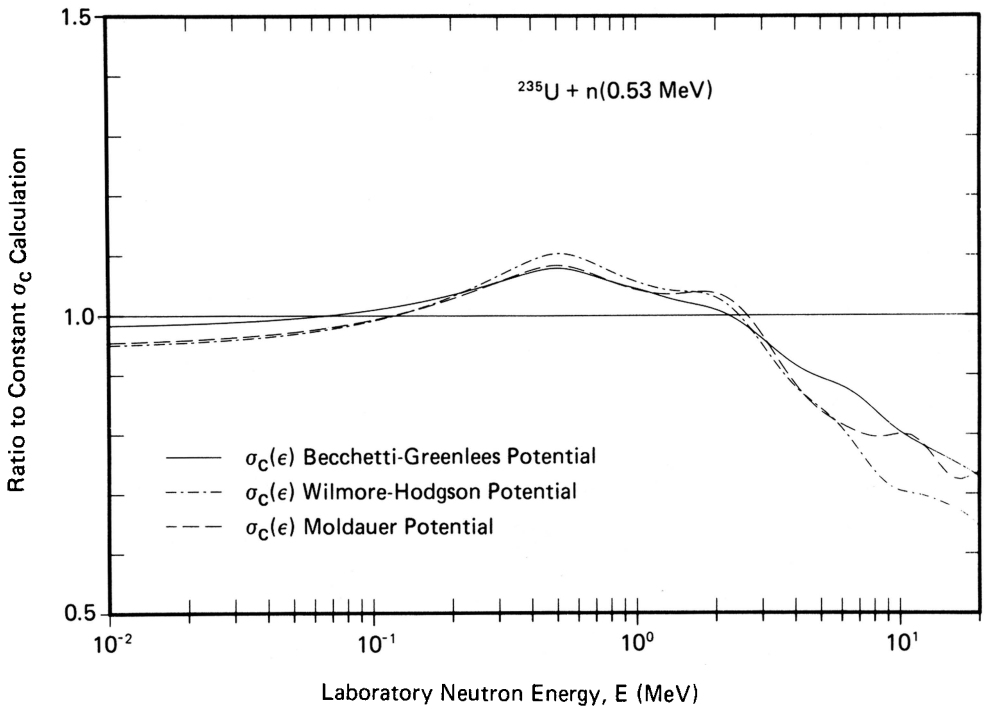

Fig. 20. Ratio of the spectra calculated using different optical model potentials to generate $\sigma_c(\epsilon)$ to the spectrum calculated with σ_c = constant, corresponding to the curves shown in Fig. 19.

data spanning the broadest possible range of bombarding energy. This conclusion is in addition to one already implied in Sec. III.A that, in applications to the fission spectrum, global potentials with explicit isospin-dependent terms are preferred.

The differences among the three spectra due to the use of different global optical model potentials are shown more clearly in Fig. 20 where the ratio of each spectrum to the constant cross-section spectrum is plotted. One observes that in the region below ~1 MeV the ratios are very nearly the same, differing at most by a few percent. However, in the region above 1 MeV relatively large differences of 5 to 10% occur between the ratios and it is, of course, in this region where the upper limits occur in the range of validity for the three potentials, namely, 1 MeV for the Moldauer potential,[39] 15 MeV for the Wilmore-Hodgson potential,[38] and 50 MeV for the Becchetti-Greenlees potential.[30] Despite these quite different limits of validity, the spectra disagree by no more than ~15%. Thus, the calculated fission spectra are somewhat insensitive to the detail of the global optical model potential used when considering a 15% level of comparison. For finer comparisons, such as testing the theory against experimentally determined fission spectra, we use the global optical model potential with the greatest range of validity and with explicit isospin-dependent terms, namely, that of Becchetti and Greenlees.[30]

IV. COMPARISON WITH EXPERIMENTAL PROMPT FISSION NEUTRON SPECTRA

We now compare the spectra calculated for both a constant compound nucleus cross section σ_c and an energy-dependent cross section $\sigma_c(\epsilon)$ with experimental data for several fissioning nuclei and excitation energies. We consider three cases of neutron-induced fission and one case of spontaneous fission, reserving Sec. VI for the discussion of spectra from multiple-chance fission.

In each comparison the experimental histogram is normalized so that its area from the lower limit of the first energy bin to the upper limit of the last energy bin equals the corresponding integral of the theoretical spectrum calculated with the energy-dependent cross section $\sigma_c(\epsilon)$. This integral is evaluated numerically. To within graphical accuracy, the same normalization would result from use of the corresponding integral of the theoretical spectrum calculated with a constant cross section σ_c, which is given in Appendix A. The formula used for normalizing experimental prompt fission neutron spectra is given in Appendix B.

In the energy-dependent cross-section calculations of this section, we use the optical model potential of Becchetti and Greenlees[30] to determine $\sigma_c(\epsilon)$. The mean and mean-square center-of-mass and laboratory energies of all calculated spectra discussed in this section are listed in Table II.

IV.A. $^{235}U + n(0.53\ MeV)$

For the fission of ^{235}U induced by 0.53-MeV neutrons, we compare in Figs. 21 and 22 our calculated spectra with the experimental data of Johansson and Holmqvist.[31] The dashed curve of Fig. 21 gives the spectrum calculated with Eq. (16) for a constant cross section and the solid curve gives the spectrum calculated with Eq. (28) using energy-dependent cross sections for neutrons incident on the average fission fragments ^{96}Sr and ^{140}Xe. Both of the calculated spectra agree well with the experiment although there is a clear preference for the energy-dependent cross-section calculation over the constant cross-section calculation. The latter spectrum is somewhat harder in the tail region above ~3 MeV. As discussed in Sec. III.C, a consequence of this is a higher average energy for the constant cross-section calculation, namely, $\langle E \rangle$ = 2.138 MeV as compared to $\langle E \rangle$ = 2.046 MeV for the energy-dependent cross-section calculation.

The preference for the energy-dependent cross-section calculation can be seen more clearly in Fig. 22 where the ratios to the constant cross-section calculation are plotted. We make three points with respect to this figure. First, the experimental data show that the physical differences between the energy-dependent cross-section calculation and the constant cross-section calculation are real and, in this case, range from approximately a +10% effect to a −25% effect. Second, all of the experimental points together with their total uncertainties, with one exception at 12.43 MeV, overlap the energy-dependent cross-section calculation. Since our calculations involve no fitting procedures, other than the slight readjustment of the level density parameter discussed in Sec. II.A, this may mean that an overly conservative uncertainty analysis was performed by Johansson and Holmqvist.[31] Third, the first four low-energy experimental points indicate the existence of a fine structure that is both stronger and more rapidly varying with energy than that of the calculation. However, these data points are in the region of greatest uncertainty in the detector efficiency,[31] and the percent magnitude of that uncertainty is approximately equal to the percent magnitude of the structure, namely, ~10%. Thus, the fine structure implied by the four data points may not be real.

IV.B. $^{235}U + n(0.60\ MeV)$

In the case of ^{235}U fission induced by 0.60-MeV neutrons, we compare in Figs. 23 and 24 our calculated spectra with the experimental data of Bertin et al.,[42] Frehaut et al.,[43] and Frehaut.[44] Again, the

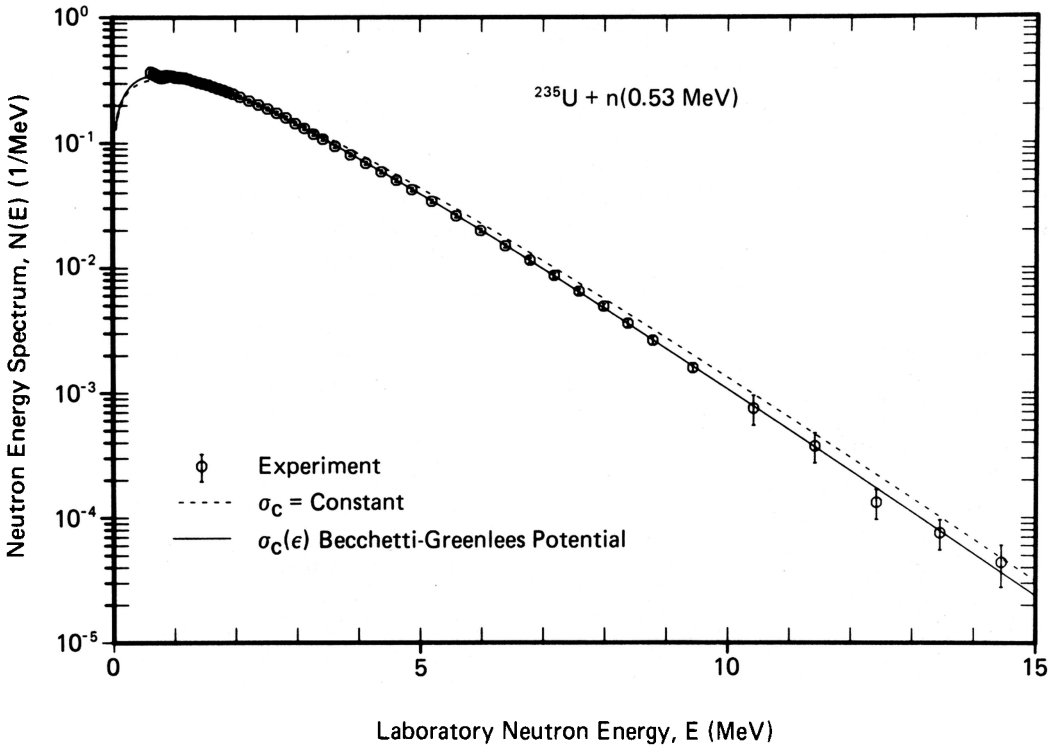

Fig. 21. Prompt fission neutron spectrum in the laboratory system for the fission of ^{235}U induced by 0.53-MeV neutrons. The dashed curve gives the spectrum calculated with Eq. (16) for a constant cross section whereas the solid curve gives the spectrum calculated with Eq. (28) for energy-dependent cross sections obtained using the optical model potential of Becchetti and Greenlees (Ref. 30). The values of the constants appearing in the calculated spectra are E_f^L = 1.062 MeV, E_f^H = 0.499 MeV, and T_m = 1.019 MeV. The experimental data are those of Johansson and Holmqvist (Ref. 31).

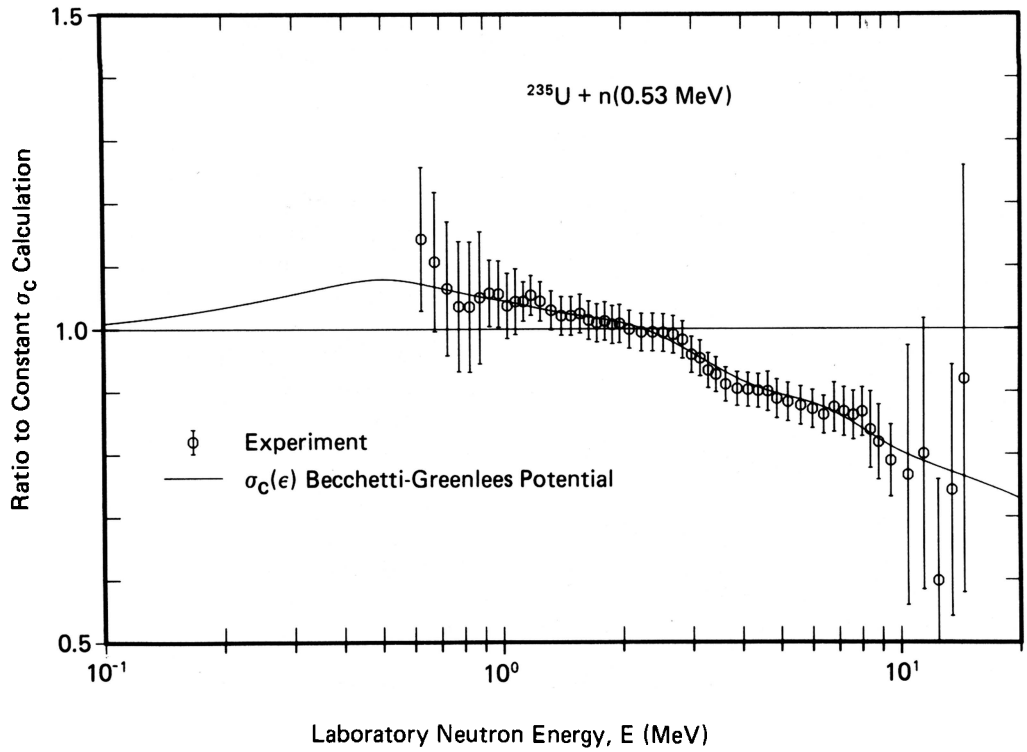

Fig. 22. Ratio of the spectrum calculated using energy-dependent cross sections and the experimental spectrum to the spectrum calculated using a constant cross section, corresponding to the curves shown in Fig. 21.

dashed curve of Fig. 23 gives the spectrum calculated with Eq. (16) for a constant cross section and the solid curve gives the spectrum calculated with Eq. (28) using energy-dependent cross sections. Since the calculations differ from those discussed in Sec. IV.A only by a 70-keV increase in incident neutron energy, the results are very similar. Indeed, T_m increases by 1 keV, E_f^L and E_f^H remain the same, and Table II shows that the average energy $\langle E \rangle$ increases by only 3 keV for the constant cross-section calculation and 2 keV for the energy-dependent cross-section calculation.

The experimental data were obtained using two different methods.[42] The fission-chamber method data are represented by circles and the sample method data are represented by triangles. Bin-width corrections were applied to the data of the two methods and separate normalizations were performed using the procedures given in Appendix B. It is clear from Fig. 23 that the agreement between theory and experiment is reasonable except in the region below ~0.6 MeV and in the region above ~9 MeV. For the latter region, the experimentalists[44] comment "all of our experimental data above 10 MeV have less credibility than the data below 10 MeV because of the increasingly complex experimental data corrections which must be applied above 10 MeV." For the former region it is perhaps noteworthy that the disagreement occurs for neutron energies at or below the incident neutron energy of 0.60 MeV. On the basis of Fig. 23 it is not possible to determine which theoretical spectrum is preferred. However, the trend of the experimental data in the ratio plot of Fig. 24 is more supportive of the energy-dependent cross-section calculation.

IV.C. $^{239}Pu + n(0.53\ MeV)$

For the fission of ^{239}Pu induced by 0.53-MeV neutrons, we compare in Figs. 25 and 26 our calculated spectra with the experimental data of Johansson et al.,[45] which are tabulated by Adams.[46] As before, the dashed curve of Fig. 25 gives the spectrum calculated with Eq. (16) for a constant cross section, and the solid curve gives the spectrum calculated with Eq. (28) using energy-dependent cross sections, but in this case for neutrons incident on the average fragments ^{100}Zr and ^{140}Xe.

It is clear from Fig. 25 that the energy-dependent cross-section calculation agrees with the experiment better than does the constant cross-section calculation. However, both calculations disagree noticeably with the experiment above ~8 MeV where the calculated spectra appear to be too hard. This result is most likely due to a slightly large calculated value of T_m because of its strong influence on the spectrum in the tail region. Inspection of Eqs. (2) and (4) show that T_m is equally sensitive to the value of the level density parameter a and the difference between the average energy release $\langle E_r \rangle$ and the total average fission-fragment kinetic energy $\langle E_f^{\text{tot}} \rangle$. As is seen in Sec. V, the calculation of the average prompt fission neutron multiplicity $\bar{\nu}_p$ for neutrons incident on ^{239}Pu is also high with respect to the experimental $\bar{\nu}_p$ data. It is shown that the calculated $\bar{\nu}_p$ is also sensitive to the difference $\langle E_r \rangle - \langle E_f^{\text{tot}} \rangle$, but is relatively insensitive to the level density parameter a. Thus, one concludes that the calculated average energy release $\langle E_r \rangle$ and/or the experimental[22] total average fission-fragment kinetic energy $\langle E_f^{\text{tot}} \rangle$ are somewhat in error for the ^{239}Pu + n system. We return to this topic in Sec. V and attempt to resolve the discrepancy in Appendix C.

Turning to the ratio curves of Fig. 26, we see that the experimental data agree with the energy-dependent cross-section calculation in the region below ~4 MeV, but disagree by ~10% at 8 MeV. A Watt distribution least-squares adjustment[45] to these data yields an average energy of 2.096 MeV whereas our calculated average energies are 2.294 MeV for the constant cross-section calculation and 2.194 MeV for the energy-dependent cross-section calculation. We note that in the region below ~1.1 MeV the structure of the data is stronger than that of the calculation, but the slopes are approximately the same. We also note that the sharp gradient observed at low energy in the experimental ratio curve of Fig. 22 for ^{235}U + n(0.53 MeV) is not present in this case.

IV.D. $^{252}Cf(sf)$

For the spontaneous fission of ^{252}Cf we compare in Figs. 27 through 30 our calculated spectra with the experimental data of Boldeman et al.[47] and Boldeman.[48] Figures 27 and 28 contain the data from experiment 1 whereas Figs. 29 and 30 contain the data from experiment 7 of Boldeman et al.[47] and Boldeman.[48] Bin-width corrections were applied to the data of the two experiments and separate normalizations were performed using the procedures given in Appendix B.

The dashed curves of Figs. 27 and 29 give the spectrum calculated with Eq. (16) for a constant cross section and the solid curves give the spectrum calculated with Eq. (28) using energy-dependent cross sections, but in this case for neutrons incident on the average fragments ^{108}Mo and ^{144}Ba. Considering experiment 1, we observe in Fig. 27 that the energy-dependent cross-section calculation is preferred in the region between ~3 and 8.5 MeV, but that both calculations agree with experiment equally well above 8.5 MeV. However, the ratio curves of Fig. 28 show that the energy-dependent cross-section calculation is also preferred in the region below 3 MeV. In fact, the figure shows that the difference between this calculation and the experiment over

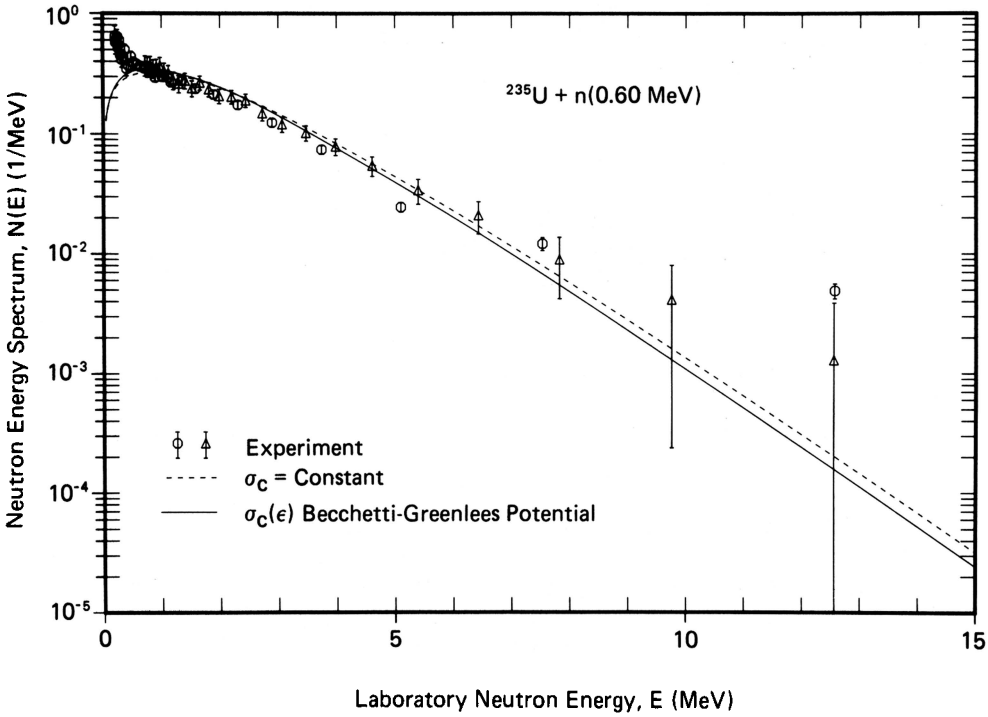

Fig. 23. Prompt fission neutron spectrum in the laboratory system for the fission of ^{235}U induced by 0.60-MeV neutrons. The dashed curve gives the spectrum calculated with Eq. (16) for a constant cross section whereas the solid curve gives the spectrum calculated with Eq. (28) for energy-dependent cross sections obtained using the optical model potential of Becchetti and Greenlees (Ref. 30). The values of the constants appearing in the calculated spectra are E_f^L = 1.062 MeV, E_f^H = 0.499 MeV, and T_m = 1.020 MeV. The experimental data are those of Bertin et al. (Ref. 42), Frehaut et al. (Ref. 43), and Frehaut (Ref. 44), with the circles corresponding to the use of the fission-chamber method and the triangles corresponding to the use of the sample method.

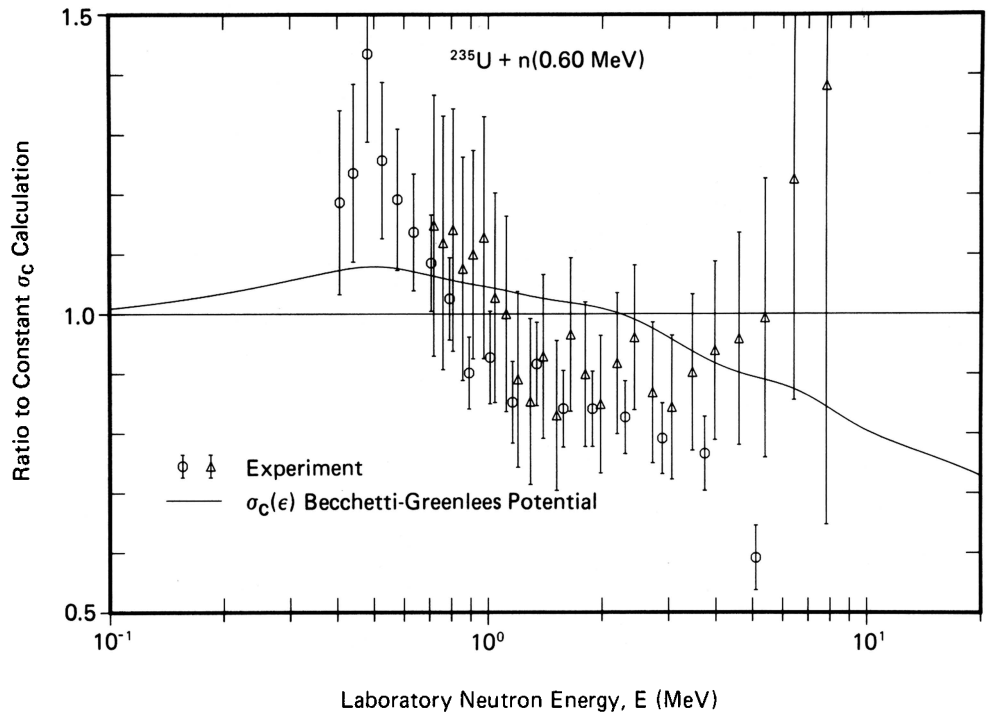

Fig. 24. Ratio of the spectrum calculated using energy-dependent cross sections and the experimental spectra to the spectrum calculated using a constant cross section, corresponding to the curves shown in Fig. 23. Note that some of the experimental ratios are off the scale of the graph.

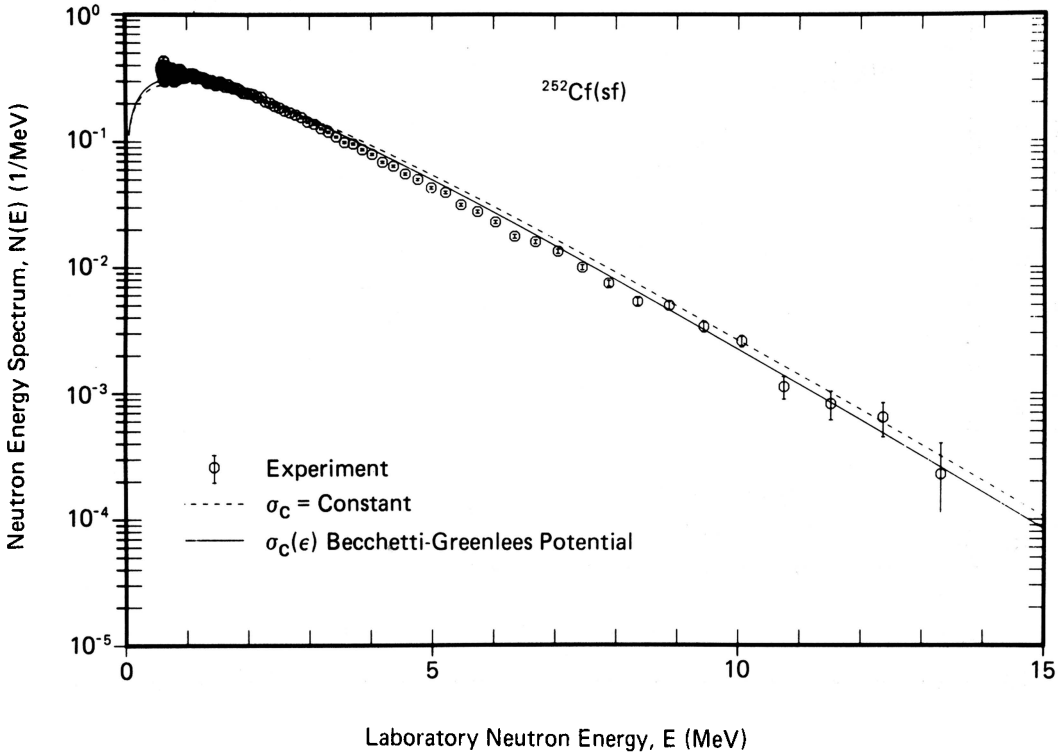

Fig. 25. Prompt fission neutron spectrum in the laboratory system for the fission of ^{239}Pu induced by 0.53-MeV neutrons. The dashed curve gives the spectrum calculated with Eq. (16) for a constant cross section whereas the solid curve gives the spectrum calculated with Eq. (28) for energy-dependent cross sections obtained using the optical model potential of Becchetti and Greenlees (Ref. 30). The values of the constants appearing in the calculated spectra are E_f^L = 1.033 MeV, E_f^H = 0.527 MeV, and T_m = 1.135 MeV. The experimental data are those of Johansson et al. (Ref. 45), which are tabulated by Adams (Ref. 46).

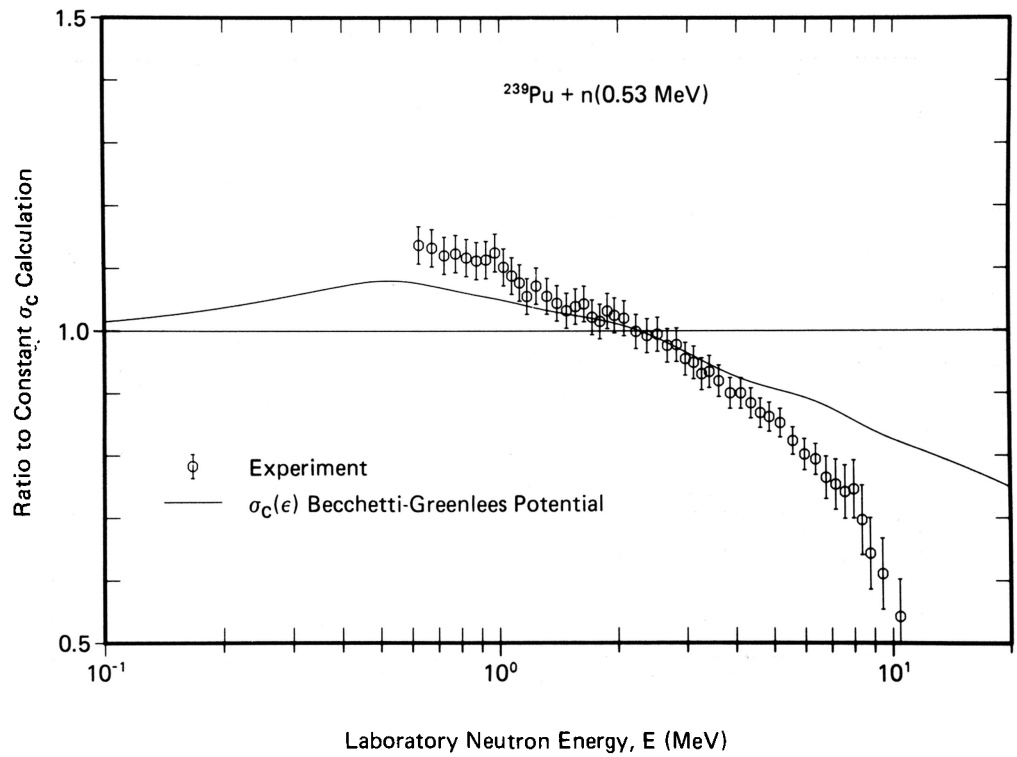

Fig. 26. Ratio of the spectrum calculated using energy-dependent cross sections and the experimental spectrum to the spectrum calculated using a constant cross section, corresponding to the curves shown in Fig. 25. Note that the experimental ratios are off the scale of the graph for energies >11 MeV.

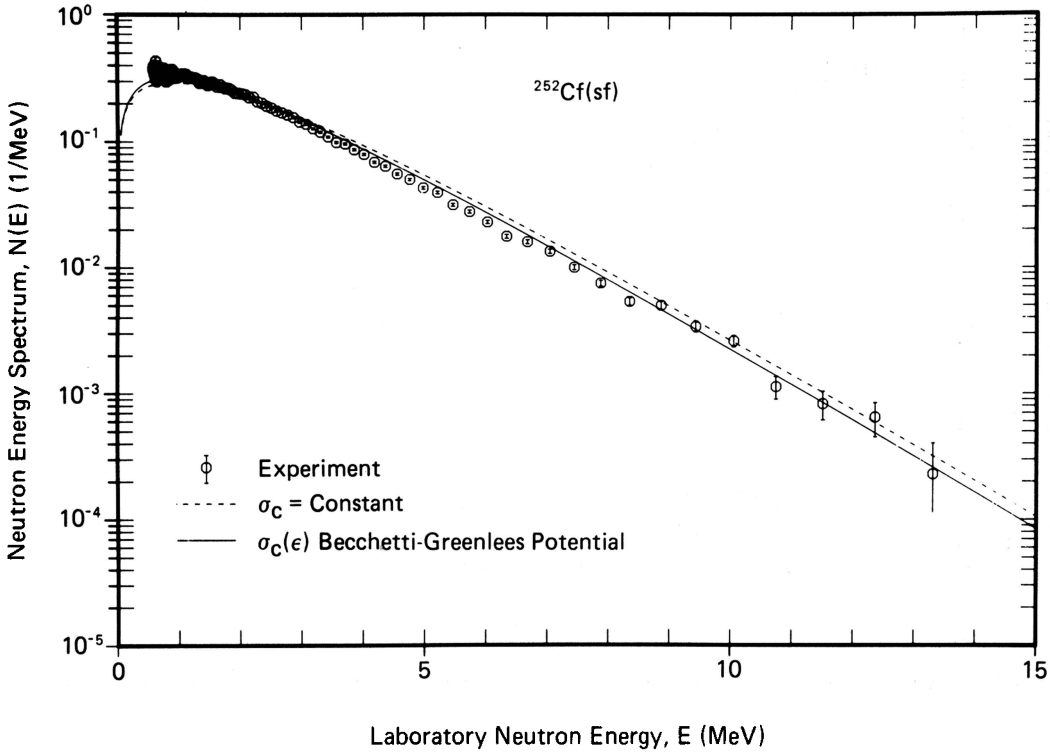

Fig. 27. Prompt fission neutron spectrum in the laboratory system for the spontaneous fission of ^{252}Cf. The dashed curve gives the spectrum calculated with Eq. (16) for a constant cross section whereas the solid curve gives the spectrum calculated with Eq. (28) for energy-dependent cross sections obtained using the optical model potential of Becchetti and Greenlees (Ref. 30). The values of the constants appearing in the calculated spectra are E_f^L = 0.984 MeV, E_f^H = 0.553 MeV, and T_m = 1.209 MeV. The experimental data are those of Boldeman et al. (Ref. 47) and Boldeman (Ref. 48), experiment 1.

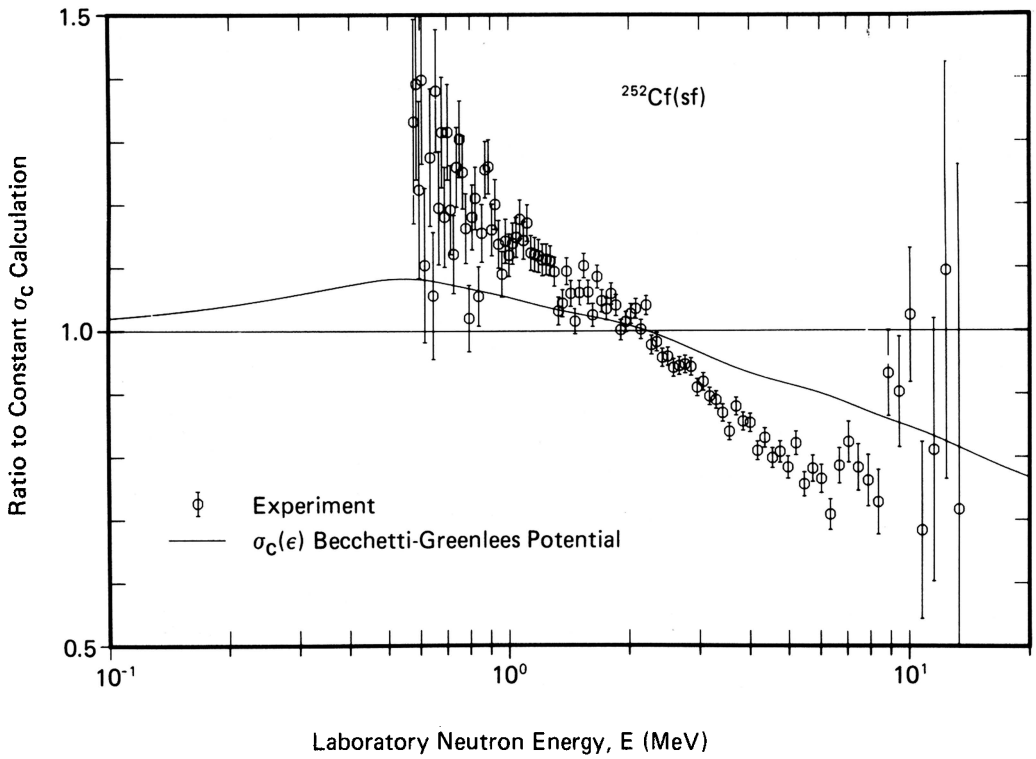

Fig. 28. Ratio of the spectrum calculated using energy-dependent cross sections and the experimental spectrum to the spectrum calculated using a constant cross section, corresponding to the curves shown in Fig. 27.

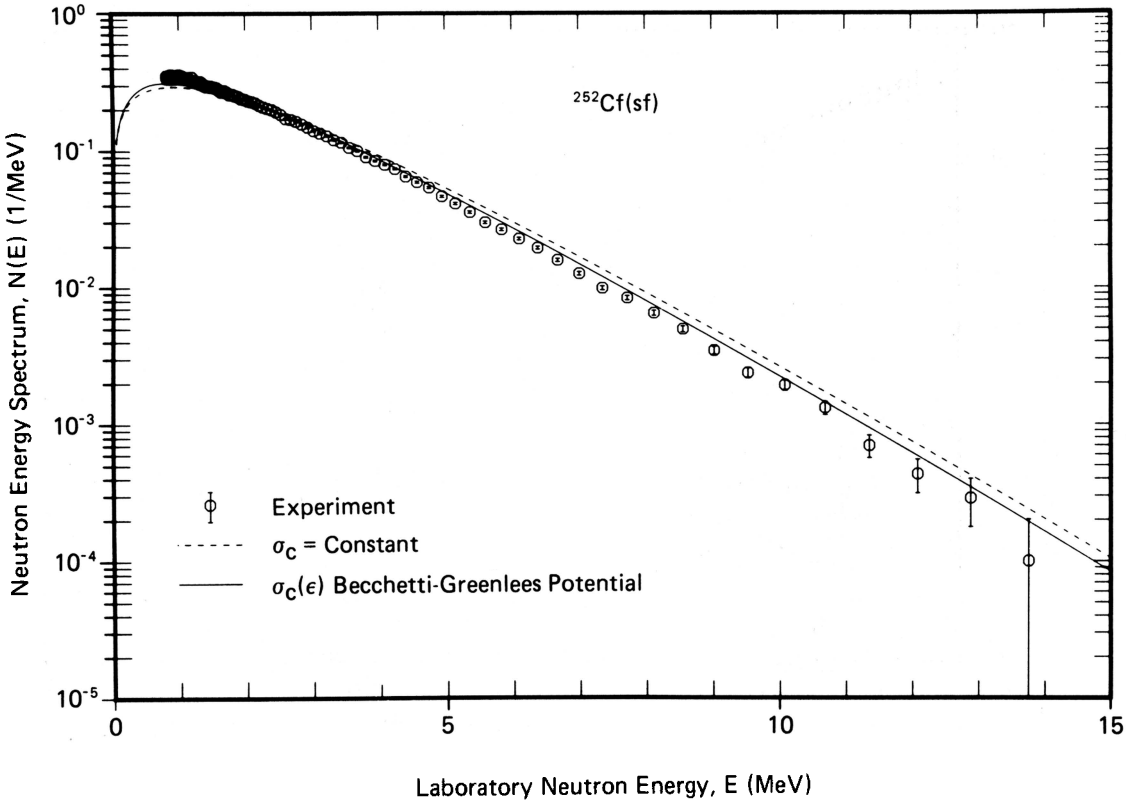

Fig. 29. Identical to Fig. 27 except that the experimental data are those of Boldeman et al. (Ref. 47) and Boldeman (Ref. 48), experiment 7.

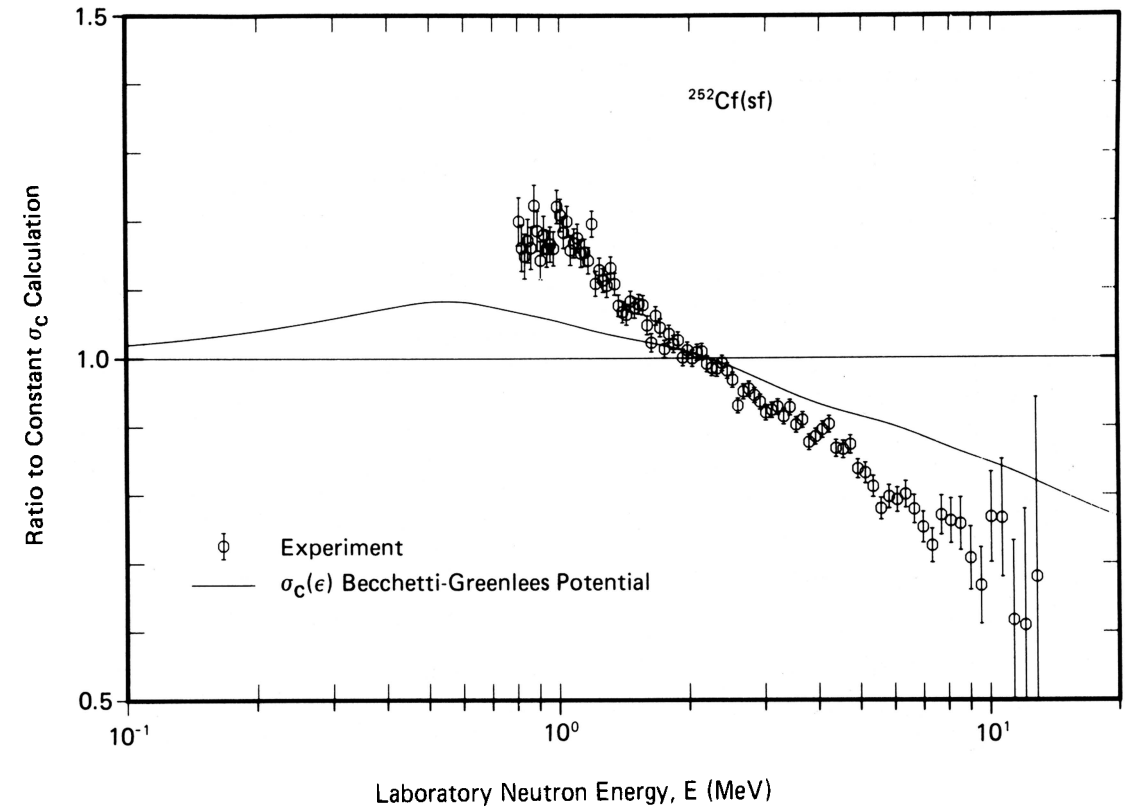

Fig. 30. Identical to Fig. 28 except that the experimental data are those of Boldeman et al. (Ref. 47) and Boldeman (Ref. 48), experiment 7.

most of the energy range is essentially one of slope, on a linear-log scale, resulting in maximum discrepancies of ~15%. A slightly stronger case is made for the energy-dependent cross-section calculation by considering the comparisons to experiment 7 shown in Figs. 29 and 30. In Fig. 29 the constant cross-section spectrum is clearly too hard relative to the experiment, and in Fig. 30 the largest discrepancies between the energy-dependent cross-section calculation and experiment are close to 10% as compared to 15% for experiment 1.

However, neither experimental spectrum is quite as hard as the energy-dependent cross-section spectrum, which has an average energy of 2.279 MeV. This could be due to a slightly large calculated value of T_m. Unlike the case of ^{239}Pu + n(0.53 MeV) discussed above, however, the calculated $\bar{\nu}_p$ for ^{252}Cf(sf) is in good agreement with experiment. Therefore, from the ^{239}Pu + n(0.53 MeV) discussion, one would conclude that in this case the level density parameter a is slightly in error, being somewhat low. This can be understood because the simple level density expression given by Eq. (5) is an approximation, the accuracy of which clearly depends on the mass region under consideration, as shown in Fig. 2. As the mass number of the fissioning nucleus increases, the average mass A_L of the light fragment mass distribution increases while the average mass A_H of the heavy fragment mass distribution remains relatively stable. Therefore, in the case of ^{252}Cf(sf) the level density parameter for A_L = 108 should be compared to that for A_L = 96 shown by the first arrow in Fig. 2. Clearly, the level density parameter increases with mass number in this region, which is the correct behavior to reduce T_m and thereby soften the calculated spectrum.

This reduction in T_m would reduce somewhat the average energy of the spectrum. For applied purposes, higher accuracy in this quantity could be achieved by adjusting the value of T_m to optimally reproduce the experimental spectrum. However, as is easily seen by comparing Figs. 28 and 30, there are experimental difficulties at both low and high energies, leading in some cases to nonreproducible measurements. Furthermore, as discussed above, the value of T_m is related physically to not only the level density parameter a but also to the average excitation energy $\langle E^* \rangle$ that affects the average prompt neutron multiplicity, to which we now turn our attention.

V. AVERAGE PROMPT NEUTRON MULTIPLICITIES

The excitation energy of fission fragments is dissipated primarily by prompt neutron emission and to a lesser extent by prompt gamma emission in cascade de-excitation processes. The average prompt neutron multiplicity $\bar{\nu}_p$ is the average total number of prompt neutrons emitted per fission from all contributing cascades. This quantity is as important as the prompt fission neutron spectrum $N(E)$ in many practical applications. Therefore, as in the case of $N(E)$, we calculate $\bar{\nu}_p$ as a function of both the fissioning nucleus and its excitation energy.

V.A. Calculation of Average Prompt Neutron Multiplicity

The total average fission-fragment excitation energy $\langle E^* \rangle$ is by energy conservation equal to the product of the average prompt neutron multiplicity $\bar{\nu}_p$ and the average energy removed per emitted neutron $\langle \eta \rangle$ plus the total average prompt gamma energy $\langle E_\gamma^{\text{tot}} \rangle$. Thus,

$$\langle E^* \rangle = \bar{\nu}_p \langle \eta \rangle + \langle E_\gamma^{\text{tot}} \rangle \ . \tag{30}$$

The average energy removed per emitted neutron $\langle \eta \rangle$ has been studied by Terrell[49] and is represented reasonably well by the sum of the average fission-fragment neutron separation energy $\langle S_n \rangle$ and the average center-of-mass energy of the emitted neutrons $\langle \epsilon \rangle$. Thus,

$$\langle \eta \rangle = \langle S_n \rangle + \langle \epsilon \rangle \ . \tag{31}$$

Combining Eqs. (30) and (31) and solving for $\bar{\nu}_p$ yields

$$\bar{\nu}_p = \frac{\langle E^* \rangle - \langle E_\gamma^{\text{tot}} \rangle}{\langle S_n \rangle + \langle \epsilon \rangle} \ . \tag{32}$$

In this equation the total average fission-fragment excitation energy $\langle E^* \rangle$ is already known as a function of the fissioning nucleus and its excitation energy and is given by Eq. (2). Similarly, the average center-of-mass energy of the emitted neutrons $\langle \epsilon \rangle$ is identical to the mean energy of the center-of-mass prompt fission neutron spectrum $\Phi(\epsilon)$ and is also known as a function of both the fissioning nucleus and its excitation energy. For the case of a constant compound nucleus cross section, $\langle \epsilon \rangle$ is given by Eq. (8), and for the case of an energy-dependent compound nucleus cross section, $\langle \epsilon \rangle$ is given by Eq. (27). Based on the result of Sec. IV that the energy-dependent cross-section calculations reproduce the experimental data better than do the constant cross-section calculations, we use values of $\langle \epsilon \rangle$ calculated with Eq. (27) for the calculations of this section. We neglect any dependence of the total average prompt gamma energy $\langle E_\gamma^{\text{tot}} \rangle$ upon the excitation energy of the fissioning nucleus, but account for its weak dependence on the mass of the fissioning nucleus by using available experimental values or the result of a least-squares adjustment, both given in the review by Hoffman and Hoffman.[23] To average over pairing effects, we take the average fission-fragment neutron separation energy $\langle S_n \rangle$ as one-half of the

average two-neutron separation energy $\langle S_{2n} \rangle$. We calculate $\langle S_{2n} \rangle$ using the same approximation as that for the calculation of the average energy release $\langle E_r \rangle$ discussed following Eq. (2). Thus, $\langle S_n \rangle$ has a dependence on the fissioning nucleus and its excitation energy from the same source as that of $\langle E_r \rangle$, although in both cases we neglect the weak dependence on excitation energy for the present calculations.

We obtain the explicit expression for the average prompt neutron multiplicity $\bar{\nu}_p$ by inserting Eq. (2) into Eq. (32) which yields

$$\bar{\nu}_p = \frac{\langle E_r \rangle + B_n + E_n - \langle E_f^{\text{tot}} \rangle - \langle E_\gamma^{\text{tot}} \rangle}{\langle S_n \rangle + \langle \epsilon \rangle} \quad . \tag{33}$$

For a given fissioning nucleus and fixed incident neutron energy E_n, the average multiplicity is quite sensitive to the difference between the two largest quantities in the numerator of Eq. (33), namely, the average energy release $\langle E_r \rangle$ and the total average fission-fragment kinetic energy $\langle E_f^{\text{tot}} \rangle$. To a lesser extent, it is also sensitive to the dominant term in the denominator which is the average neutron separation energy $\langle S_n \rangle$. Thus, good agreement between an experimental and a calculated average multiplicity suggests that the quantities $\langle E_r \rangle - \langle E_f^{\text{tot}} \rangle$ and $\langle S_n \rangle$ are substantially correct. Since the maximum temperature T_m appearing in the prompt fission neutron spectrum $N(E)$ is also quite sensitive to the former quantity, the good agreement also provides a measure of confidence in the corresponding prompt fission neutron spectrum. This is certainly an important observation especially in view of the fact that average neutron multiplicities can be measured very accurately. Moreover, the comparison of experimental and calculated average neutron multiplicities is not strongly dependent on nuclear level density parameter considerations because in Eq. (33) only the average center-of-mass energy $\langle \epsilon \rangle$ depends on the level density, and $\langle \epsilon \rangle$ is typically <20% of the denominator of the equation. It is therefore clear that the prompt fission neutron spectrum $N(E)$ and the average prompt neutron multiplicity $\bar{\nu}_p$ should be calculated and compared to experiment simultaneously.

Equation (33) is valid for neutron-induced, first-chance fission and spontaneous fission in which case E_n and B_n are set equal to zero. For incident neutron energies E_n less than the second-chance fission threshold, ~6 MeV, an explicit dependence of $\bar{\nu}_p$ on E_n is obtained using the constant cross-section result $\langle \epsilon \rangle = (4/3)T_m$ in Eq. (33). This yields the form

$$\bar{\nu}_p(E_n) = \frac{\alpha + E_n}{\beta + \gamma(1 + \delta E_n)^{1/2}} \quad , \tag{34}$$

where α, β, γ, and δ all depend weakly on E_n. The predicted energy dependence consists in a slight departure from the usual linear assumption[50] in that the square-root term causes a downward curvature that increases with increasing neutron energy. This is a small effect for cases of practical interest. However, it is nonnegligible where high accuracy is required. A similar, but more nearly exact, dependence on E_n is obtained with values of $\langle \epsilon \rangle$ calculated numerically by the use of energy-dependent cross sections in Eq. (27).

V.B. Comparison with Experimental Average Prompt Neutron Multiplicities

We now compare average prompt neutron multiplicities calculated with Eq. (33) to experimental data for several fissioning nuclei and excitation energies. We consider five cases of neutron-induced, first-chance fission and one case of spontaneous fission, reserving Sec. VI for the discussion of neutron multiplicities from multiple-chance fission. In Eq. (33) we use values of the average center-of-mass neutron energy $\langle \epsilon \rangle$ calculated with Eq. (27) using the optical model potential of Becchetti and Greenlees.[30] Many of the experimental data used in the comparisons have been measured relative to the average prompt neutron multiplicity for the spontaneous fission of ^{252}Cf. These data have been renormalized using the current value $\bar{\nu}_p[^{252}\text{Cf(sf)}] = 3.757$ obtained by subtracting the average delayed neutron multiplicity reported by Amiel[51] from the measured average total neutron multiplicity as evaluated by Smith.[52] For the neutron-induced fission cases, we compare our calculations to experimental results in Figs. 31 through 35 and list the calculated values in Table III.A for incident neutron energies of 0, 3, and 6 MeV. For the single spontaneous fission case studied, the calculated and experimental results are given in Table III.B.

We consider first the neutron-induced fission of three uranium isotopes ^{233}U, ^{235}U, and ^{238}U. The comparisons for the three cases are shown, respectively, in Figs. 31, 32, and 33 wherein the zero of the vertical scale is suppressed in order to enhance the comparative detail. The input quantities for the calculated curves are given in Table I except for the total average prompt gamma energy $\langle E_\gamma^{\text{tot}} \rangle$ and the average fission-fragment neutron separation energy $\langle S_n \rangle$. These are 6.69 and 5.274 MeV for ^{233}U + n, 6.71 and 4.998 MeV for ^{235}U + n, and 6.782 and 4.915 MeV for ^{238}U + n, respectively. As noted previously, the values of $\langle E_\gamma^{\text{tot}} \rangle$ are taken from Ref. 23 and the values of $\langle S_n \rangle$ are obtained using Refs. 24 and 25. Figure 31 shows that for the ^{233}U + n system the calculated average prompt neutron multiplicities are somewhat larger than the experimental values for the entire range of experimental incident neutron energies. The discrepancy ranges from an ~4% effect at thermal neutron

TABLE III

Average Prompt Neutron Multiplicities

A. Neutron-Induced Fission $\bar{\nu}_p(E_n)$				
Fission Reaction	$\sigma_c(\epsilon)$	$\bar{\nu}_p(0)$	$\bar{\nu}_p$(3 MeV)	$\bar{\nu}_p$(6 MeV)
$^{233}U + n$	B-G potential[a]	2.585	3.004	3.414
$^{235}U + n$	B-G potential	2.403	2.845	3.278
$^{238}U + n$	B-G potential	2.350	2.799	3.240
$^{239}Pu + n$	B-G potential	3.144	3.557	3.963
$^{240}Pu + n$	B-G potential	3.029	3.443	3.849

B. Spontaneous Fission $\bar{\nu}_p$(sf)			
Fission Reaction	$\sigma_c(\epsilon)$	$\bar{\nu}_p$(sf)	$\bar{\nu}_p^{exp}$(sf)
^{252}Cf(sf)	B-G potential	3.803	3.757 ± 0.009[b]

[a]Optical model potential of Becchetti and Greenlees (Ref. 30).

[b]Obtained from the experimental data contained in Refs. 51 and 52 as discussed in the text.

energies to almost 7% near 4 MeV. Since the total average fission-fragment kinetic energy $\langle E_f^{tot}\rangle$ and the total average prompt gamma energy $\langle E_\gamma^{tot}\rangle$ are measured quantities in this case, and since they were measured at thermal neutron energies, the 4% discrepancy can be attributed primarily to uncertainties in the average energy release $\langle E_r\rangle$ and/or $\langle S_n\rangle$ provided one neglects the experimental uncertainties in $\langle E_f^{tot}\rangle$ and $\langle E_\gamma^{tot}\rangle$. If the discrepancy is attributed entirely to the uncertainty in $\langle E_r\rangle$, one obtains agreement with experiment by a 0.7-MeV or 0.4% reduction in $\langle E_r\rangle$. This amount is within the 1-MeV uncertainty limit that has been estimated in Sec. II.A for calculating $\langle E_r\rangle$. Note, however, that since the fragment masses used to calculate $\langle E_r\rangle$ are a subset of those used to calculate $\langle S_n\rangle$, a correlated uncertainty can exist for $\langle S_n\rangle$. The sources of the discrepancy of almost 7% at the other end of the experimental range, ~4 MeV, are more difficult to assess because in addition to the uncertainties in $\langle E_r\rangle$ and $\langle S_n\rangle$ due to mass uncertainties, the slight dependencies of $\langle E_r\rangle$, $\langle S_n\rangle$, $\langle E_f^{tot}\rangle$, and $\langle E_\gamma^{tot}\rangle$ on the incident neutron energy E_n have been neglected. Thus, values of the

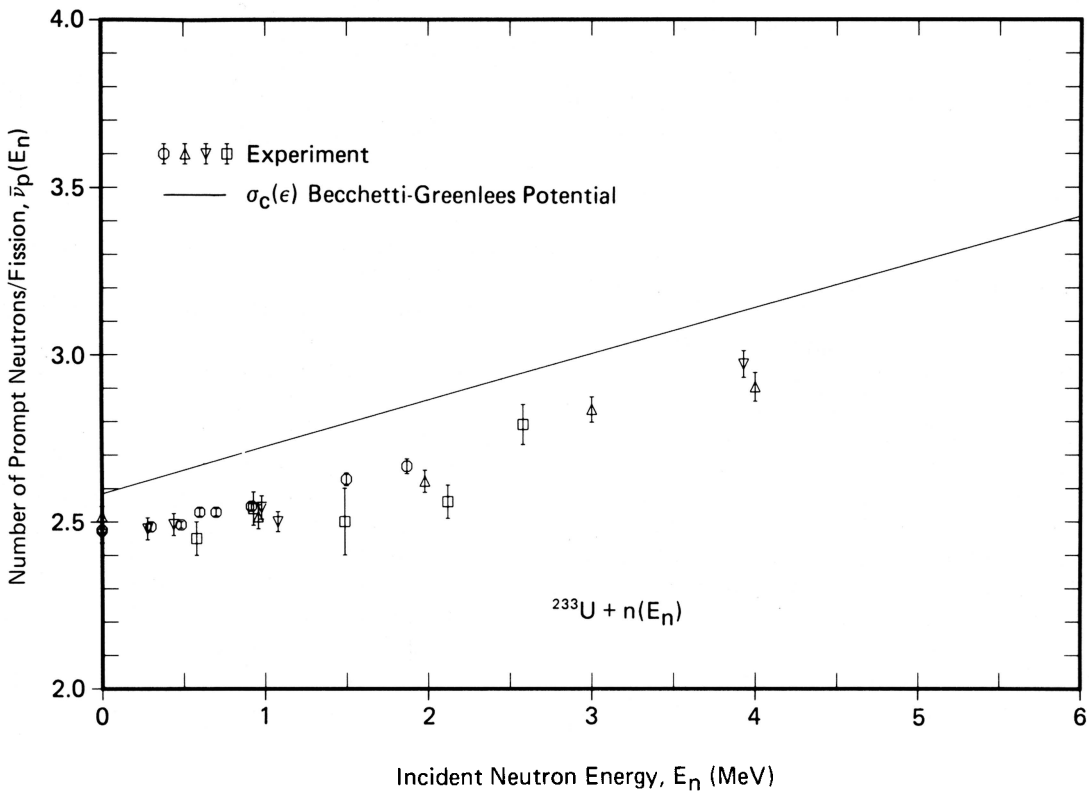

Fig. 31. Average prompt neutron multiplicity as a function of the incident neutron energy for the neutron-induced fission of ^{233}U. The solid curve gives the multiplicity calculated with Eq. (33) using the optical model potential of Becchetti and Greenlees (Ref. 30) to determine the average center-of-mass energy $\langle\epsilon\rangle$. The experimental data are those of Walsh and Boldeman (Ref. 53), ○; Mather et al. (Ref. 54), △; Hopkins and Diven (Ref. 55), ▽; and Colvin and Sowerby (Ref. 56), □. Note the suppressed zero of the vertical scale.

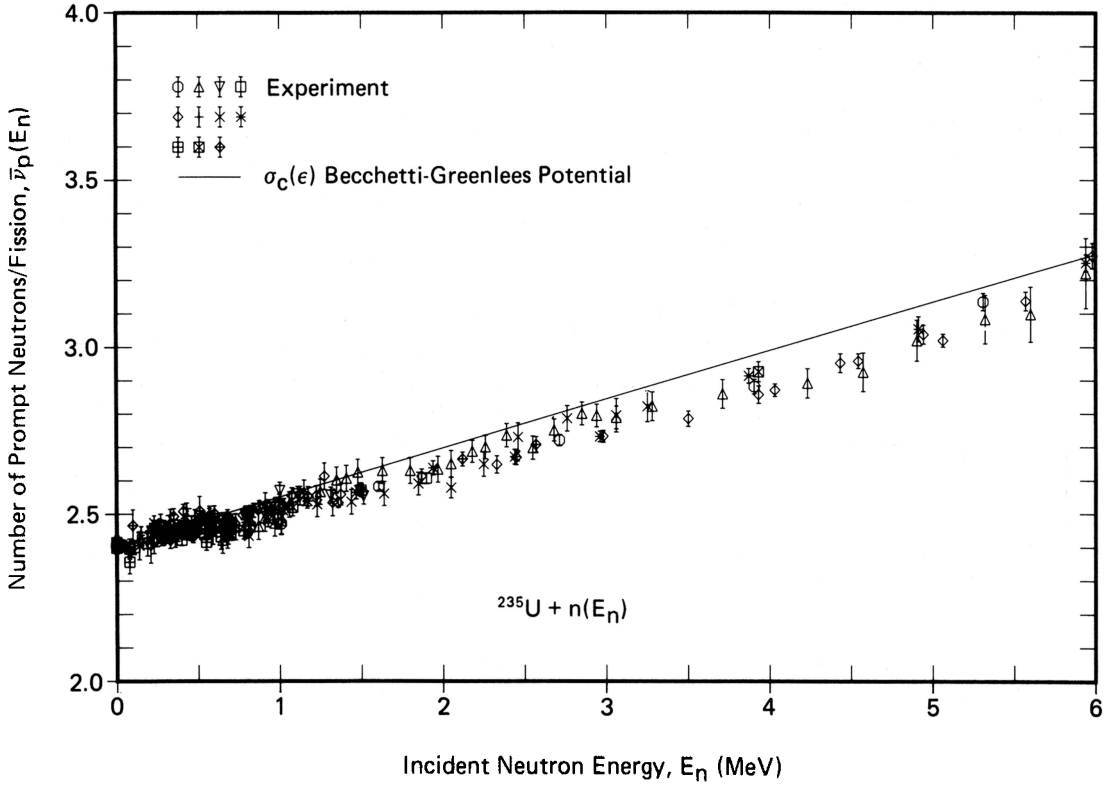

Fig. 32. Average prompt neutron multiplicity as a function of the incident neutron energy for the neutron-induced fission of ^{235}U. The solid curve gives the multiplicity calculated with Eq. (33) using the optical model potential of Becchetti and Greenlees (Ref. 30) to determine the average center-of-mass energy $\langle\epsilon\rangle$. The experimental data are those of Gwin et al. (Ref. 57), ○; Savin et al. (Ref. 58), △; Nesterov et al. (Ref. 59), ▽; Boldeman and Walsh (Ref. 60), □; Soleilhac et al. (Ref. 61), ◇; Meadows and Whalen (Ref. 62), +; Prokhorova and Smirenkin (Ref. 63), ×; Mather et al. (Ref. 54), *; Blyumkina et al. (Ref. 64), ⊞; Hopkins and Diven (Ref. 55), ⊠; and Colvin and Sowerby (Ref. 56), ⊕. Note the suppressed zero of the vertical scale.

derivatives $d\langle E_r\rangle/dE_n$, $d\langle S_n\rangle/dE_n$, $d\langle E_f^{tot}\rangle/dE_n$, and $d\langle E_\gamma^{tot}\rangle/dE_n$ are required as a function of E_n. We have not accounted for the four derivatives in this work because they have not yet been measured over an adequate range of neutron energy. It is known that $d\langle E_f^{tot}\rangle/dE_n$ is usually negative[23] and that $d\langle E_\gamma^{tot}\rangle/dE_n$ is positive for certain cases.[44] The negative derivative of $\langle E_f^{tot}\rangle$ would increase the discrepancy for the $^{233}U + n$ case whereas the positive derivative of $\langle E_\gamma^{tot}\rangle$ would decrease the discrepancy.

Calculated and experimental average prompt neutron multiplicities are more in agreement for the $^{235}U + n$ system as shown by Fig. 32. In this case the agreement is better than 1% for thermal neutron energies up to ~1 MeV and again at 6 MeV. However, in the region from ~1.5 to 5.5 MeV, the experimental values are somewhat less than the calculated values. In addition, whereas the curvature of the data appears to be concave upward in the region of ~3 to 6 MeV, the calculation is linear to first order in this region. The maximum discrepancy also occurs within this region at ~4.5 MeV where the calculation is ~3% high. We believe that this discrepancy and the slight concave-upward curvature between 3 and 6 MeV in the data can be understood in terms of the dependencies of $\langle E_r\rangle$, $\langle S_n\rangle$, $\langle E_f^{tot}\rangle$, and $\langle E_\gamma^{tot}\rangle$ on the incident neutron energy. As noted in the preceding discussion of the $^{233}U + n$ system, some of these dependencies have canceling effects in their contribution to $\bar{\nu}_p(E_n)$. Thus, not only are experimental measurements of these dependencies required as a function of the incident neutron energy, they are required with high accuracy.

The comparison of calculated and experimental average prompt neutron multiplicities for the $^{238}U + n$ system is shown in Fig. 33. In this case the calculation is between ~1 and 3% high with respect to the experimental data except in the region between ~2 and 4 MeV. Here, the data display a concave-upward curvature similar to that observed between 3 and 6 MeV in the $^{235}U + n$ case. The maximum discrepancy between calculation and experiment occurs at the center of this region, ~3 MeV, and is ~5%. Again, we believe that the behavior of the experimental data in this region, as in the similar

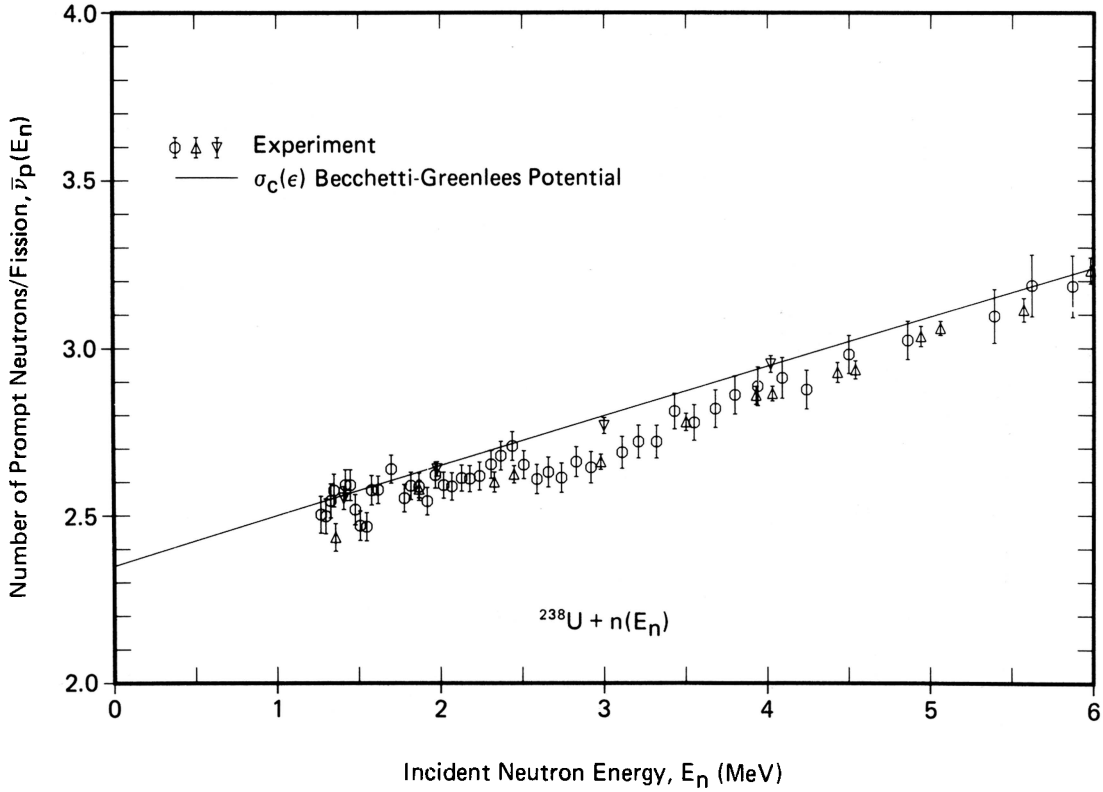

Fig. 33. Average prompt neutron multiplicity as a function of the incident neutron energy for the neutron-induced fission of ^{238}U. The solid curve gives the multiplicity calculated with Eq. (33) using the optical model potential of Becchetti and Greenlees (Ref. 30) to determine the average center-of-mass energy $\langle\epsilon\rangle$. The experimental data are those of Savin et al. (Ref. 65), ○; Soleilhac et al. (Ref. 61), △; and Mather et al. (Ref. 54), ▽. Note the suppressed zero of the vertical scale.

region for the $^{235}U + n$ case, is explicable in terms of the dependencies of $\langle E_r\rangle$, $\langle S_n\rangle$, $\langle E_f^{tot}\rangle$, and $\langle E_\gamma^{tot}\rangle$ on the incident neutron energy.

We now consider the neutron-induced fission of the two plutonium isotopes ^{239}Pu and ^{240}Pu. The comparisons of calculated and experimental average prompt neutron multiplicities for these two cases are shown in Figs. 34 and 35. The input quantities for the calculated curves are given in Table I except for $\langle E_\gamma^{tot}\rangle$ and $\langle S_n\rangle$. These are 6.77 and 5.220 MeV for $^{239}Pu + n$ and 6.838 and 5.241 MeV for $^{240}Pu + n$, respectively. The values of $\langle E_\gamma^{tot}\rangle$ are taken from Ref. 23 and the values of $\langle S_n\rangle$ are obtained using Refs. 24 and 25. Figure 34 shows that for the $^{239}Pu + n$ system the calculation is larger than experiment for the entire 6-MeV range. This result is similar to that obtained in comparisons of the prompt fission neutron spectrum for the same system in that the calculated spectrum is harder than the experimental spectrum as shown by Fig. 25. The discrepancy here ranges from an ~10% effect at thermal neutron energies to ~6% at 6 MeV. Noting that $\langle E_f^{tot}\rangle$ and $\langle E_\gamma^{tot}\rangle$ are quantities measured at thermal neutron energy, we could attribute the 10% discrepancy primarily to uncertainties in $\langle E_r\rangle$ and/or $\langle S_n\rangle$ by neglecting the experimental uncertainties in $\langle E_f^{tot}\rangle$ and $\langle E_\gamma^{tot}\rangle$. Assuming that the discrepancy is due entirely to an erroneous value of $\langle E_r\rangle$, one obtains agreement with experiment by a 2.1-MeV reduction in $\langle E_r\rangle$. This amount is over a factor of 2 larger than our estimated uncertainty limit of 1 MeV given in Sec. II.A.

There are two possible sources of error in our calculation of $\langle E_r\rangle$ for this system. One source is that 6 of the 14 fragment masses required in the calculation are systematic masses from Wapstra and Bos,[24] which could be in error. The second source is that the choice of ^{100}Zr and ^{140}Xe as the average fragments of the two mass peaks, based on the work of Unik et al.,[22] could be in error. Of course, either or both of these sources would also contribute to an error in the calculation of $\langle S_n\rangle$. Note, however, that whereas the calculated average neutron multiplicity depends on $\langle S_n\rangle$, the fission-neutron-spectrum calculation is independent of $\langle S_n\rangle$. Finally, the maximum combined experimental uncertainty in $\langle E_f^{tot}\rangle$ and $\langle E_\gamma^{tot}\rangle$ for this case is 0.8 MeV. Some or all of the above possible errors and experimental uncertainties could resolve the discrepancy between calculation and experiment shown in Fig. 34 for the average multiplicity $\bar{\nu}_p(E_n)$ and shown in Fig. 25 for the fission spectrum $N(E)$. In Appendix C we

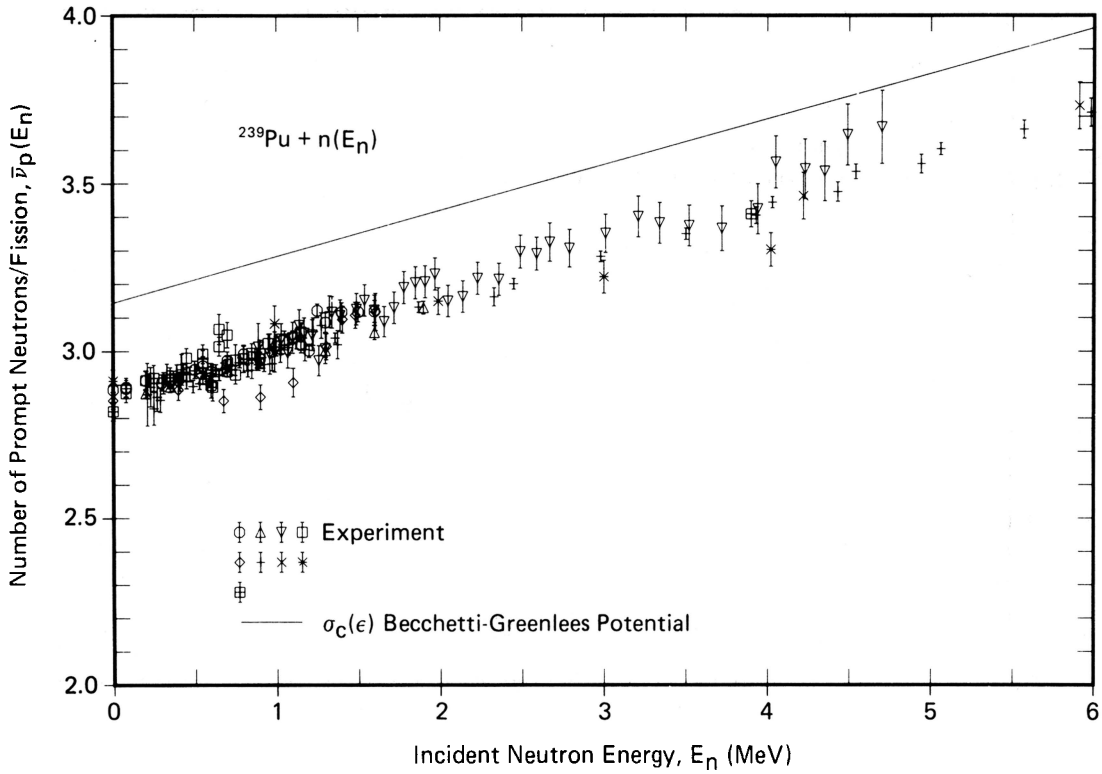

Fig. 34. Average prompt neutron multiplicity as a function of the incident neutron energy for the neutron-induced fission of ^{239}Pu. The solid curve gives the multiplicity calculated with Eq. (33) using the optical model potential of Becchetti and Greenlees (Ref. 30) to determine the average center-of-mass energy $\langle\epsilon\rangle$. The experimental data are those of Bolodin et al. (Ref. 66), ○; Walsh and Boldeman (Ref. 67), △; Savin et al. (Ref. 58), ▽; Mather et al. (Ref. 68), □; Nesterov et al. (Ref. 59), ◇; Soleilhac et al. (Ref. 61), +; Condé et al. (Ref. 69), ×; Mather et al. (Ref. 54), ∗; and Hopkins and Diven (Ref. 55), ⊞. Note the suppressed zero of the vertical scale.

investigate the effects of different determinations of the average fission fragments and the measured value of $\langle E_f^{tot}\rangle$ on $N(E)$ and $\bar{\nu}_p(E_n)$ for the ^{239}Pu + n system. The conclusion for the present calculation of these quantities is that the calculated total average fission-fragment excitation energy $\langle E^*\rangle$ is too large, by perhaps as much as 8% in the worst case, to explain the experimental data. This relatively large difference must be explained before addressing the possible fine structure of the data in Fig. 34 at higher incident neutron energies.

The comparison of calculated and experimental average prompt neutron multiplicities for the ^{240}Pu + n system is shown in Fig. 35. In this case the calculation is on the average ~3% higher than the average of the experimental data up to ~4 MeV. A 3% discrepancy at 3 MeV corresponds to an error of ~0.7 MeV or 0.3% in the calculation of $\langle E_r\rangle$ assuming all other quantities are known. Above 4 MeV the three data points suggest the existence of another concave-upward curvature as observed in the ^{235}U + n and ^{238}U + n cases. We would expect to explain this curvature with the same energy-dependent quantities discussed in those two cases.

Our calculation of the average prompt neutron multiplicity for the spontaneous fission of ^{252}Cf is performed using values of the input parameters listed in Table I, except for values of $\langle E_\gamma^{tot}\rangle$ = 6.95 MeV and $\langle S_n\rangle$ = 5.473 MeV, which are obtained from Ref. 23 and Refs. 24 and 25, respectively. The result is $\bar{\nu}_p[^{252}\text{Cf(sf)}]$ = 3.803, whereas a current evaluation of the measured value gives $\bar{\nu}_p[^{252}\text{Cf(sf)}]$ = 3.757 ± 0.009, as listed in Table III.B. The calculated value is 1.2% high with respect to the evaluation. This difference, however, is well within the expected accuracy of the calculation based on the approximations that we have used.

VI. MULTIPLE-CHANCE FISSION

At high incident neutron energy, above ~6 MeV, the excitation energy of the compound nucleus is sufficiently large that fission is possible following the emission of one or more neutrons. Thus, at some excitation energy the first-chance fission (n,f) reaction is in competition with the second-chance fission $(n,n'f)$ reaction; at some higher excitation energy these two reactions are in competition with

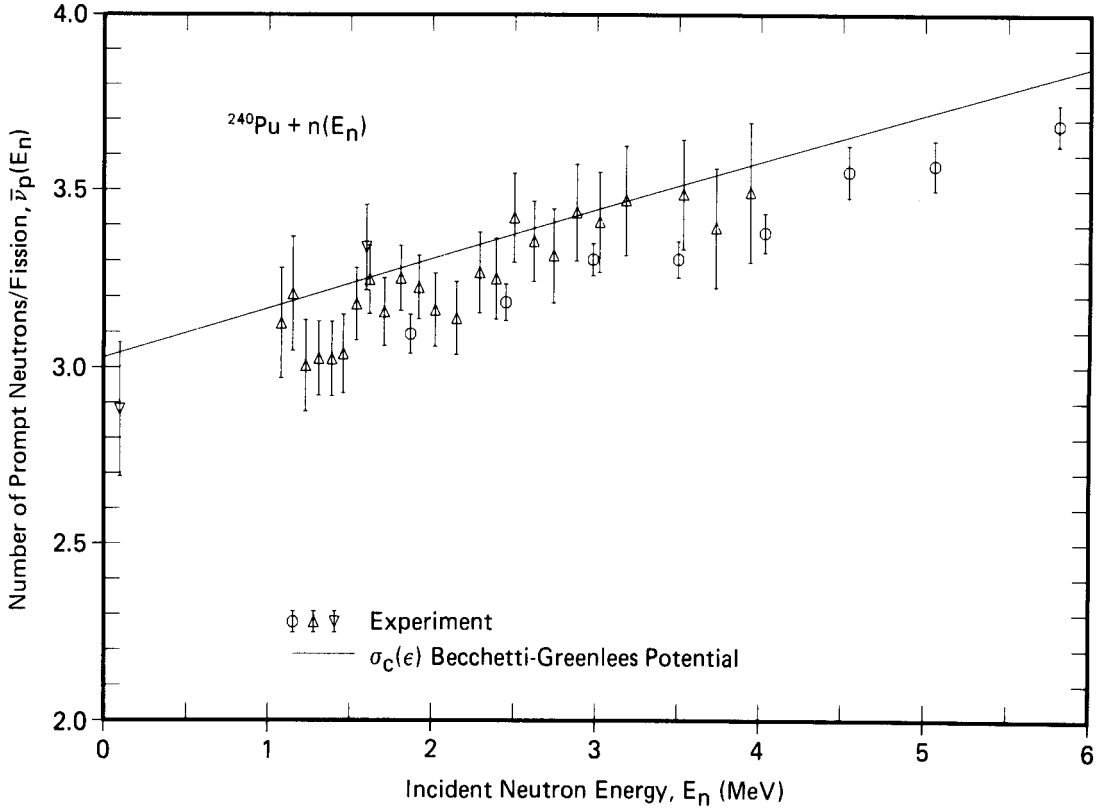

Fig. 35. Average prompt neutron multiplicity as a function of the incident neutron energy for the neutron-induced fission of ^{240}Pu. The solid curve gives the multiplicity calculated with Eq. (33) using the optical model potential of Becchetti and Greenlees (Ref. 30) to determine the average center-of-mass energy $\langle\epsilon\rangle$. The experimental data are those of de Vroey et al. (Ref. 70), ○; Savin et al. (Ref. 58), △; and Frehaut et al. (Ref. 71), ▽. Note the suppressed zero of the vertical scale.

each other and with the third-chance fission $(n,n'n''f)$ reaction, and so on. Although the neutrons emitted prior to fission have no direct connection with the fission process, whereas those emitted following fission do, both groups are nevertheless in coincidence with the fission event from the standpoint of any physical measurement. Thus, both groups must be accounted for in calculating the prompt fission neutron spectrum $N(E)$ and the average prompt neutron multiplicity $\bar{\nu}_p$ when the fissioning nucleus is at high excitation energy.

In this section we account for the effects of and competition between multiple-chance fission processes up through third-chance fission in the calculation of $N(E)$ and $\bar{\nu}_p$. Using the resulting formalism, we present calculations of these quantities and comparisons to experimental data for the neutron-induced fission of ^{235}U.

VI.A. Multiple-Chance Fission Probabilities

The competition between first-, second-, and third-chance fission events can be described by the probabilities for these reactions to occur as shown, for example, in the studies by Boyce et al.[72] and Benzi et al.[73] Here, the multiple-chance fission probabilities are defined in terms of the cross sections for open reaction channels in the neutron-plus-actinide scattering system. We have

$$\begin{aligned}\sigma_a &= \sigma_c + \sigma_{dr} \\ &= \sigma_{ce} + \sigma(n,n') + \sigma(n,\gamma) + \sigma(n,xn) + \sigma(n,f) \\ &\quad + \sigma(n,n'f) + \sigma(n,n'n''f) + \sigma_{dr} \ , \end{aligned} \tag{35}$$

where

σ_a = total absorption cross section

σ_c = total compound nucleus cross section

σ_{dr} = total direct reaction cross section including semidirect and knockout processes

σ_{ce} = total compound elastic cross section

$\sigma(n,n')$ = total compound inelastic cross section

$\sigma(n,\gamma)$ = total compound neutron capture cross section

$\sigma(n,xn)$ = total compound cross section for the (n,xn) reaction,

and where the remaining compound multiple-chance fission cross sections have already been defined. For incident neutron energies near and above the

threshold for second-chance fission, σ_{ce} and $\sigma(n,\gamma)$ are negligibly small and σ_{dr} is small relative to the fission and (n,xn) cross sections. We therefore approximate these three cross sections by zero, identify the absorption cross section and the total compound nucleus cross section with the optical model absorption cross section, and divide Eq. (35) by the optical model absorption cross section giving

$$P(n,n') + P(n,xn) + P(n,f) + P(n,n'f) + P(n,n'n''f) = 1 \ , \qquad (36)$$

where the notation for each probability is analogous to that of Eq. (35). With the approximation used in Eq. (36), $P(n,f)$ is the probability that there are no neutrons in the exit channel whereas $[1 - P(n,f)]$ is the probability that there is a neutron in the exit channel. The total fission probability P_f^{tot} is equal to the sum of the last three terms of Eq. (36), namely,

$$P_f^{tot} = P(n,f) + P(n,n'f) + P(n,n'n''f) \qquad (37)$$

or

$$P_f^A[E_n + B_n(A)] = P_{f_1}^A[E_n + B_n(A)] + P_{f_2}^A[E_n + B_n(A)] + P_{f_3}^A[E_n + B_n(A)] \ , \qquad (38)$$

where A is the mass number of the fissioning compound nucleus (Z,A) of excitation energy $E_n + B_n(A)$; E_n and $B_n(A)$ are the kinetic energy and separation energy of the neutron inducing fission; and the subscripts f_1, f_2, and f_3 refer to first-, second-, and third-chance fission, respectively. Equation (38) is identical to Eq. (37) except for the convenient notation change for developing the solution to the equation.

Let $D_1(E^*)$ equal the normalized distribution of excitation energy in the excited $(Z,A-1)$ nucleus having been created by a neutron evaporating from the (Z,A) nucleus at the specific excitation energy $E_n + B_n(A)$. Then, Eq. (38) can be written as

$$P_f^A[E_n + B_n(A)] = P_{f_1}^A[E_n + B_n(A)] + \left[\int_0^{E_n} P_f^{A-1}(E^*)D_1(E^*)dE^*\right] \times \{1 - P_{f_1}^A[E_n + B_n(A)]\} \ , \qquad (39)$$

where $P_f^{A-1}(E^*)$ is the total fission probability of the $(Z,A-1)$ nucleus at excitation energy E^*. The first term on the right side of this equation is, of course, the first-chance fission probability of the (Z,A) nucleus at an excitation energy of $E_n + B_n(A)$. The second term is the product of an average total fission probability of the $(Z,A-1)$ nucleus, in large square brackets, and the probability that there is a neutron in the exit channel of the (Z,A) nucleus at an excitation energy $E_n + B_n(A)$, in curly braces. More specifically, the factor in large square brackets is the integral of the total fission probability of the $(Z,A-1)$ nucleus, weighted by the normalized distribution of excitation energy in the $(Z,A-1)$ nucleus, over the total range of excitation energy available to the $(Z,A-1)$ nucleus. Representing this factor by $\langle P_f^{A-1}(E_n)\rangle$ and solving Eq. (39) for $P_{f_1}^A$, we obtain

$$P_{f_1}^A[E_n + B_n(A)] = \frac{P_f^A[E_n + B_n(A)] - \langle P_f^{A-1}(E_n)\rangle}{1 - \langle P_f^{A-1}(E_n)\rangle} \ . \qquad (40)$$

Equation (40) gives the first-chance fission probability of the (Z,A) nucleus as a function of the incident neutron energy E_n in terms of quantities that are known or can be calculated.

Let $D_2(E^*)$ equal the normalized distribution of excitation energy in the excited $(Z,A-2)$ nucleus having been created by a neutron evaporating from the $(Z,A-1)$ nucleus at an average excitation energy $[E_n + B_n(A)] - [\langle \mathscr{E}_1\rangle + B_n(A)] = E_n - \langle \mathscr{E}_1\rangle$, where $\langle \mathscr{E}_1\rangle$ is the mean kinetic energy of the neutron evaporated from the (Z,A) nucleus. Then, similar to Eq. (39), we have

$$P_f^{A-1}(E_n - \langle \mathscr{E}_1\rangle) = P_{f_1}^{A-1}(E_n - \langle \mathscr{E}_1\rangle) + \left[\int_0^{E_n - \langle \mathscr{E}_1\rangle - B_n(A-1)} P_f^{A-2}(E^*)D_2(E^*)dE^*\right] \times [1 - P_{f_1}^{A-1}(E_n - \langle \mathscr{E}_1\rangle)] \ , \qquad (41)$$

where $P_f^{A-2}(E^*)$ is the total fission probability of the $(Z,A-2)$ nucleus at excitation energy E^* and $B_n(A-1)$ is the neutron separation energy of the $(Z,A-1)$ nucleus. Representing the factor in large square brackets by $\langle P_f^{A-2}[E_n - \langle \mathscr{E}_1\rangle - B_n(A-1)]\rangle$ and solving Eq. (41) for $P_{f_1}^{A-1}$, we obtain

$$P_{f_1}^{A-1}(E_n - \langle \mathscr{E}_1\rangle) = \frac{P_f^{A-1}(E_n - \langle \mathscr{E}_1\rangle) - \langle P_f^{A-2}[E_n - \langle \mathscr{E}_1\rangle - B_n(A-1)]\rangle}{1 - \langle P_f^{A-2}[E_n - \langle \mathscr{E}_1\rangle - B_n(A-1)]\rangle} \ . \qquad (42)$$

Equation (42) gives the first-chance fission probability of the $(Z,A-1)$ nucleus as a function of its average excitation energy $E_n - \langle \mathscr{E}_1\rangle$ in terms of quantities that are known or can be calculated.

Let $D_3(E^*)$ equal the normalized distribution of excitation energy in the excited $(Z,A-3)$ nucleus having been created by a neutron evaporating from the $(Z,A-2)$ nucleus at an average excitation energy

$[E_n + B_n(A)] - [\langle \mathscr{E}_1 \rangle + B_n(A)] - [\langle \mathscr{E}_2 \rangle + B_n(A-1)] = [E_n - \langle \mathscr{E}_1 \rangle - \langle \mathscr{E}_2 \rangle - B_n(A-1)]$, where $\langle \mathscr{E}_2 \rangle$ is the mean kinetic energy of the neutron evaporated from the $(Z,A-1)$ nucleus. Then, similar to Eq. (41), we have

$$P_f^{A-2}[E_n - \langle \mathscr{E}_1 \rangle - \langle \mathscr{E}_2 \rangle - B_n(A-1)] = P_{f_1}^{A-2}[E_n - \langle \mathscr{E}_1 \rangle - \langle \mathscr{E}_2 \rangle - B_n(A-1)] + \left[\int_0^{E_n - \langle \mathscr{E}_1 \rangle - \langle \mathscr{E}_2 \rangle - B_n(A-1) - B_n(A-2)} P_f^{A-3}(E^*) D_3(E^*) dE^*\right] \{1 - P_{f_1}^{A-2}[E_n - \langle \mathscr{E}_1 \rangle - \langle \mathscr{E}_2 \rangle - B_n(A-1)]\} , \quad (43)$$

where $P_f^{A-3}(E^*)$ is the total fission probability of the $(Z,A-3)$ nucleus at excitation energy E^* and $B_n(A-2)$ is the neutron separation energy of the $(Z,A-2)$ nucleus. Representing the factor in large square brackets by $\langle P_f^{A-3}[E_n - \langle \mathscr{E}_1 \rangle - \langle \mathscr{E}_2 \rangle - B_n(A-1) - B_n(A-2)] \rangle$ and solving Eq. (43) for $P_{f_1}^{A-2}$, we obtain

$$P_{f_1}^{A-2}[E_n - \langle \mathscr{E}_1 \rangle - \langle \mathscr{E}_2 \rangle - B_n(A-1)] = \frac{P_f^{A-2}[E_n - \langle \mathscr{E}_1 \rangle - \langle \mathscr{E}_2 \rangle - B_n(A-1)] - \langle P_f^{A-3}[E_n - \langle \mathscr{E}_1 \rangle - \langle \mathscr{E}_2 \rangle - B_n(A-1) - B_n(A-2)] \rangle}{1 - \langle P_f^{A-3}[E_n - \langle \mathscr{E}_1 \rangle - \langle \mathscr{E}_2 \rangle - B_n(A-1) - B_n(A-2)] \rangle} . \quad (44)$$

Equation (44) gives the first-chance fission probability of the $(Z,A-2)$ nucleus as a function of its average excitation energy $[E_n - \langle \mathscr{E}_1 \rangle - \langle \mathscr{E}_2 \rangle - B_n(A-1)]$ in terms of quantities that are known or can be calculated. We note that this equation and Eqs. (40) and (42) are all of the form $P = (X - Y)/(1 - Y)$.

Upon comparing Eq. (38) with the sequence of Eqs. (39), (41), and (43) and noting that average fission probabilities are approximately equal to fission probabilities evaluated at average excitation energies, we obtain the approximate relations

$$P_{f_1}^{A}[E_n + B_n(A)] = P_{f_1}^{A}[E_n + B_n(A)] , \quad (45)$$

$$P_{f_2}^{A}[E_n + B_n(A)] = P_{f_1}^{A-1}(E_n - \langle \mathscr{E}_1 \rangle) \times \{1 - P_{f_1}^{A}[E_n + B_n(A)]\} , \quad (46)$$

and

$$P_{f_3}^{A}[E_n + B_n(A)] = P_{f_1}^{A-2}[E_n - \langle \mathscr{E}_1 \rangle - \langle \mathscr{E}_2 \rangle - B_n(A-1)] \times [1 - P_{f_1}^{A-1}(E_n - \langle \mathscr{E}_1 \rangle)] \times \{1 - P_{f_1}^{A}[E_n + B_n(A)]\} , \quad (47)$$

which are evaluated using Eqs. (40), (42), and (44). Equations (45), (46), and (47) give, respectively, the probabilities of first-, second-, and third-chance fission of the (Z,A) fissioning compound nucleus at an excitation energy $E_n + B_n(A)$.

We now discuss the excitation energy distributions $D_1(E^*)$, $D_2(E^*)$, and $D_3(E^*)$ that are required in the solutions of Eqs. (40), (42), and (44). The excitation energy distribution $D(E^*)$ is the complement of the neutron energy distribution of the neutrons emitted prior to fission in the multiple-chance fission process. This distribution is identical to the expression for the center-of-mass neutron energy spectrum $\phi(\epsilon)$ given by Eq. (1) for the case of a constant cross section for the inverse process of compound nucleus formation and given by Eq. (22) for the case of an energy-dependent cross section. For the calculations of this section, we use Eq. (22) with energy-dependent cross sections calculated from an actinide optical model potential. We neglect the distinction between center-of-mass and laboratory systems for the neutrons emitted prior to fission because an actinide nucleus is kinematically a good approximation to an infinite mass nucleus for the neutron energies considered here. Thus,

$$\phi(E,\sigma_c) = k(T)\sigma_c(E)E \exp(-E/T) , \quad (48)$$

where E is the laboratory neutron energy and all other quantities are defined as in Eq. (22). Note that we have earlier designated the mean energy of this spectrum by the symbol $\langle \mathscr{E} \rangle$. The required complement of this spectrum is

$$D(E^*,\sigma_c) = c(T)\phi(E_m - E^*,\sigma_c) , \quad (49)$$

where E^* is the excitation energy, E_m is the maximum excitation energy, and $c(T)$ is the renormalization constant due to the finite value of E_m, namely,

$$c(T) = \left[\int_0^{E_m} \phi(E_m - E^*,\sigma_c) dE^*\right]^{-1} .$$

The residual nuclear temperature T used in Eqs. (48) and (49) is obtained using the Fermi gas model $E_m = aT^2$ where the nuclear level density parameter a is given by Eq. (5).

Accordingly, the excitation energy distributions required in the solution of Eqs. (40), (42), and (44) are given by

$$D_1(E^*,\sigma_{c_1}) = c(T_1)\phi_1(E_{m_1} - E^*,\sigma_{c_1}) , \quad (50a)$$

where

$$E_{m_1} = E_n \ , \tag{50b}$$

$$T_1 = [(11 \text{ MeV})E_{m_1}/A]^{1/2} \ , \tag{50c}$$

and σ_{c_1} is calculated for the $n + (Z,A-1)$ scattering system;

$$D_2(E^*,\sigma_{c_2}) = c(T_2)\phi_2(E_{m_2} - E^*,\sigma_{c_2}) \ , \tag{51a}$$

where

$$E_{m_2} = E_n - \langle \mathscr{E}_1 \rangle - B_n(A-1) \ , \tag{51b}$$

$$T_2 = [(11 \text{ MeV})E_{m_2}/(A-1)]^{1/2} \ , \tag{51c}$$

and σ_{c_2} is calculated for the $n + (Z,A-2)$ scattering system; and

$$D_3(E^*,\sigma_{c_3}) = c(T_3)\phi_3(E_{m_3} - E^*,\sigma_{c_3}) \ , \tag{52a}$$

where

$$E_{m_3} = E_n - \langle \mathscr{E}_1 \rangle - \langle \mathscr{E}_2 \rangle - B_n(A-1) - B_n(A-2) \ , \tag{52b}$$

$$T_3 = [(11 \text{ MeV})E_{m_3}/(A-2)]^{1/2} \ , \tag{52c}$$

and σ_{c_3} is calculated for the $n + (Z,A-3)$ scattering system.

In these equations, whereas E_{m_1} is the maximum excitation energy, E_{m_2} and E_{m_3} are maximum average excitation energies because in each of these cases mean neutron energies $\langle \mathscr{E}_i \rangle$ are used to determine the average energy cost per emitted neutron for the preceding nuclei in the cascade.

We next consider the total fission probabilities P_f^A, P_f^{A-1}, P_f^{A-2}, and P_f^{A-3} that are required in the solutions of Eqs. (40), (42), and (44). We construct these by using experimental total fission probabilities for excitation energies below the neutron separation energy and by using the ratio of a measured total fission cross section to a calculated compound nucleus cross section above the neutron separation energy. As in the calculation of the excitation energy distributions $D(E^*)$, we use an actinide optical model potential to calculate these cross sections. In the case of P_f^{A-1}, for example, we use an experimental value $P_f^{A-1}(\text{exp})$ for excitation energies $E^* < B_n(A-1)$ and form the ratio of the experimental total fission cross section to the calculated compound nucleus cross section, both determined for the $n + (Z,A-2)$ scattering system, for excitation energies $E^* \geqq B_n(A-1)$.

As an example of the formulation given by Eqs. (38) through (52), we calculate the probabilities for first-, second-, third-chance, and total fission for the neutron-induced fission of ^{235}U. We perform these calculations utilizing the numerical integration techniques described in Sec. III. We consider incident neutron energies E_n ranging from 0.01 to 15 MeV. The values of $B_n(236)$, $B_n(235)$, and $B_n(234)$ used are obtained from Table I and are 6.546, 5.298, and 6.844 MeV, respectively. Experimental total fission probabilities for excitation energies less than $B_n(235)$ and $B_n(234)$ are obtained from Back et al.[74] and Back et al.,[75] respectively. All required compound nucleus cross sections are calculated with the Iteration 1 actinide optical model potential of Madland and Young.[76] This potential is a spherical approximation used in the development of a more accurate deformed coupled-channel optical potential for actinide nuclei. We use the simpler spherical approximation here in light of the other assumptions that we have made. The total fission cross section for neutrons incident on ^{235}U is that of the Evaluated Nuclear Data File[77] (ENDF/B-V). The total fission cross section of ^{235}U*, for excitation energies greater than $B_n(235)$, is obtained from the ratio measurement of Behrens and Carlson[78] for neutrons incident on ^{234}U. Similarly, the total fission cross section of ^{234}U*, for excitation energies greater than $B_n(234)$, is obtained from the ratio measurement of Carlson and Behrens[79] for neutrons incident on ^{233}U. In both cases the ratio measurement is converted to an absolute cross section using the total fission cross section of Ref. 77. For incident neutron energies of 15 MeV or less, the quantity $P_f^{A-3}(E^*) = P_f^{233}(E^*)$ in Eq. (43) is identically zero. Therefore, $D_3(E^*,\sigma_{c_3})$ need not be calculated in this case.

Our results are plotted in Fig. 36 and listed in Table IV. The tabulated probabilities include total uncertainties calculated by propagation of estimated errors in the quantities P_f^{236}, P_f^{235}, P_f^{234}, $\langle P_f^{235} \rangle$, and $\langle P_f^{234} \rangle$. We estimate 10% uncertainty in each of these five quantities for all values of the incident neutron energy. For purposes of clarity, we have not included the total uncertainties in Fig. 36 where there are two features that we wish to address. The first is that the agreement between the total fission probability calculated with Eq. (38) and the experimental fission probability, above the second-chance fission threshold, provides a consistency check on the method of calculation. The greatest discrepancy in this comparison is at 12.5 MeV where the calculated value is ~7% low. Thus, the overall consistency is reasonably good. However, there are two regions where the discrepancies are most apparent, namely, the 8-MeV region where there is a steep rise in the second-chance fission probability and the 13-MeV region where the third-chance fission probability is beginning to rise. Hence, threshold regions are the least accurately calculated using the approach given here. Second, the first-chance fission probability has a plateau in the region between 10 and 13 MeV. This arises because after its onset, the first-chance fission probability of the $(Z,A-1)$ nucleus is nearly constant until after the onset of second-chance fission for this nucleus is reached.

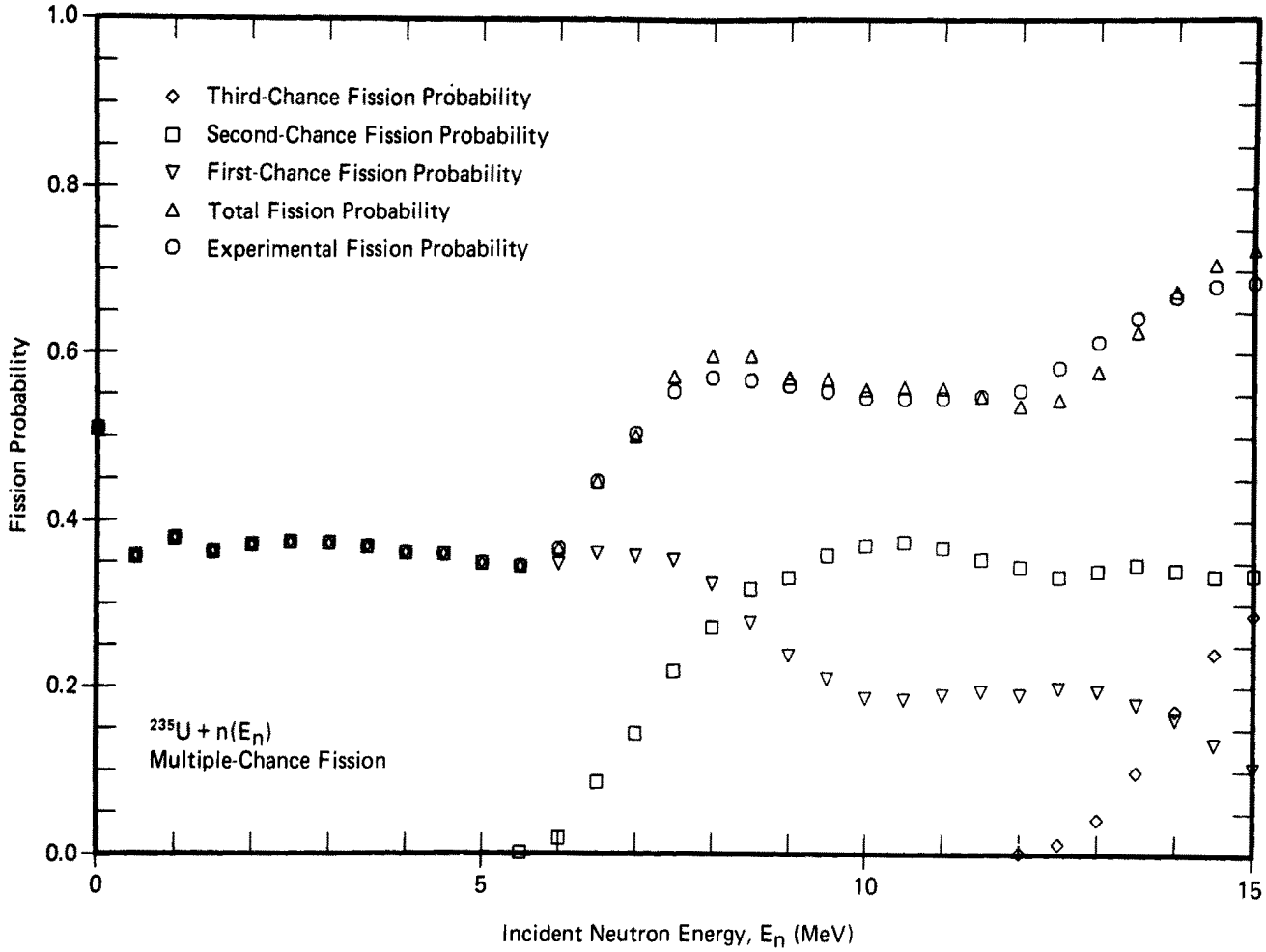

Fig. 36. Multiple-chance fission probabilities as a function of the incident neutron energy for the neutron-induced fission of ^{235}U. The third-, second-, first-chance, and total fission probabilities are calculated with Eqs. (47), (46), (45), and (38), respectively, using the calculational procedure and input quantities given in the text. The experimental fission probability is obtained by forming the ratio of the total fission cross section of Ref. 77 and the compound nucleus cross section calculated using the Iteration 1 optical model potential of Ref. 76. The values of the probabilities together with their estimated uncertainties are given in Table IV.

This results in a plateau, as can be seen from Eqs. (40) and (42).

In the remainder of Sec. VI, we use the fission probabilities $P_{f_1}^{236}$, $P_{f_2}^{236}$, and $P_{f_3}^{236}$ presented in Table IV to study the effects of multiple-chance fission on prompt fission neutron spectra and average prompt neutron multiplicities.

VI.B. Prompt Fission Neutron Spectra

We obtain the prompt fission neutron spectrum for neutron-induced, multiple-chance fission by construction, using the expression for the prompt fission neutron spectrum $N(E)$ due to first-chance fission, the expression for the evaporation spectrum $\phi(E)$ due to neutron emission prior to fission, and the multiple-chance fission probabilities $P_{f_i}^A$. The total prompt fission neutron spectrum due to first-, second-, and third-chance fission events is given in the laboratory system by

$$N(E) = \{P_{f_1}^A \bar{\nu}_{p_1} N_1(E) + P_{f_2}^A [\phi_1(E) + \bar{\nu}_{p_2} N_2(E)] + P_{f_3}^A [\phi_1(E) + \phi_2(E) + \bar{\nu}_{p_3} N_3(E)]\} / [P_{f_1}^A \bar{\nu}_{p_1} + P_{f_2}^A (1 + \bar{\nu}_{p_2}) + P_{f_3}^A (2 + \bar{\nu}_{p_3})] \ , \quad (53)$$

where E is the energy of the emitted neutron and A is the mass number of the fissioning compound nucleus. The first term of this equation is the first-chance fission component; the second and third terms are the second-chance fission component; and the fourth, fifth, and sixth terms are the third-chance fission component of the spectrum. The spectrum constructed in this way gives unit normalization when integrated from zero to infinity. The laboratory

TABLE IV

Fission Probabilities for the Neutron-Induced Fission of ^{235}U

E_n (MeV)	$P_{f_1}^{236}$	$P_{f_2}^{236}$	$P_{f_3}^{236}$	P_f^{236}	P_f^{236}(exp)
0.01	0.509 ± 0.051	---	---	0.509 ± 0.051	0.509 ± 0.051
0.5	0.357 ± 0.036	---	---	0.357 ± 0.036	0.357 ± 0.036
1.0	0.379 ± 0.038	---	---	0.379 ± 0.038	0.379 ± 0.038
1.5	0.363 ± 0.036	---	---	0.363 ± 0.036	0.363 ± 0.036
2.0	0.371 ± 0.037	---	---	0.371 ± 0.037	0.371 ± 0.037
2.5	0.374 ± 0.037	---	---	0.374 ± 0.037	0.374 ± 0.037
3.0	0.373 ± 0.037	---	---	0.373 ± 0.037	0.373 ± 0.037
3.5	0.369 ± 0.037	---	---	0.369 ± 0.037	0.369 ± 0.037
4.0	0.362 ± 0.036	---	---	0.362 ± 0.036	0.362 ± 0.036
4.5	0.361 ± 0.036	---	---	0.361 ± 0.036	0.361 ± 0.036
5.0	0.350 ± 0.035	---	---	0.350 ± 0.035	0.350 ± 0.035
5.5	0.345 ± 0.035	0.001[a] ± 0.0001[a]	---	0.346 ± 0.035	0.346 ± 0.035
6.0	0.349 ± 0.038	0.019 ± 0.002	---	0.367 ± 0.037	0.367 ± 0.037
6.5	0.361 ± 0.053	0.086 ± 0.011	---	0.447 ± 0.046	0.447 ± 0.045
7.0	0.358 ± 0.068	0.144 ± 0.021	---	0.501 ± 0.055	0.505 ± 0.050
7.5	0.353 ± 0.086	0.219 ± 0.036	---	0.572 ± 0.061	0.554 ± 0.055
8.0	0.324 ± 0.098	0.272 ± 0.048	---	0.597 ± 0.064	0.570 ± 0.057
8.5	0.278 ± 0.106	0.318 ± 0.057	---	0.596 ± 0.067	0.567 ± 0.057
9.0	0.238 ± 0.112	0.332 ± 0.059	---	0.570 ± 0.071	0.561 ± 0.056
9.5	0.210 ± 0.116	0.359 ± 0.064	---	0.569 ± 0.073	0.554 ± 0.055
10.0	0.186 ± 0.117	0.370 ± 0.065	---	0.556 ± 0.074	0.546 ± 0.055
10.5	0.185 ± 0.117	0.375 ± 0.066	---	0.559 ± 0.074	0.546 ± 0.055
11.0	0.190 ± 0.116	0.368 ± 0.064	---	0.558 ± 0.073	0.546 ± 0.055
11.5	0.195 ± 0.116	0.354 ± 0.062	---	0.549 ± 0.074	0.548 ± 0.055
12.0	0.191 ± 0.121	0.345 ± 0.062	0.002[b] ± 0.0003[b]	0.538 ± 0.077	0.556 ± 0.056
12.5	0.199 ± 0.134	0.333 ± 0.066	0.013 ± 0.003	0.545 ± 0.084	0.583 ± 0.058
13.0	0.195 ± 0.155	0.340 ± 0.078	0.042 ± 0.010	0.578 ± 0.090	0.614 ± 0.061
13.5	$0.180 \pm \frac{0.182}{0.180}$	0.348 ± 0.097	0.099 ± 0.027	0.627 ± 0.095	0.643 ± 0.064
14.0	$0.162 \pm \frac{0.212}{0.162}$	0.341 ± 0.120	0.172 ± 0.055	0.675 ± 0.100	0.669 ± 0.067
14.5	$0.132 \pm \frac{0.239}{0.132}$	0.335 ± 0.147	0.241 ± 0.087	0.708 ± 0.105	0.682 ± 0.068
15.0	$0.104 \pm \frac{0.257}{0.104}$	0.336 ± 0.171	0.287 ± 0.113	0.727 ± 0.108	0.686 ± 0.069

[a]To three significant figures the value is $(1.23 \pm 0.14) \times 10^{-3}$.
[b]To three significant figures the value is $(1.63 \pm 0.32) \times 10^{-3}$.

energy moments $\langle E^n \rangle$ of the spectrum are given by

$$\langle E^n \rangle = [P_{f_1}^A \bar{\nu}_{p_1} \langle E_1^n \rangle + P_{f_2}^A (\langle \mathscr{E}_1^n \rangle + \bar{\nu}_{p_2} \langle E_2^n \rangle) + P_{f_3}^A (\langle \mathscr{E}_1^n \rangle + \langle \mathscr{E}_2^n \rangle + \bar{\nu}_{p_3} \langle E_3^n \rangle)] / [P_{f_1}^A \bar{\nu}_{p_1} + P_{f_2}^A (1 + \bar{\nu}_{p_2}) + P_{f_3}^A (2 + \bar{\nu}_{p_3})] \quad . \tag{54}$$

We outline the solutions of Eqs. (53) and (54) for the case of energy-dependent cross sections to describe all inverse processes of compound nucleus formation. The first-, second-, and third-chance fission probabilities are given by Eqs. (45), (46), and (47), respectively. The average prompt neutron multiplicities $\bar{\nu}_{p_i}$ are calculated using Eq. (33) with values of the average center-of-mass neutron energy $\langle \epsilon_i \rangle$ that are obtained from Eq. (27). The prompt fission neutron spectra $N_i(E)$ and their energy moments $\langle E_i^n \rangle$ are calculated using Eqs. (24), (28), and (29). The neutron evaporation spectra $\phi_i(E,\sigma_{c_i})$ and their energy moments $\langle \mathscr{E}_i^n \rangle$ are obtained using Eq. (48). The total average fission-fragment excitation energy $\langle E_i^* \rangle$ is used in the calculation of both

$\bar{\nu}_{p_i}$ and the maximum temperature T_{m_i} of Eqs. (24), (27), (28), and (29). The value of $\langle E_1^* \rangle$ is given identically by Eq. (2) whereas $\langle E_2^* \rangle$ and $\langle E_3^* \rangle$ are given by

$$\langle E_2^* \rangle = \langle E_{r_2} \rangle + E_n - \langle \mathscr{E}_1 \rangle - \langle E_{f_2}^{\text{tot}} \rangle \tag{55}$$

and

$$\langle E_3^* \rangle = \langle E_{r_3} \rangle + E_n - \langle \mathscr{E}_1 \rangle - \langle \mathscr{E}_2 \rangle - B_n(A-1) - \langle E_{f_3}^{\text{tot}} \rangle \ . \tag{56}$$

The temperatures T_i used in the calculation of both P_{fi}^A and $\phi_i(E,\sigma_{c_i})$ are given in Eqs. (50c), (51c), and (52c). Finally, appropriate optical model potentials are required to calculate compound nucleus cross sections for the average light and heavy fission fragments associated with each $N_i(E)$ and for the actinide nucleus associated with each $\phi_i(E,\sigma_{c_i})$.

Using this procedure, we calculate the prompt fission neutron spectrum and its mean and mean-square energies for the fission of ^{235}U induced by 7- and 14-MeV neutrons. We use the multiple-chance fission probabilities of Table IV corresponding to 7 and 14 MeV, the appropriate quantities from Table I to calculate the constants appearing in the spectra, the optical model potential of Becchetti and Greenlees[30] to calculate average fission-fragment compound nucleus cross sections, and the Iteration 1 optical model potential of Madland and Young[76] to calculate actinide compound nucleus cross sections. The constants appearing in each individual spectrum of Eq. (53), the first and second energy moments of each of these spectra, and other quantities related to Eqs. (53) through (56) are given in Table V for the two values of the incident neutron energy.

Our results are presented in Figs. 37, 38, and 39 for 7-MeV neutron energy and in Figs. 40, 41, and 42 for 14-MeV neutron energy. The values of the mean and mean-square neutron energies for the two cases are contained in Table II. At 7 MeV the fission probabilities of Table IV and Fig. 36 show that ~71% of the fission events are first-chance fission, that ~29% are second-chance fission, and that third-chance fission is not energetically allowed. The contributions to the prompt fission neutron spectrum due to these proportions are shown in Fig. 37 together with their sum, the total multiple-chance fission spectrum. The figure shows that the

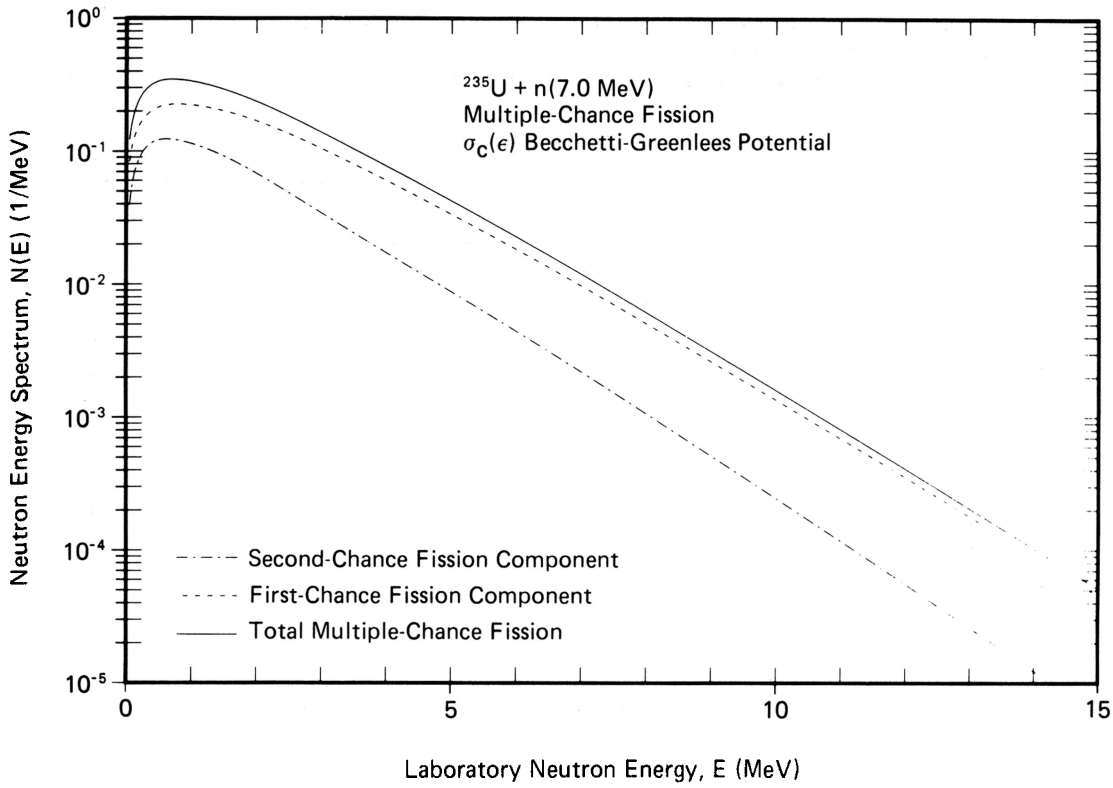

Fig. 37. Multiple-chance fission components of the prompt fission neutron spectrum in the laboratory system for the fission of ^{235}U induced by 7-MeV neutrons. The dot-dashed curve gives the second-chance fission component calculated with the second and third terms of Eq. (53). The dashed curve gives the first-chance fission component calculated with the first term of Eq. (53). The solid curve gives their sum, the total multiple-chance fission spectrum. The energy-dependent cross sections used in the calculation of $N_1(E)$ and $N_2(E)$ are obtained using the optical model potential of Becchetti and Greenlees (Ref. 30). The values of the constants appearing in the spectra are given in Table V.

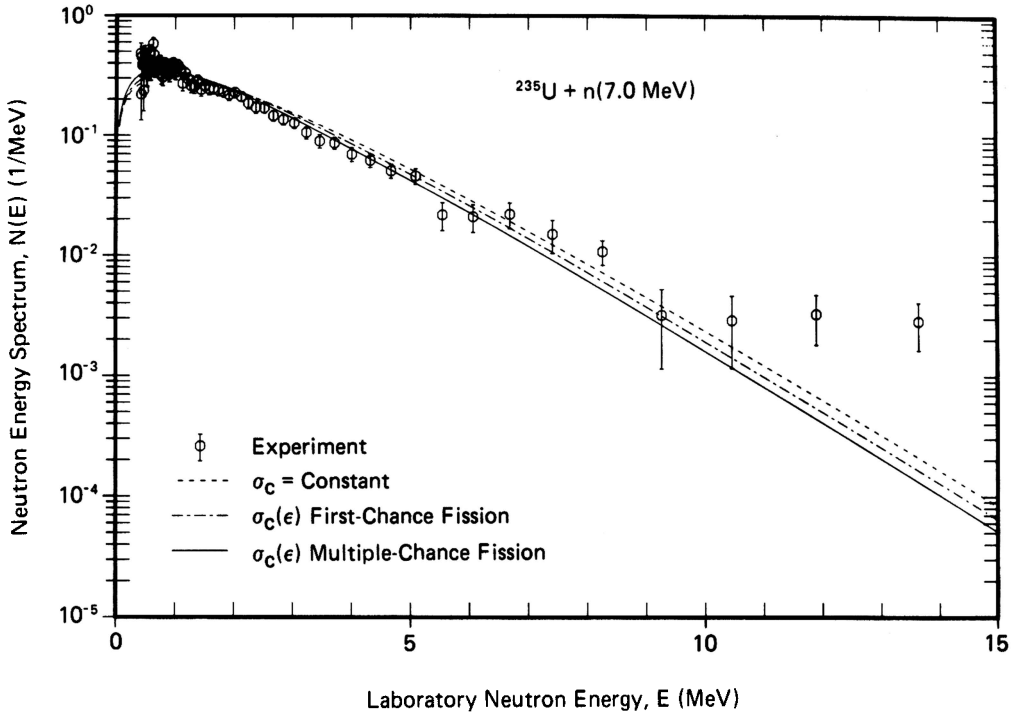

Fig. 38. Prompt fission neutron spectrum in the laboratory system for the fission of ^{235}U induced by 7-MeV neutrons. The dashed curve gives the spectrum calculated with Eq. (16) for a constant cross section assuming first-chance fission whereas the dot-dashed curve gives the spectrum calculated with Eq. (28) under the same assumption, but using energy-dependent cross sections. The solid curve gives the total multiple-chance fission spectrum calculated with Eq. (53) and is identical to the solid curve of Fig. 37. The energy-dependent cross sections used in the calculation of $N_1(E)$ and $N_2(E)$ are obtained using the optical model potential of Becchetti and Greenlees (Ref. 30). The values of the constants appearing in the spectra are given in Table V. The experimental data are those of Bertin et al. (Ref. 42), Frehaut et al. (Ref. 43), and Frehaut (Ref. 44), using the fission-chamber method.

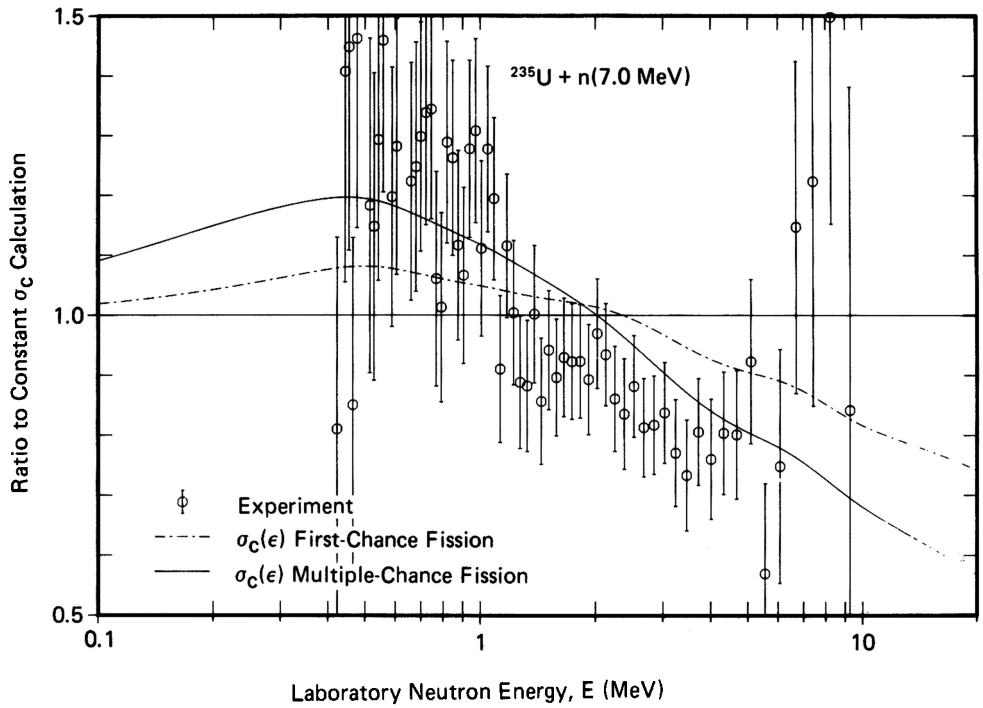

Fig. 39. Ratio of the total multiple-chance fission spectrum and the first-chance fission spectrum calculated using energy-dependent cross sections, and the experimental spectrum, to the first-chance fission spectrum calculated using a constant cross section, corresponding to the curves shown in Fig. 38. Note that some of the experimental ratios are off the scale of the graph.

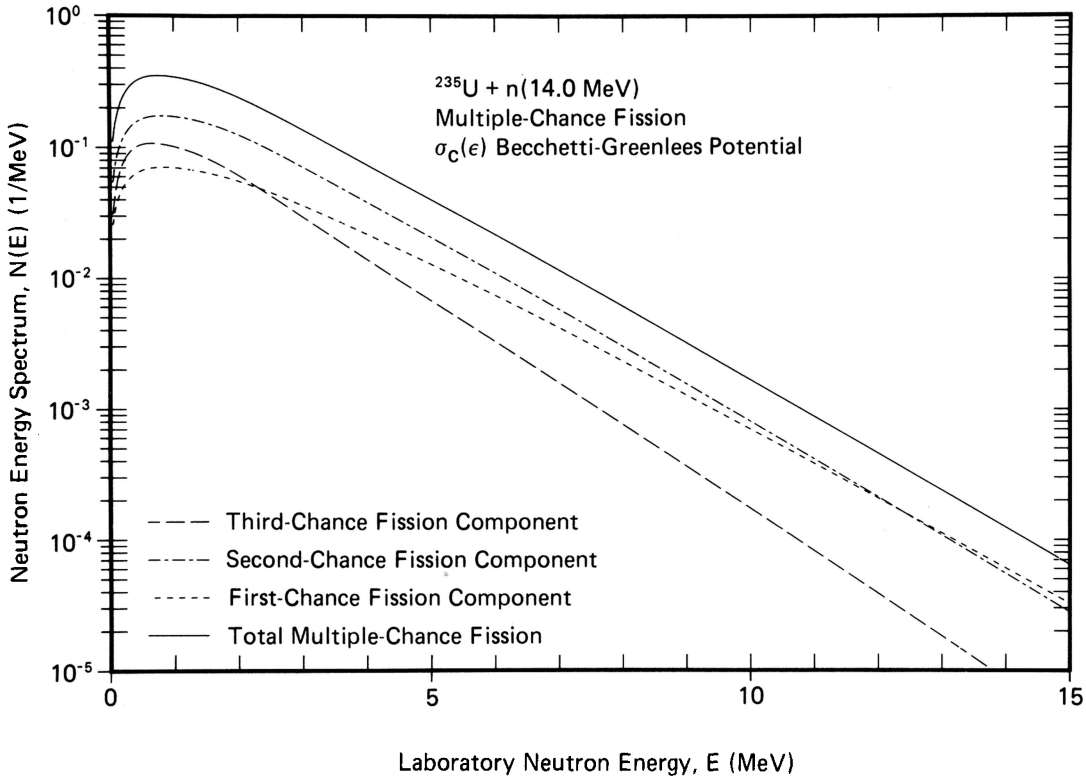

Fig. 40. Multiple-chance fission components of the prompt fission neutron spectrum in the laboratory system for the fission of ^{235}U induced by 14-MeV neutrons. The long-dashed curve gives the third-chance fission component calculated with the fourth, fifth, and sixth terms of Eq. (53). The dot-dashed curve gives the second-chance fission component calculated with the second and third terms of Eq. (53). The short-dashed curve gives the first-chance fission component calculated with the first term of Eq. (53). The solid curve gives their sum, the total multiple-chance fission spectrum. The energy-dependent cross sections used in the calculation of $N_1(E)$, $N_2(E)$, and $N_3(E)$ are obtained using the optical model potential of Becchetti and Greenlees (Ref. 30). The values of the constants appearing in the spectra are given in Table V.

first-chance fission component dominates the total spectrum, that the peak of the second-chance fission component is somewhat lower in energy than the peak of the first-chance fission component, and that the second-chance fission component decreases more rapidly with increasing energy than does the first-chance fission component. These latter two effects are due in part to the influence of the neutron evaporation spectrum $\phi_1(E,\sigma_{c_1})$ on the second-chance fission component. One therefore expects similar effects in the peak and tail regions of the total multiple-chance fission spectrum when compared to that calculated on the basis of first-chance fission alone.

This is shown in Figs. 38 and 39 where the total multiple-chance fission spectrum, which peaks at 710 keV, is compared to two fission spectra calculated on the basis of first-chance fission, namely, the constant cross-section calculation of Eq. (16), which peaks at 870 keV, and the energy-dependent cross-section calculation of Eq. (28), which peaks at 790 keV. The figures show that as one proceeds from the constant cross-section first-chance fission spectrum to the energy-dependent cross-section multiple-chance fission spectrum the peak shifts lower in energy, by 80-keV steps in this case, the tail region becomes softer, and the peak region becomes more enhanced. Consequently, the mean and mean-square laboratory neutron energies of the spectra shift lower in similar steps as shown by Table II. Perhaps the most illuminating comparison is between the energy-dependent cross-section first- and multiple-chance fission spectrum ratios shown in Fig. 39. The difference between the two ratio curves shows that the main effect of multiple-chance fission at 7-MeV incident neutron energy is to increase the number of emitted neutrons between ~100 keV and 2 MeV, by perhaps 10%, at the expense of decreasing the number of emitted neutrons above 2 MeV by the same amount.

We also show the experimental data of Bertin et al.,[42] Frehaut et al.,[43] and Frehaut[44] in Figs. 38 and 39. Bin-width corrections were applied to the data and a normalization was performed using the procedures given in Appendix B. It is clear from Fig. 38 that the agreement between theory and experiment is reasonable except in the region below ~0.6 MeV and in the region above ~10 MeV. For

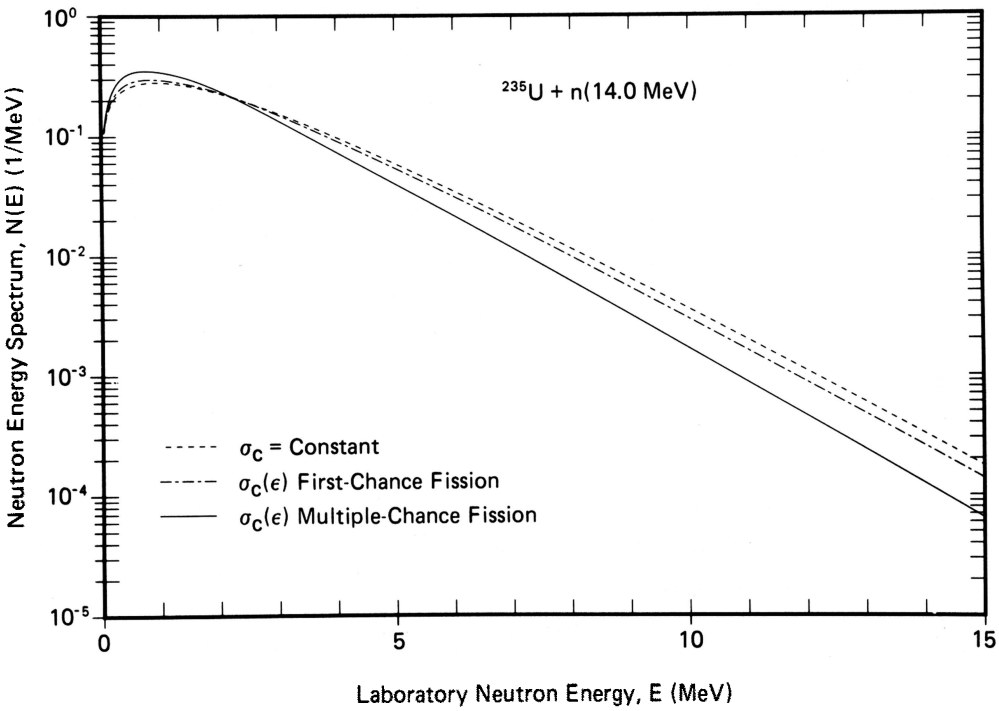

Fig. 41. Prompt fission neutron spectrum in the laboratory system for the fission of ^{235}U induced by 14-MeV neutrons. The dashed curve gives the spectrum calculated with Eq. (16) for a constant cross section assuming first-chance fission whereas the dot-dashed curve gives the spectrum calculated with Eq. (28) under the same assumption, but using energy-dependent cross sections. The solid curve gives the total multiple-chance fission spectrum calculated with Eq. (53) and is identical to the solid curve of Fig. 40. The energy-dependent cross sections used in the calculation of $N_1(E)$, $N_2(E)$, and $N_3(E)$ are obtained using the optical model potential of Becchetti and Greenlees (Ref. 30). The values of the constants appearing in the spectra are given in Table V.

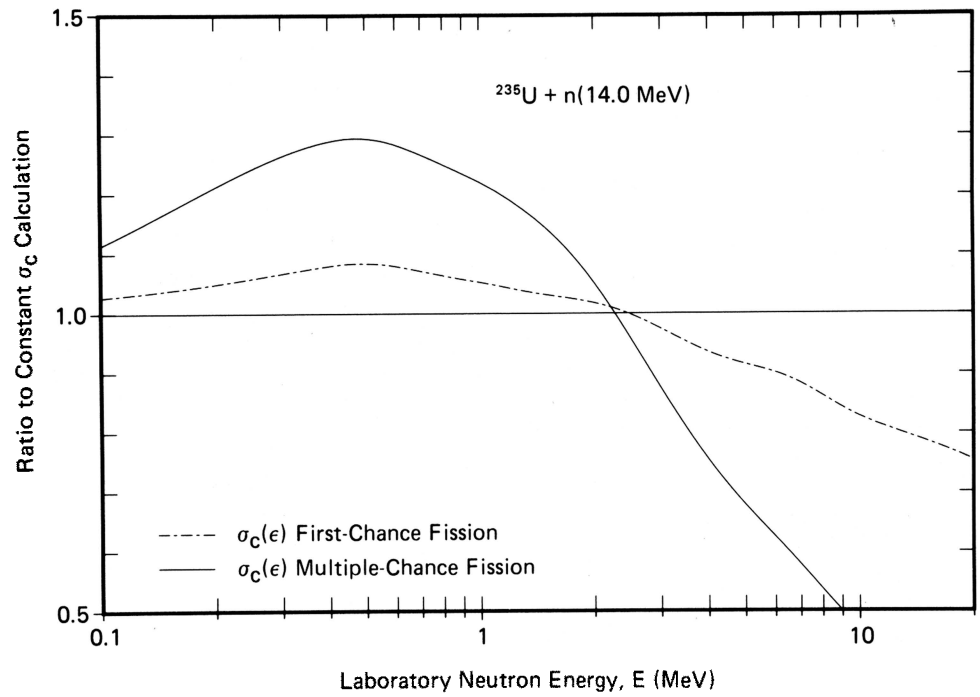

Fig. 42. Ratio of the total multiple-chance fission spectrum and the first-chance fission spectrum calculated using energy-dependent cross sections to the first-chance fission spectrum calculated using a constant cross section, corresponding to the curves shown in Fig. 41.

TABLE V

Quantities Used in Calculating the Multiple-Chance Fission Components of the Prompt Fission Neutron Spectrum, the Mean and Mean-Square Energies of the Spectrum, and the Average Prompt Neutron Multiplicities for the Neutron-Induced Fission of ^{235}U at 7 and 14 MeV*

Quantity	E_n = 7 MeV	E_n = 14 MeV
$E_{f_1}^L$	1.062	1.062
$E_{f_1}^H$	0.499	0.499
T_{m_1}	1.157	1.290
$\langle\epsilon_1\rangle$	1.439	1.606
$\langle E_1\rangle$	2.219	2.386
$\langle E_1^2\rangle$	7.999	9.307
$\bar{\nu}_{p_1}$	3.420	4.394
T_1	0.571	0.808
$\langle\mathscr{E}_1\rangle$	1.145	1.606
$\langle\mathscr{E}_1^2\rangle$	1.958	3.835
$E_{f_2}^L$	1.059	1.059
$E_{f_2}^H$	0.505	0.505
T_{m_2}	1.034	1.173
$\langle\epsilon_2\rangle$	1.285	1.459
$\langle E_2\rangle$	2.068	2.241
$\langle E_2^2\rangle$	6.888	8.162
$\bar{\nu}_{p_2}$	2.514	3.437
T_2	---	0.576
$\langle\mathscr{E}_2\rangle$	---	1.155
$\langle\mathscr{E}_2^2\rangle$	---	1.994
$E_{f_3}^L$	---	1.076
$E_{f_3}^H$	---	0.503
T_{m_3}	---	1.036
$\langle\epsilon_3\rangle$	---	1.287
$\langle E_3\rangle$	---	2.076
$\langle E_3^2\rangle$	---	6.946
$\bar{\nu}_{p_3}$	---	2.457

*Energies and temperatures are expressed in units of million electron volts (MeV).

the latter region, the experimentalists give the same comment as for their 0.60-MeV data discussed in Sec. IV.B. On the basis of Fig. 38, it is not possible to determine which theoretical spectrum is preferred. However, the trend of the experimental data in the ratio plot of Fig. 39 is clearly more supportive of the multiple-chance fission calculation.

The calculations at 14-MeV incident neutron energy are shown in Figs. 40, 41, and 42. In this case the fission probabilities of Table IV and Fig. 36 show that ~24% of the fission events are first-chance fission, that ~51% are second-chance fission, and that ~25% are third-chance fission. The contributions to the prompt fission neutron spectrum due to these proportions are shown in Fig. 40 together with their sum, the total multiple-chance fission spectrum. The figure shows that the second-chance fission component dominates the total spectrum and that although there are approximately equal numbers of first- and third-chance fission events, the third-chance fission component is much softer than the first-chance fission component. This is, in part, due to the presence of two neutron evaporation spectra, $\phi_1(E,\sigma_{c_1})$ and $\phi_2(E,\sigma_{c_2})$, in the third-chance fission component. As expected, the peaks of the second- and third-chance fission components are at lower energies than the peak of the first-chance fission component, which is also the hardest of the three component spectra in the tail region.

Again, we study the effects of the multiple-chance fission components by comparing the total multiple-chance fission spectrum to that calculated on the basis of first-chance fission alone. This comparison is made in Figs. 41 and 42 and is analogous to that made in Figs. 38 and 39 for 7-MeV incident neutron energy. In Figs. 41 and 42 the constant cross-section and energy-dependent cross-section first-chance fission calculations peak at 920 and 830 keV, respectively, whereas the energy-dependent cross-section, multiple-chance fission calculation peaks at 750 keV. Thus, the spectrum peak shifts lower, in average steps of 85 keV in this case, for each added physical effect. The net decrease in the mean and mean-square laboratory neutron energies is more significant being 420 keV and 2995 keV^2, respectively. In fact, Table II shows that the difference between the mean and mean-square laboratory energies for the 14-MeV neutron-induced fission and the 0.53-MeV neutron-induced fission of ^{235}U are only 35 keV and 425 keV^2, respectively, when energy-dependent cross sections and multiple-chance fission are taken into account. Moreover, the mean and mean-square laboratory neutron energies are slightly less for 14-MeV incident neutrons than they are for 7-MeV neutrons, the differences being 17 keV and 101 keV^2, respectively. This is because second-chance fission dominates the 14-MeV case whereas first-chance fission dominates the 7-MeV case.

The comparison between the energy-dependent cross-section first- and multiple-chance fission spectrum ratios of Fig. 42 shows, again, that the main effect of multiple-chance fission is to increase the number of low-energy neutrons emitted at the expense of the number of high-energy neutrons.

The figure shows that at 14-MeV incident neutron energy there are perhaps 20% more neutrons emitted with energies between ~100 keV and 2 MeV for the multiple-chance fission calculation.

We note in concluding this section that Table II also contains the mean and mean-square center-of-mass neutron energies $\langle\epsilon\rangle$ and $\langle\epsilon^2\rangle$ calculated for multiple-chance fission. These are calculated with an equation that is entirely analogous to Eq. (54) for the laboratory energy moments. Their behavior is somewhat different than that of the corresponding laboratory moments because the center-of-mass moments $\langle\epsilon_i^n\rangle$ are similar in magnitude to the moments $\langle\mathcal{E}_i^n\rangle$ of each contributing neutron evaporation spectrum, whereas the laboratory moments $\langle E_i^n\rangle$ are generally larger and therefore tend to dominate more. Thus, the mean center-of-mass neutron energy $\langle\epsilon\rangle$ for the fission of ^{235}U induced by 14-MeV neutrons is significantly larger than that due to 0.53-MeV neutrons whereas the mean laboratory neutron energies $\langle E\rangle$ are quite similar, when energy-dependent cross sections and multiple-chance fission are taken into account. Physically, the larger value of $\langle\epsilon\rangle$ at 14 MeV is due to the large amount of excitation energy available for neutron emission prior to fission in the compound nucleus ^{236}U. While these evaporation neutrons have the effect of raising $\langle\epsilon\rangle$, they have the opposite effect of lowering $\langle E\rangle$ because they are emitted from a stationary nucleus as opposed to a fast moving fission fragment.

VI.C. Average Prompt Neutron Multiplicities

We obtain the average prompt neutron multiplicity for neutron-induced multiple-chance fission by construction, using the expression for the average prompt neutron multiplicity $\bar{\nu}_p$ due to first-chance fission and the multiple-chance fission probabilities $P_{f_i}^A$. The total average prompt neutron multiplicity due to first-, second-, and third-chance fission events is given by

$$\bar{\nu}_p = [P_{f_1}^A \bar{\nu}_{p_1} + P_{f_2}^A(1 + \bar{\nu}_{p_2}) + P_{f_3}^A(2 + \bar{\nu}_{p_3})]/(P_{f_1}^A + P_{f_2}^A + P_{f_3}^A) \ , \qquad (57)$$

where A is the mass number of the fissioning compound nucleus. The first term of this equation is the first-chance fission component; the second and third terms are the second-chance fission component; and the fourth and fifth terms are the third-chance fission component of the total average multiplicity.

We outline the solution of Eq. (57) as a function of the incident neutron energy E_n for the case of energy-dependent cross sections to describe all inverse processes of compound nucleus formation. The first-, second-, and third-chance fission probabilities are given as a function of the incident neutron energy by Eqs. (45), (46), and (47), respectively. The average prompt neutron multiplicities $\bar{\nu}_{p_i}$ are calculated as a function of the incident neutron energy using Eq. (33). In this equation the value of the total average fission-fragment excitation energy $\langle E_i^*\rangle$ is given by Eqs. (2), (55), and (56) for first-, second-, and third-chance fission, respectively. The value of the average center-of-mass neutron energy $\langle\epsilon_i\rangle$ used in Eq. (33) is calculated as a function of incident neutron energy using Eq. (27) wherein the maximum temperature T_{m_i} is determined using Eqs. (2), (55), and (56) for first-, second-, and third-chance fission, respectively. Finally, an appropriate optical model potential is required to calculate compound nucleus cross sections for the average light and heavy fission fragments associated with the calculation of each $\langle\epsilon_i\rangle$.

Using this procedure we calculate the average prompt neutron multiplicity for the neutron-induced fission of ^{235}U with incident neutron energies ranging from 0 to 15 MeV. We use the multiple-chance fission probabilities of Table IV, the appropriate quantities from Table I, and the optical model potential of Becchetti and Greenlees.[30] The values of the total average prompt gamma energy $\langle E_\gamma^{\text{tot}}\rangle$ and the average fission-fragment neutron separation energy $\langle S_n\rangle$ required in Eq. (33) are given in Sec. V.B except for the excited fissioning nucleus ^{235}U* for which they are 6.67 and 5.151 MeV, respectively, from the references given in Sec. V.A. Note that the evaluation of Eq. (57) can be carried out for neutron energies of 7 and 14 MeV by direct use of Tables IV and V.

Our results are presented in Fig. 43 where the 0- through 6-MeV region has already been discussed in Fig. 32 of Sec. V.B. In the multiple-chance fission region beginning near 5.5 MeV, the agreement of both the first- and multiple-chance fission calculations with experiment is very good, being of the order of 1%. This is better agreement than expected based on the simplifying assumptions that have been made. The multiple-chance fission calculation introduces a smooth upward step at the second-chance fission threshold near 5.5 MeV and a very slight dip at the third-chance fission threshold near 12 MeV, relative to the smoother first-chance fission calculation. On the basis of our calculations, therefore, it appears that multiple-chance fission processes introduce only slight structure into the variation of the average prompt neutron multiplicity with incident neutron energy.

VII. SIMULATED ENERGY DEPENDENCE OF THE COMPOUND NUCLEUS CROSS SECTION

For computational ease we present in this section an approximate way to simulate the energy dependence of the compound nucleus cross section $\sigma_c(\epsilon)$.

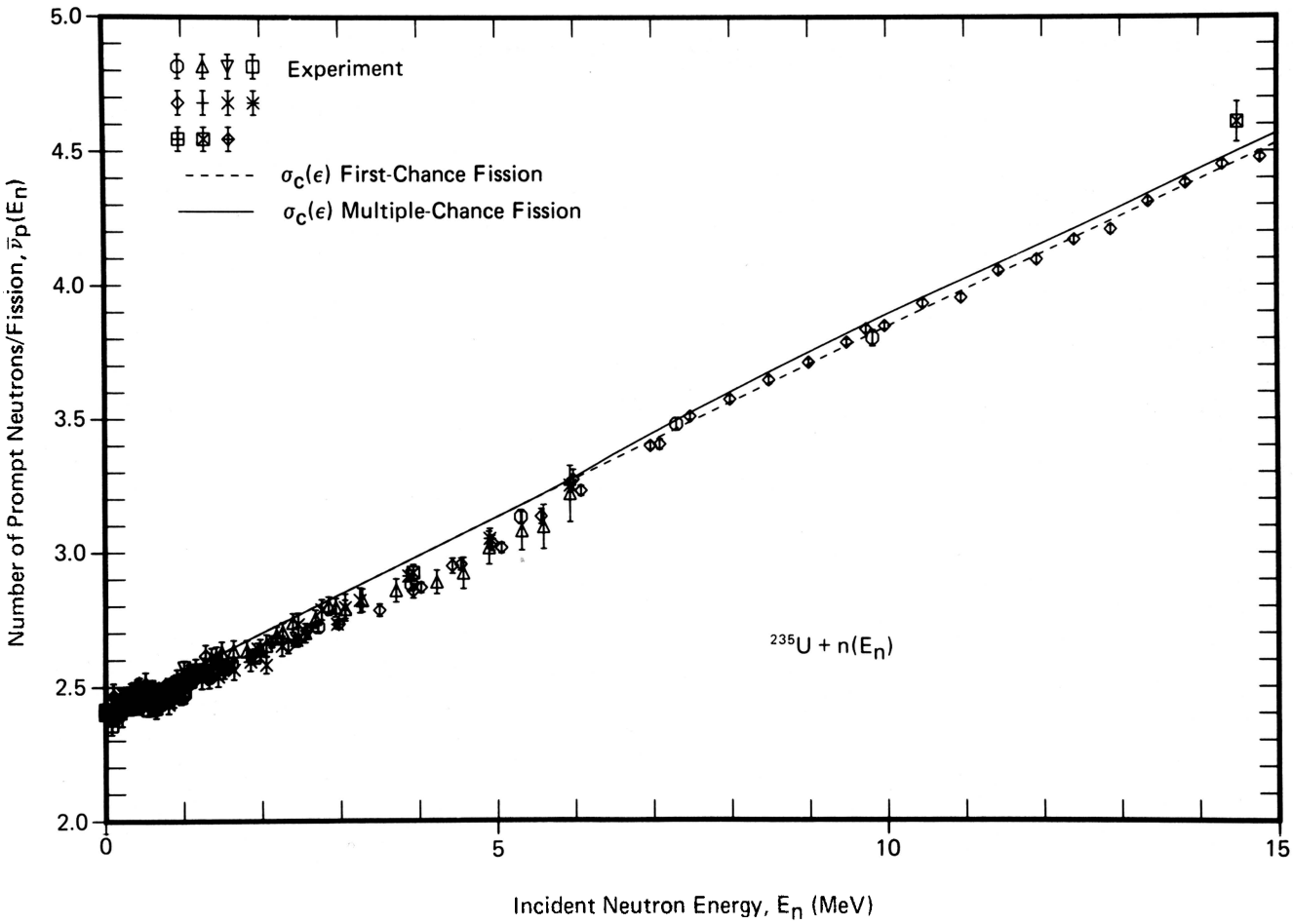

Fig. 43. Average prompt neutron multiplicity as a function of the incident neutron energy for the neutron-induced fission of ^{235}U. The dashed curve gives the multiplicity calculated with Eq. (33) assuming first-chance fission whereas the solid curve gives the multiplicity calculated with Eq. (57) assuming multiple-chance fission. In both cases, the optical model potential of Becchetti and Greenlees (Ref. 30) is used to determine the center-of-mass average energies used in the equations. The portion of the dashed curve between 0 and 6 MeV is identical to the solid curve of Fig. 32, and the experimental data symbols and references of Fig. 32 apply also to this figure. Note the suppressed zero of the vertical scale.

We perform the simulation through a slight readjustment of the nuclear level density parameter a which is described in the present work by Eq. (5). The simulation allows the prompt fission neutron spectrum $N(E)$ and the average prompt neutron multiplicity $\bar{\nu}_p$ to be expressed in closed form and therefore easily calculated on most modern computers. Moreover, the integral of $N(E)$ over an arbitrary energy interval can then be directly calculated using the expression given in Appendix A.

VII.A. Prompt Fission Neutron Spectra

An inspection of Figs. 21 through 30 shows that in every case the constant cross-section spectrum given by Eq. (16) is higher in the tail region than the more nearly exact energy-dependent cross-section calculation given by Eq. (28). Since the behavior of the tail region is largely determined by the value of the maximum temperature T_m, a slight readjustment of this quantity should bring the calculation of Eq. (16) into closer agreement with that of Eq. (28), thereby simulating the energy dependence of the cross section $\sigma_c(\epsilon)$.

We have already discussed the dependence of the tail region of the spectrum on the magnitude of T_m in Sec. II.D, where the sensitivity to slight changes in the total average fission-fragment kinetic energy $\langle E^* \rangle$ and the nuclear level density parameter a is shown in Figs. 9 and 10. Since the average prompt neutron multiplicity $\bar{\nu}_p$ depends strongly on $\langle E^* \rangle$ and only weakly on a, we conclude that the adjustment of T_m is best accomplished by a slight readjustment of the nuclear level density parameter given by Eq. (5).

One method of adjusting the level density parameter is to equate the first moment or mean energy of the constant cross-section spectrum to that of

the more nearly exact energy-dependent cross-section spectrum. Using Eqs. (4), (17), and (29), we obtain for the effective level density parameter

$$a_{\text{eff}} = \frac{16\langle E^* \rangle}{9\left[\langle E \rangle - \frac{1}{2}(E_f^L + E_f^H)\right]^2} , \quad (58)$$

where $\langle E \rangle$ is the first moment of the energy-dependent cross-section spectrum obtained by numerical integration of Eq. (29). The quantities $\langle E^* \rangle$, E_f^L, and E_f^H are given by Eqs. (2), (14), and (15), respectively. Applying this method to the case of the fission of ^{235}U induced by 0.53-MeV neutrons and converting the result to the form of Eq. (5) gives $a_{\text{eff}} = A/(9.548\ \text{MeV})$. Similarly, applying the method to the spontaneous fission of ^{252}Cf and converting the result to the form of Eq. (5) gives $a_{\text{eff}} = A/(9.655\ \text{MeV})$. For the former case, we compare in Figs. 44 and 45 the simulated energy-dependence spectrum calculated with Eq. (16) using $a_{\text{eff}} = A/(9.548\ \text{MeV})$ to the exact energy-dependent cross-section spectrum calculated with Eq. (28) using the value of a given by Eq. (5). If the simulation were perfect, the dashed and solid curves of Fig. 44 would be coincident and the solid curve of Fig. 45 would have unit value. As Fig. 45 shows, the simulation is good to within 5% for energies up to ~7 MeV, to within 10% for energies up to ~9 MeV, and to within 25% for energies up to ~12 MeV. For the latter case of the spontaneous fission of ^{252}Cf, similar results are obtained by using the value $a_{\text{eff}} = A/(9.655\ \text{MeV})$. Thus, the method of equal first moments gives a reasonable simulation of the effects of the energy-dependent cross sections. Moreover, the denominator of the readjusted level density model is quite similar for two cases that are widely spaced in actinide mass number, being 9.548 MeV for $A = 236$ and 9.655 MeV for $A = 252$.

Applying the same method, but instead equating second moments or mean-square energies improves the agreement between simulated energy-dependence spectra and exact spectra at high neutron energy. The improvements, however, are slight. In this case the denominator of the readjusted level density parameter is 9.677 MeV for $A = 236$ and 9.818 MeV for $A = 252$. These values represent increases of ~1.5% over those obtained in the method of equal first moments. Use instead of third or higher moments, where greater emphasis is placed on the tail of the spectrum, would increase the denominator of the readjusted level density parameter still further. Accordingly, we choose the convenient value 10 MeV as a reasonable compromise, which gives

$$a_{\text{eff}} = A/(10\ \text{MeV}) . \quad (59)$$

Applying this result to the fission of ^{235}U induced by 0.53-MeV neutrons, we compare in Figs. 46 and 47 the simulated spectrum calculated with Eq. (16) using $a_{\text{eff}} = A/(10\ \text{MeV})$ to the exact spectrum calculated with Eq. (28) using the value of a given by Eq. (5). The figures clearly demonstrate the improvement given by Eq. (59), especially at higher energy. Figure 47 shows that the simulation is good to within 5% for energies up to ~12 MeV, to within 10% for energies up to ~14 MeV, and to within 25% for energies up to ~18 MeV. Similar results are obtained using Eq. (59) in other fission reactions as shown in Table VI where we present the mean and mean-square energies of prompt fission neutron spectra obtained by simulating the energy dependence in this way. Each entry in Table VI is

TABLE VI

Mean and Mean-Square Energies of Calculated Prompt Fission Neutron Spectra Obtained by Simulation of the Energy Dependence of $\sigma_c(\epsilon)$

Fission Reaction	$\sigma_c(\epsilon)$	Center-of-Mass System		Laboratory System	
		$\langle \epsilon \rangle$ (MeV)	$\langle \epsilon^2 \rangle$ (MeV^2)	$\langle E \rangle$ (MeV)	$\langle E^2 \rangle$ (MeV^2)
^{235}U + n(0.53 MeV)	Constant[a]	1.295	2.829	2.075	6.885
^{235}U + n(0.60 MeV)	Constant	1.297	2.838	2.077	6.900
^{239}Pu + n(0.53 MeV)	Constant	1.443	3.515	2.223	7.940
^{252}Cf(sf)	Constant	1.537	3.989	2.306	8.564
^{235}U + n(7.0 MeV)[b]	Constant	1.471	3.652	2.251	8.166
^{235}U + n(14.0 MeV)[b]	Constant	1.640	4.541	2.421	9.497

[a]The constant cross section replaces the energy-dependent cross section by use of the effective level density parameter $a_{\text{eff}} = A/(10\ \text{MeV})$ to simulate the energy dependence.

[b]Calculated assuming first-chance fission only.

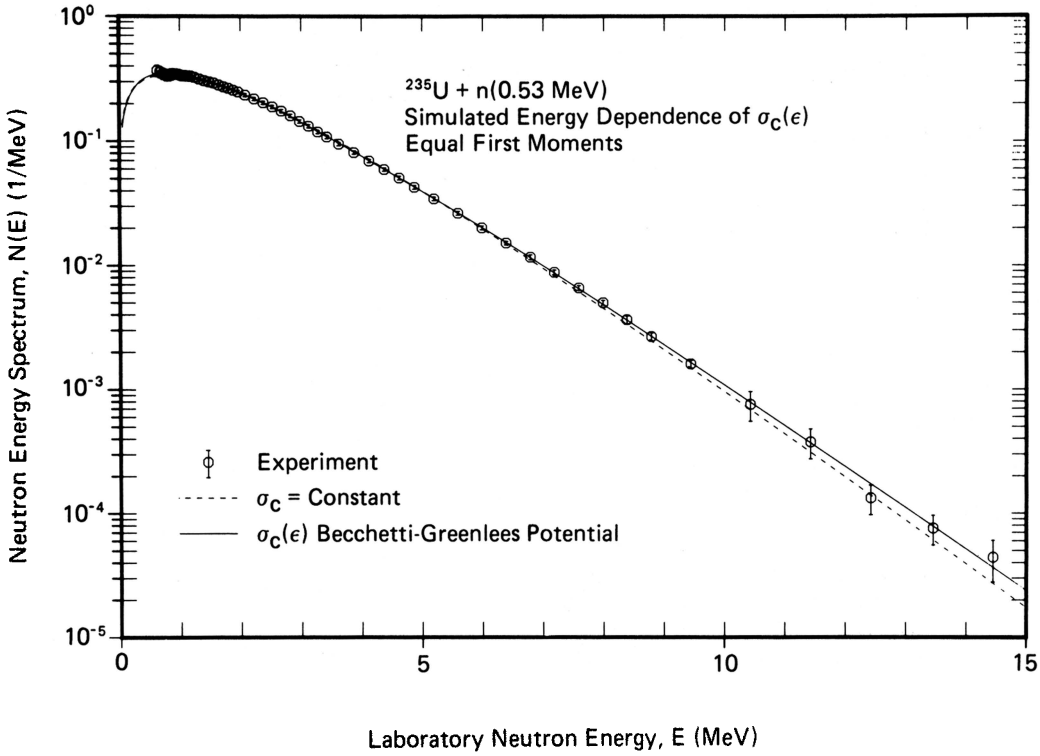

Fig. 44. Prompt fission neutron spectrum in the laboratory system for the fission of ^{235}U induced by 0.53-MeV neutrons, illustrating the simulated energy dependence of $\sigma_c(\epsilon)$. The two calculated spectra are identical to those of Fig. 21 except that the level density parameter used in the constant cross-section calculation, shown by the dashed curve, is given by Eq. (58) instead of Eq. (5). The values of the constants appearing in the calculated spectra are given in the caption to Fig. 21 except that T_m = 0.949 MeV for the constant cross-section calculation. The experimental data are those of Johansson and Holmqvist (Ref. 31).

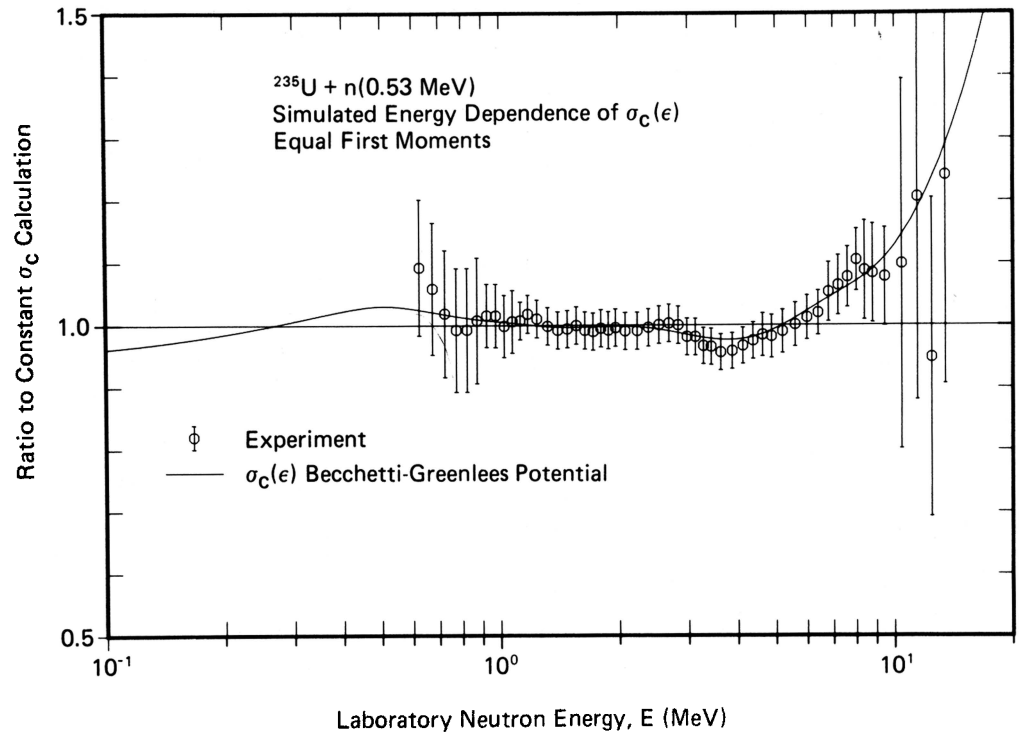

Fig. 45. Ratio of the spectrum calculated using energy-dependent cross sections and the experimental spectrum to the spectrum calculated using a constant cross section, corresponding to the curves shown in Fig. 44.

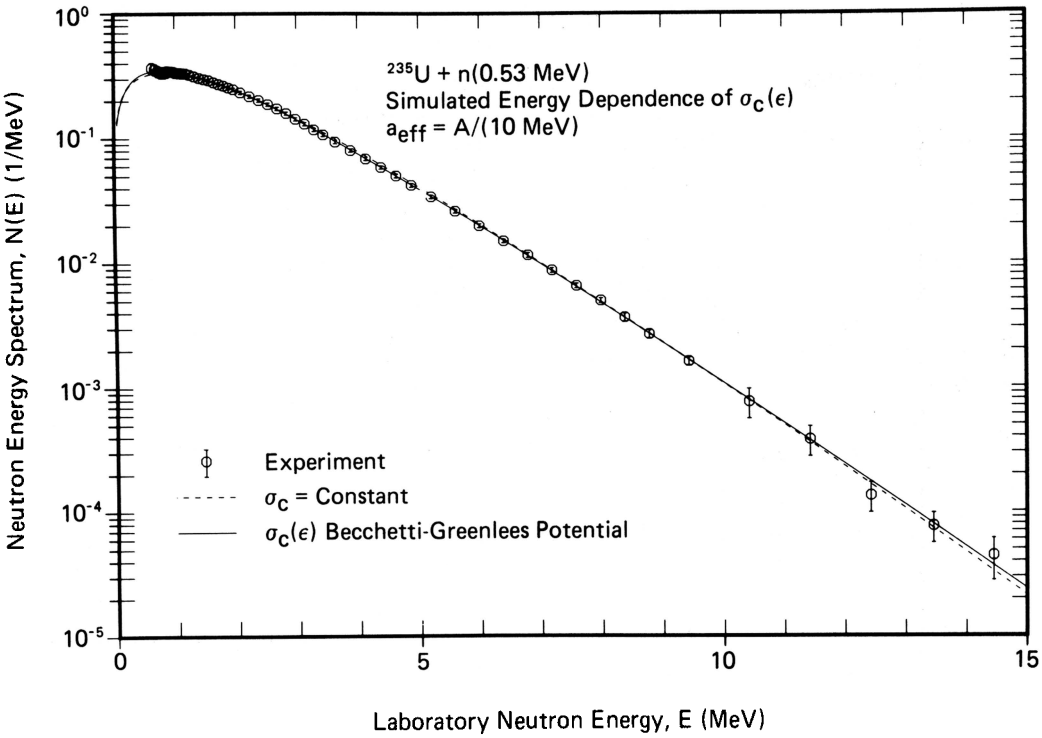

Fig. 46. Prompt fission neutron spectrum in the laboratory system for the fission of ^{235}U induced by 0.53-MeV neutrons, illustrating the simulated energy dependence of $\sigma_c(\epsilon)$. The two calculated spectra are identical to those of Fig. 21 except that the level density parameter used in the constant cross-section calculation, shown by the dashed curve, is given by Eq. (59) instead of Eq. (5). The values of the constants appearing in the calculated spectra are given in the caption to Fig. 21 except that T_m = 0.971 MeV for the constant cross-section calculation. The experimental data are those of Johansson and Holmqvist (Ref. 31).

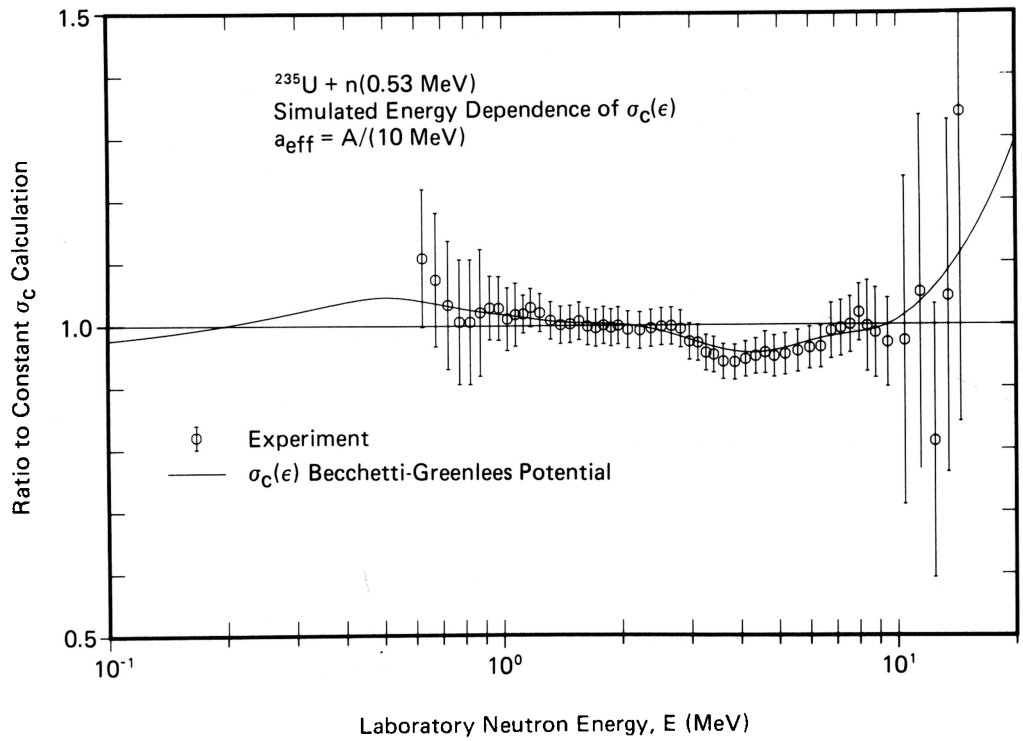

Fig. 47. Ratio of the spectrum calculated using energy-dependent cross sections and the experimental spectrum to the spectrum calculated using a constant cross section, corresponding to the curves shown in Fig. 46.

to be compared with its corresponding entry in Table II determined using energy-dependent cross sections. When this comparison is made for the mean center-of-mass energy $\langle\epsilon\rangle$ and the mean laboratory energy $\langle E\rangle$, for example, one finds on the average only a 30-keV difference between the two tables. We conclude that the most accurate simulation of the energy-dependent cross section $\sigma_c(\epsilon)$ is obtained using the readjusted level density parameter given by Eq. (59). We note that the multiple-chance fission calculations of Sec. VI would be greatly simplified by use of the simulated energy-dependence approach given here.

VII.B. Average Prompt Neutron Multiplicities

The average prompt neutron multiplicity $\bar{\nu}_p$ is only slightly dependent on the nuclear level density parameter as Eq. (33) shows. The average center-of-mass energy $\langle\epsilon\rangle$, given by the numerical integration of Eq. (27), is the only quantity in the equation that depends on the level density parameter and the energy-dependent cross sections $\sigma_c(\epsilon)$. We show in this section the effects on $\bar{\nu}_p$ due to the replacement of Eq. (27) by Eq. (8), namely, $\langle\epsilon\rangle = (4/3)T_m$. We evaluate Eq. (8) using the results of Sec. VII.A for the simulation of the energy dependence of $\sigma_c(\epsilon)$.

By way of example, we show in Fig. 48 the average prompt neutron multiplicity as a function of the incident neutron energy for the neutron-induced fission of ^{235}U. The dot-dashed and dashed curves give the simulated energy-dependence calculations which are to be compared to the solid curve for the exact calculation. By construction, the dot-dashed curve and solid curve are equal at incident neutron energy E_n = 0.53 MeV. The differences

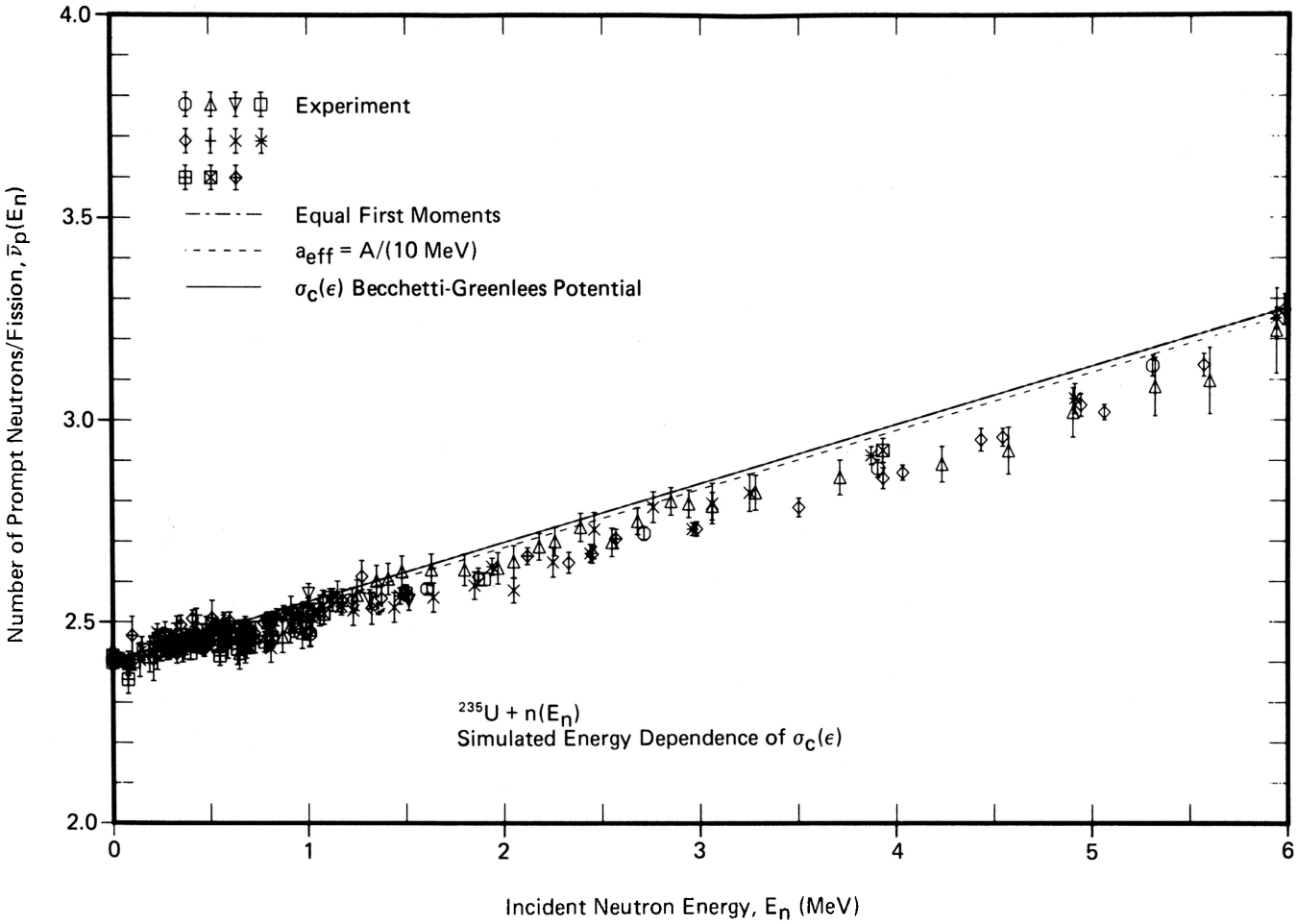

Fig. 48. Average prompt neutron multiplicity as a function of the incident neutron energy for the neutron-induced fission of ^{235}U illustrating the simulated energy dependence of $\sigma_c(\epsilon)$. The dot-dashed and dashed curves are calculated with Eq. (33) except that the average center-of-mass energy $\langle\epsilon\rangle$ is replaced by $(4/3)T_m$, where T_m is calculated using $a_{\text{eff}} = A/(9.548\text{ MeV})$ for the dot-dashed curve and $a_{\text{eff}} = A/(10\text{ MeV})$ for the dashed curve. The solid curve and the experimental data are identical to those of Fig. 32.

between the three curves are very small showing that the approximate Eq. (8) is as good as the exact Eq. (27) for the purpose of calculating $\bar{\nu}_p$. Based on the results of Sec. VII.A, we use Eq. (59) in the remainder of this section.

Table VII summarizes our results for the calculation of $\bar{\nu}_p$ in five cases of neutron-induced fission and one spontaneous fission case. Each entry of the table has a corresponding entry in Table III where the exact energy-dependent cross-section calculations are presented. A comparison of the two tables shows that in every case the difference between the two calculated values is approximately one unit in the second decimal place, that is, ~0.3%. We conclude that $\bar{\nu}_p$ can be accurately calculated in closed form by using Eqs. (8) and (59).

VIII. CONCLUSIONS

We have calculated the prompt fission neutron spectrum $N(E)$ and average prompt neutron multiplicity $\bar{\nu}_p$ as functions of the fissioning nucleus and its excitation energy by using conventional nuclear physics concepts and certain well-measured, fission-related quantities. We have shown that $N(E)$ and $\bar{\nu}_p$ can be accurately predicted to within a few percent for a single choice of the nuclear level density parameter and without the use of any further adjustable parameters. We have found that it is necessary to take into account the facts that fission fragments are formed with a distribution of excitation energy and that the inverse process of compound nucleus formation is energy dependent. We have learned that it is essential to calculate $N(E)$ and $\bar{\nu}_p$ simultaneously to ensure accurate results. We have shown that the dependence of $\bar{\nu}_p$ on incident neutron energy is not strictly linear as is almost always assumed, but that the dependence is somewhat weaker than a linear assumption. Using a method to extract multiple-chance fission probabilities from total fission cross-section measurements, we have determined that at high excitation of the fissioning nucleus, multiple-chance fission processes must be included in the calculation of $N(E)$ but that they have only a slight effect on $\bar{\nu}_p$. Finally, we have developed a method by which our exact calculations involving numerical integrations can be simulated with closed-form expressions, which simplifies enormously the application of our approach to practical problems.

Certain additional studies are suggested by the present work. These include an improved calculation of the average fission energy release $\langle E_r \rangle$, the use of a more realistic form of the fission-fragment nuclear temperature distribution $P(T)$ than the triangular form presently used, and the relaxation of the assumption that, on the average, equal numbers of neutrons are emitted by the light and heavy fragment groups. However, even in its present form, the approach described here can be used to predict accurately the prompt fission neutron spectrum and average prompt fission neutron multiplicity as functions of both the fissioning nucleus and its excitation energy. We hope that in the coming years its use leads to improved results in calculations of the complex physical processes occurring in practical nuclear applications.

TABLE VII

Average Prompt Neutron Multiplicities Obtained by Simulation of the Energy Dependence of $\sigma_c(\epsilon)$

A. Neutron-Induced Fission $\bar{\nu}_p(E_n)$				
Fission Reaction	$\sigma_c(\epsilon)$	$\bar{\nu}_p(0)$	$\bar{\nu}_p$(3 MeV)	$\bar{\nu}_p$(6 MeV)
$^{233}U + n$	Constant[a]	2.573	2.990	3.398
$^{235}U + n$	Constant	2.392	2.831	3.262
$^{238}U + n$	Constant	2.338	2.785	3.223
$^{239}Pu + n$	Constant	3.131	3.542	3.945
$^{240}Pu + n$	Constant	3.016	3.427	3.832

B. Spontaneous Fission $\bar{\nu}_p$(sf)			
Fission Reaction	$\sigma_c(\epsilon)$	$\bar{\nu}_p$(sf)	$\bar{\nu}_p^{exp}$(sf)
^{252}Cf(sf)	Constant[a]	3.788	3.757 ± 0.009[b]

[a]The constant cross section replaces the energy-dependent cross section by use of the effective level density parameter $a_{eff} = A/(10\ \text{MeV})$ to simulate the energy dependence.

[b]Obtained from the experimental data contained in Refs. 51 and 52 as discussed in the text.

APPENDIX A

INTEGRATION OF THE PROMPT FISSION NEUTRON SPECTRUM FOR CONSTANT COMPOUND NUCLEUS CROSS SECTION OVER AN ARBITRARY ENERGY INTERVAL

For applied purposes we present a closed-form expression for the integral of Eq. (13) over an arbitrary energy interval (a,b). Use of this expression in Eq. (16) yields the desired closed-form expression for the fission-spectrum integral.

We set $\alpha = \sqrt{T_m}$ and $\beta = \sqrt{E_f}$. Then, using the notation of Eq. (13) we set

$$u_2(a) = (\sqrt{a} + \sqrt{E_f})^2/T_m$$
$$= (\sqrt{a} + \beta)^2/\alpha^2$$
$$= A \ , \qquad \text{(A.1)}$$

$$u_2(b) = (\sqrt{b} + \beta)^2/\alpha^2 = B \ , \tag{A.2}$$

$$u_1(a) = (\sqrt{a} - \beta)^2/\alpha^2 = A' \ , \tag{A.3}$$

and

$$u_1(b) = (\sqrt{b} - \beta)^2/\alpha^2 = B' \ . \tag{A.4}$$

The integral of Eq. (13) is then obtained by a change of variable and integration by parts. There are three different expressions for the result depending on the magnitudes of a and b with respect to E_f.

Region I ($a \geqq E_f, b > E_f$):

$$\begin{aligned} 3\alpha\beta \int_a^b N(E,E_f)dE = &\left[\left(\frac{2}{5}\alpha^2 B^{5/2} - \frac{1}{2}\alpha\beta B^2\right) E_1(B) - \left(\frac{2}{5}\alpha^2 A^{5/2} - \frac{1}{2}\alpha\beta A^2\right) E_1(A)\right] \\ &- \left[\left(\frac{2}{5}\alpha^2 B'^{5/2} + \frac{1}{2}\alpha\beta B'^2\right) E_1(B') - \left(\frac{2}{5}\alpha^2 A'^{5/2} + \frac{1}{2}\alpha\beta A'^2\right) E_1(A')\right] \\ &+ [(\alpha^2 B - 2\alpha\beta B^{1/2})\gamma(3/2,B) - (\alpha^2 A - 2\alpha\beta A^{1/2})\gamma(3/2,A)] - [(\alpha^2 B' + 2\alpha\beta B'^{1/2})\gamma(3/2,B') \\ &- (\alpha^2 A' + 2\alpha\beta A'^{1/2})\gamma(3/2,A')] - \frac{3}{5}\alpha^2[\gamma(5/2,B) - \gamma(5/2,A) - \gamma(5/2,B') + \gamma(5/2,A')] \\ &- \frac{3}{2}\alpha\beta[(1+B)\exp(-B) - (1+A)\exp(-A) + (1+B')\exp(-B') - (1+A')\exp(-A')] \ . \end{aligned} \tag{A.5}$$

Region II ($a < E_f, b \leqq E_f$):

$$\begin{aligned} 3\alpha\beta \int_a^b N(E,E_f)dE = &\left[\left(\frac{2}{5}\alpha^2 B^{5/2} - \frac{1}{2}\alpha\beta B^2\right) E_1(B) - \left(\frac{2}{5}\alpha^2 A^{5/2} - \frac{1}{2}\alpha\beta A^2\right) E_1(A)\right] \\ &- \left[\left(\frac{2}{5}\alpha^2 B'^{5/2} - \frac{1}{2}\alpha\beta B'^2\right) E_1(B') - \left(\frac{2}{5}\alpha^2 A'^{5/2} - \frac{1}{2}\alpha\beta A'^2\right) E_1(A')\right] \\ &+ [(\alpha^2 B - 2\alpha\beta B^{1/2})\gamma(3/2,B) - (\alpha^2 A - 2\alpha\beta A^{1/2})\gamma(3/2,A)] - [(\alpha^2 B' - 2\alpha\beta B'^{1/2})\gamma(3/2,B') \\ &- (\alpha^2 A' - 2\alpha\beta A'^{1/2})\gamma(3/2,A')] - \frac{3}{5}\alpha^2[\gamma(5/2,B) - \gamma(5/2,A) - \gamma(5/2,B') + \gamma(5/2,A')] \\ &- \frac{3}{2}\alpha\beta[(1+B)\exp(-B) - (1+A)\exp(-A) - (1+B')\exp(-B') + (1+A')\exp(-A')] \ . \end{aligned} \tag{A.6}$$

Region III ($a < E_f, b > E_f$):

$$\begin{aligned} 3\alpha\beta \int_a^b N(E,E_f)dE = &\left[\left(\frac{2}{5}\alpha^2 B^{5/2} - \frac{1}{2}\alpha\beta B^2\right) E_1(B) - \left(\frac{2}{5}\alpha^2 A^{5/2} - \frac{1}{2}\alpha\beta A^2\right) E_1(A)\right] \\ &- \left[\left(\frac{2}{5}\alpha^2 B'^{5/2} + \frac{1}{2}\alpha\beta B'^2\right) E_1(B') - \left(\frac{2}{5}\alpha^2 A'^{5/2} - \frac{1}{2}\alpha\beta A'^2\right) E_1(A')\right] \\ &+ [(\alpha^2 B - 2\alpha\beta B^{1/2})\gamma(3/2,B) - (\alpha^2 A - 2\alpha\beta A^{1/2})\gamma(3/2,A)] - [(\alpha^2 B' + 2\alpha\beta B'^{1/2})\gamma(3/2,B') \\ &- (\alpha^2 A' - 2\alpha\beta A'^{1/2})\gamma(3/2,A')] - \frac{3}{5}\alpha^2[\gamma(5/2,B) - \gamma(5/2,A) - \gamma(5/2,B') + \gamma(5/2,A')] \\ &- \frac{3}{2}\alpha\beta[(1+B)\exp(-B) - (1+A)\exp(-A) + (1+B')\exp(-B') + (1+A')\exp(-A') - 2] \ . \end{aligned} \tag{A.7}$$

A test of the Region III integration is that when the interval $(a,b) = (0,\infty)$ the evaluation of Eq. (A.7) must yield $3\alpha\beta$.

APPENDIX B

BIN-WIDTH CORRECTIONS AND NORMALIZATION OF EXPERIMENTAL PROMPT FISSION NEUTRON SPECTRA

Assuming that an experimental prompt fission neutron time-of-flight spectrum $N_{exp}(t)$ has been correctly transformed to the corresponding neutron energy spectrum $N_{exp}(E)$, there are two points that we wish to address. The first concerns a bin-width correction to $N_{exp}(E)$, and the second concerns the normalization of $N_{exp}(E)$.

Bin-Width Correction

The bin-width correction consists in determining a set of bin energies E_b by which the experimental histogram $N_{exp}(E)$ can be represented with a set of experimental points. In the tail region of the spectrum, the choice of the bin midpoint as E_b introduces a substantial error because there are more counts in the low-energy side of the bin than in the high-energy side due to the exponential-like behavior of the spectrum. Consequently, in this region E_b is determined in the following manner.

For a given histogram element or bin of magnitude N_b with lower limit E_1 and upper limit E_2, the true spectrum $N(E)$ intersects the histogram element at energy E_b. This definition of E_b ensures that the experimental point representing the histogram element falls on the curve $N(E)$ whose integral over the bin has been measured. Thus, two equations must be satisfied for each bin:

$$\int_{E_1}^{E_2} N(E)dE = N_b(E_2 - E_1) \tag{B.1}$$

and

$$N(E_b) = N_b \ . \tag{B.2}$$

By making an exponential approximation

$$N(E) = k \exp(-E/T) \ , \tag{B.3}$$

one finds that

$$E_b = T \ln \left\{ \frac{E_2 - E_1}{T[\exp(-E_1/T) - \exp(-E_2/T)]} \right\} \tag{B.4}$$

for the bin in question. The value of T can be determined by iterating the solutions to Eq. (B.4) for a number of adjacent bins, or T can be equated to the value obtained in a least-squares fit of Eq. (B.3) to the tail of the spectrum prior to bin-width corrections, or more simply, a Maxwellian temperature T_M obtained from a similar experiment or calculated with the formula just below Eq. (21) can be used. However, the use of a Maxwellian temperature T_M underestimates T somewhat.

The bin-width correction must be applied when the bin widths in the tail region are large and the bin midpoint energy is used to characterize the bin. The simple correction given here cannot be applied, however, unless the bin limits E_1 and E_2 are well defined, that is, unless the width of the detector response function is small compared to the bin width.

Normalization

Experimental prompt fission neutron energy spectra $N_{exp}(E)$ are usually given in arbitrary units between energy limits E_u and E_v, which are, respectively, the lower limit of the first energy bin and the upper limit of the last energy bin. Theoretical prompt fission neutron spectra $N_{th}(E)$ are usually normalized to unity when integrated from zero to infinity. Theory and experiment are compared by integrating the theoretical spectrum over the energy range of the experiment, namely

$$\int_{E_u}^{E_v} N_{th}(E)dE = k < 1 \ , \tag{B.5}$$

and summing the experimental histogram $N_{exp}(E)$, namely,

$$\sum_i N_{exp}^{(i)}(E_i)\Delta E_i = M \ . \tag{B.6}$$

Multiplying each element $N_{exp}^{(i)}(E_i)$ of the experimental histogram by the factor (k/M) provides the required normalization.

APPENDIX C

ADDITIONAL CALCULATIONS OF THE PROMPT FISSION NEUTRON SPECTRUM AND AVERAGE PROMPT NEUTRON MULTIPLICITY FOR THE ^{239}Pu + n SYSTEM

We present in this Appendix additonal calculations of the prompt fission neutron spectrum $N(E)$ and average prompt neutron multiplicity $\bar{\nu}_p(E_n)$ for the neutron-induced fission of ^{239}Pu. We do this because for this system the calculations of $N(E)$ and $\bar{\nu}_p(E_n)$ that are described in the body of the text both have relatively large systematic errors when compared with the experimental data. This is evidenced by inspection of Figs. 25 and 34. These anomalous results are somewhat surprising because the input quantities to all of our calculations have been obtained from the same set of sources, as described in Sec. II.A. Based on the good to excellent agreement between calculation and experiment obtained in all cases except the present one, we conclude that the method is sound, but that some of the input quantities are in error.

It is argued in the discussion of Figs. 25 and 34 that the source of the error is in the somewhat large difference between the average energy release $\langle E_r \rangle$ and the total average fission-fragment kinetic energy $\langle E_f^{\text{tot}} \rangle$. This difference, obtained using the results of Unik et al.[22] together with Wapstra and Bos[24] masses, is from Table I given by $\langle E_r \rangle - \langle E_f^{\text{tot}} \rangle = 21.054$ MeV. It is noted in the discussion of Fig. 34 that the possible sources of error in $\langle E_r \rangle$ include 6 systematic masses out of the 14 masses used from Wapstra and Bos[24] and the choice, based on the work of Unik et al.,[22] of ^{100}Zr and ^{140}Xe as the average fragments of the two mass peaks. Since the systematic masses of Wapstra and Bos[24] are probably as good as those from any mass formula, we do not adjust these masses. We also do not adjust the mass numbers $A_L = 100$ and $A_H = 140$ of the average fragments of each mass peak as they are obtained directly from experiment. However, the atomic numbers $Z_L = 40$ and $Z_H = 54$ are inferred by Unik et al.[22] using an approximate expression for the charge division in fission. We therefore change the atomic numbers of the average fragments by one unit to $Z_L = 41$ and $Z_H = 53$. This choice is in the direction away from the mean fragment and toward the most probable fragment of each mass peak, according to Fig. 1 of Unik et al.[22] The average fragments therefore become ^{100}Nb and ^{140}I leading to an average energy release $\langle E_r \rangle = 196.987$ MeV.

It is further noted in the discussion of Fig. 34 that the experimental uncertainty in $\langle E_f^{\text{tot}} \rangle$ is perhaps nonnegligible. This uncertainty is given by Unik et al.[22] as 0.5 MeV out of 177.1 MeV. If, instead of this value, we use the averaged value obtained from the experimental compilation of Hoffman and Hoffman,[23] the result is $\langle E_f^{\text{tot}} \rangle = 177.6 \pm 0.6$ MeV. Using this value of $\langle E_f^{\text{tot}} \rangle$ together with the recalculated value of $\langle E_r \rangle$ gives a difference $\langle E_r \rangle - \langle E_f^{\text{tot}} \rangle = 19.387$ MeV, which is a reduction of 1.667 MeV from the original value. This corresponds to a reduction of ~6% in the total average fission-fragment excitation energy $\langle E^* \rangle$ at incident thermal neutron energy.

The recalculated fission spectrum $N(E)$ and average neutron multiplicity $\bar{\nu}_p(E_n)$ are shown by the solid curves of Figs. C.1 and C.2, respectively, where they are compared to the original calculations from Figs. 25 and 34 shown by the dashed curves and the

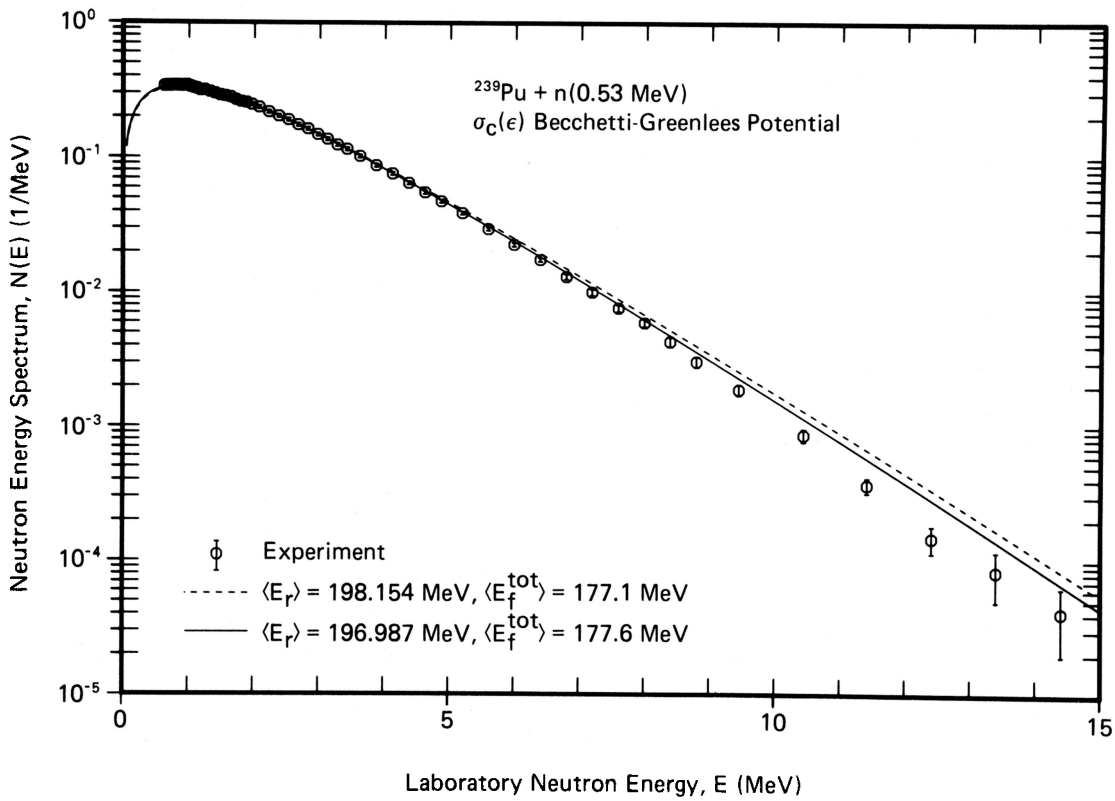

Fig. C.1. Prompt fission neutron spectrum in the laboratory system for the fission of ^{239}Pu induced by 0.53-MeV neutrons. The dashed curve is identical to the energy-dependent cross-section calculation shown by the solid curve in Fig. 25. The solid curve gives the same calculation except for the changes indicated in the average energy release $\langle E_r \rangle$ and the total average fission-fragment kinetic energy $\langle E_f^{\text{tot}} \rangle$. The values of the constants appearing in this spectrum are $E_f^L = 1.036$ MeV, $E_f^H = 0.529$ MeV, and $T_m = 1.101$ MeV. The experimental data are identical to those of Fig. 25.

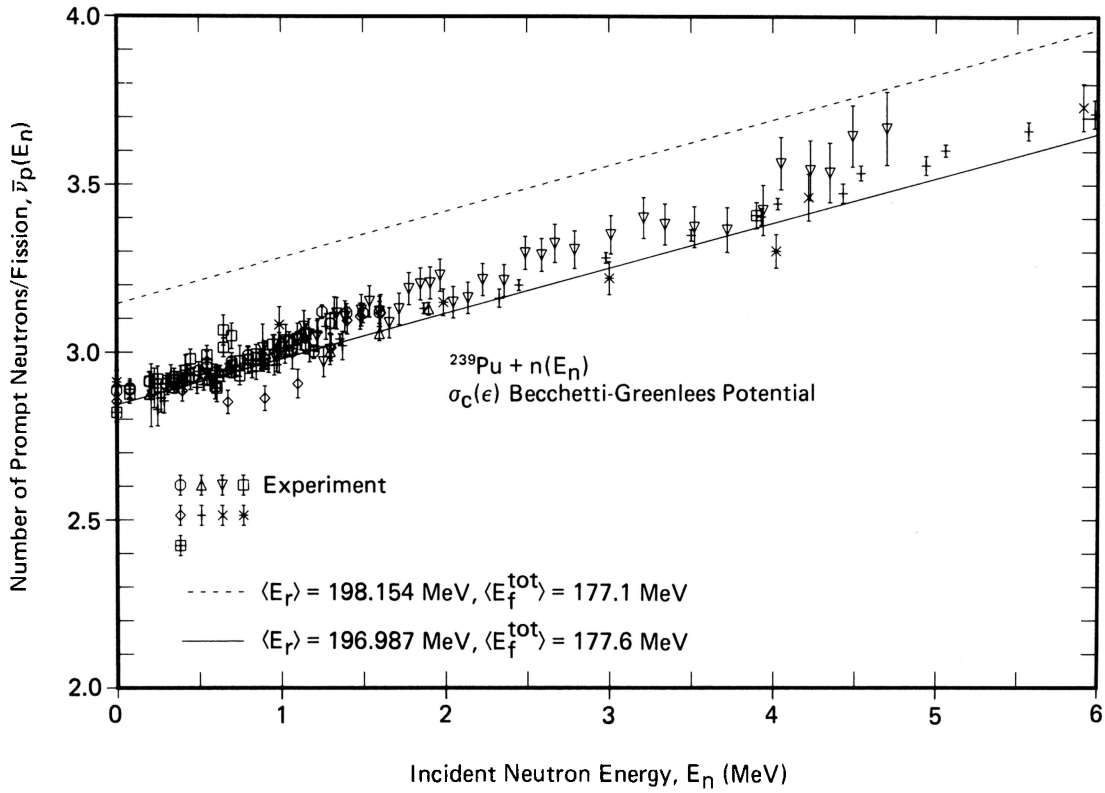

Fig. C.2. Average prompt neutron multiplicity as a function of the incident neutron energy for the neutron-induced fission of ^{239}Pu. The dashed curve is identical to the energy-dependent cross-section calculation shown by the solid curve in Fig. 34. The solid curve gives the same calculation except for the changes indicated in the average energy release $\langle E_r \rangle$ and the total average fission-fragment kinetic energy $\langle E_f^{tot} \rangle$. The experimental data are identical to those of Fig. 34.

experimental data. We see in Fig. C.1 that the agreement with experiment is improved but that a discrepancy still exists in the tail region of the spectrum. The average energy in the present calculation is $\langle E \rangle$ = 2.154 MeV whereas it is $\langle E \rangle$ = 2.194 MeV in the original calculation. The comparison of the present and original calculations of $\bar{\nu}_p(E_n)$ with experimental data in Fig. C.2 shows excellent agreement in the thermal neutron energy range up to ~1 MeV and good agreement for the remaining region except for the possible structure in the data between ~2.5 and 3.5 MeV and also just above 4 MeV.

ACKNOWLEDGMENTS

We are grateful to G. Auchampaugh, J. W. Boldeman, H. C. Britt, D. E. Cullen, J. Frehaut, B. Holmqvist, P. I. Johansson, L. Stewart, B. Suydam, and T. Wiedling for stimulating discussions and communications concerning this work; to P. G. Young, Jr. for the use of his code FISRAT for transforming fission cross-section ratio measurements to absolute fission cross sections; to J. R. Huizenga for supplying us with a copy of his figure showing the dependence of the level density parameter on mass number; and to D. C. George for her assistance in the preparation of figures.

This work was supported by the U.S. Department of Energy.

REFERENCES

[1]N. FEATHER, "Emission of Neutrons from Moving Fission Fragments," BM-148, British Mission (1942).

[2]B. E. WATT, *Phys. Rev.*, **87**, 1037 (1952).

[3]J. TERRELL, *Phys. Rev.*, **113**, 527 (1959).

[4]R. B. LEACHMAN, *Phys. Rev.*, **101**, 1005 (1956).

[5]L. CRANBERG, G. FRYE, N. NERESON, and L. ROSEN, *Phys. Rev.*, **103**, 662 (1956).

[6]J. TERRELL, *Proc. Symp. Physics and Chemistry of Fission*, Salzburg, Austria, March 22-26, 1965, Vol. II, p. 3, International Atomic Energy Agency, Vienna (1965).

[7]H. R. BOWMAN, J. C. D. MILTON, S. G. THOMPSON, and W. J. SWIATECKI, *Phys. Rev.*, **129**, 2133 (1963).

[8]S. S. KAPOOR, R. RAMANNA, and P. N. RAMA RAO, *Phys. Rev.*, **131**, 283 (1963).

[9]K. SKARSVÅG and K. BERGHEIM, *Nucl. Phys.*, **45**, 72 (1963).

[10]D. W. LANG, *Nucl. Phys.*, **53**, 113 (1964).

[11]C. P. SARGENT, W. BERTOZZI, P. T. DEMOS, J. L. MATTHEWS, and W. TURCHINETZ, *Phys. Rev.*, **137**, B89 (1965).

[12]G. KLUGE, *Phys. Lett.*, **37B**, 217 (1971).

[13]G. KLUGE, *Proc. Consultants' Mtg. Prompt Fission Neutron Spectra*, Vienna, Austria, August 25-27, 1971, p. 149, International Atomic Energy Agency, Vienna (1972).

[14]J. C. BROWNE and F. S. DIETRICH, *Phys. Rev. C*, **10**, 2545 (1974).

[15]F. S. DIETRICH and J. C. BROWNE, *Trans. Am. Nucl. Soc.*, **32**, 728 (1979).

[16]D. G. MADLAND and J. R. NIX, *Trans. Am. Nucl. Soc.*, **32**, 726 (1979).

[17]D. G. MADLAND and J. R. NIX, *Bull. Am. Phys. Soc.*, **24**, 885 (1979).

[18]D. G. MADLAND and J. R. NIX, *Proc. Int. Conf. Nuclear Cross Sections for Technology*, Knoxville, Tennessee, October 22-26, 1979, p. 788, NBS Special Publication 594, U.S. National Bureau of Standards (1980).

[19]D. G. MADLAND and J. R. NIX, *Proc. Int. Conf. Nuclear Physics*, Berkeley, California, August 24-30, 1980, Vol. I Abstracts, p. 290, Lawrence Berkeley Laboratory, University of California, Berkeley (1980).

[20]V. F. WEISSKOPF, *Phys. Rev.*, **52**, 295 (1937).

[21]J. M. BLATT and V. F. WEISSKOPF, *Theoretical Nuclear Physics*, p. 365, John Wiley and Sons, Inc., New York (1952).

[22]J. P. UNIK, J. E. GINDLER, L. E. GLENDENIN, K. F. FLYNN, A. GORSKI, and R. K. SJOBLOM, *Proc. Third IAEA Symp. Physics and Chemistry of Fission*, Rochester, New York, August 13-17, 1973, Vol. II, p. 19, International Atomic Energy Agency, Vienna (1974).

[23]D. C. HOFFMAN and M. M. HOFFMAN, *Ann. Rev. Nucl. Sci.*, **24**, 151 (1974).

[24]A. H. WAPSTRA and K. BOS, *At. Data Nucl. Data Tables*, **19**, 175 (1977).

[25]W. D. MYERS, *Droplet Model of Atomic Nuclei*, IFI/Plenum Data Company, New York (1977).

[26]V. E. VIOLA, Jr., *Nucl. Data A*, **1**, 391 (1966).

[27]J. R. HUIZENGA, *Proc. Int. Conf. Statistical Properties of Nuclei*, Albany, New York, August 23-27, 1971, p. 425, Plenum Press, New York (1972).

[28]J. R. HUIZENGA and L. G. MORETTO, *Ann. Rev. Nucl. Sci.*, **22**, 427 (1972).

[29]M. ABRAMOWITZ and I. A. STEGUN, Eds., *Handbook of Mathematical Functions*, p. 227, U.S. National Bureau of Standards, Washington, D.C. (1964).

[30]F. D. BECCHETTI, Jr. and G. W. GREENLEES, *Phys. Rev.*, **182**, 1190 (1969).

[31]P. I. JOHANSSON and B. HOLMQVIST, *Nucl. Sci. Eng.*, **62**, 695 (1977).

[32]K. J. Le COUTEUR, *Proc. Phys. Soc.*, **A65**, 718 (1952).

[33]M. ABRAMOWITZ and I. A. STEGUN, Eds., *Handbook of Mathematical Functions*, p. 253, National Bureau of Standards, Washington, D.C. (1964).

[34]J. TERRELL, *Phys. Rev.*, **127**, 880 (1962).

[35]N. AUSTERN, *Direct Nuclear Reaction Theories*, p. 30, John Wiley and Sons, Inc., New York (1970).

[36]N. CINDRO, *Rev. Mod. Phys.*, **38**, 391 (1966).

[37]A. M. LANE, *Nucl. Phys.*, **35**, 676 (1962).

[38]D. WILMORE and P. E. HODGSON, *Nucl. Phys.*, **55**, 673 (1964).

[39]P. MOLDAUER, *Nucl. Phys.*, **47**, 65 (1963).

[40]J. M. BLATT and V. F. WEISSKOPF, *Theoretical Nuclear Physics*, pp. 349 and 366, John Wiley and Sons, Inc., New York (1952).

[41]D. G. MADLAND, Los Alamos National Laboratory report (to be published).

[42]A. BERTIN, R. BOIS, and J. FREHAUT, "Mesure du Spectre en Energie des Neutrons de Fission pour la Fission de ^{235}U et de ^{238}U Induite par des Neutrons Rapides," CEA-R-4913, Commissariat à l'Energie Atomique, Centre d'Etudes de Bruyères-le-Châtel (1978).

[43]J. FREHAUT, A. BERTIN, and R. BOIS, *Trans. Am. Nucl. Soc.*, **32**, 732 (1979).

[44]J. FREHAUT, Private Communication (July 1979).

[45]P. I. JOHANSSON, B. HOLMQVIST, T. WIEDLING, and L. JEKI, *Proc. Conf. Nuclear Cross Sections and Technology*, Washington, D.C., March 3-7, 1975, Vol. II, p. 572, NBS Special Publication 425, U.S. National Bureau of Standards (1975).

[46]J. M. ADAMS, *Proc. Specialists' Mtg. Inelastic Scattering and Fission Neutron Spectra*, Harwell, United Kingdom, April 14-16, 1975, Appendix A, AERE-R-8636, U.K. Atomic Energy Authority, Harwell (1977).

[47]J. W. BOLDEMAN, D. CULLEY, and R. J. CAWLEY, *Trans. Am. Nucl. Soc.*, **32**, 733 (1979).

[48]J. W. BOLDEMAN, Private Communication (July 1979).

[49]J. TERRELL, *Phys. Rev.*, **108**, 783 (1957).

[50]R. J. HOWERTON, *Nucl. Sci. Eng.*, **62**, 438 (1977).

[51]S. AMIEL, *Proc. Second IAEA Symp. Physics and Chemistry of Fission*, Vienna, Austria, July 28–August 1, 1969, p. 569, International Atomic Energy Agency, Vienna (1969).

[52]J. R. SMITH, *Proc. Symp. Nuclear Data Problems for Thermal Reactor Applications*, Brookhaven National Laboratory, May 22-24, 1978, EPRI-NP-1093, p. 5-1, Electric Power Research Institute (1979).

[53]R. L. WALSH and J. W. BOLDEMAN, *J. Nucl. Energy*, **25**, 321 (1971).

[54]D. S. MATHER, P. FIELDHOUSE, and A. MOAT, *Nucl. Phys.*, **66**, 149 (1965).

[55]J. C. HOPKINS and B. C. DIVEN, *Nucl. Phys.*, **48**, 433 (1963).

[56]D. W. COLVIN and M. G. SOWERBY, Private Communication to the National Nuclear Data Center, CSISRS Library, 1964, Brookhaven National Laboratory, Upton, New York.

[57]R. GWIN, R. R. SPENCER, R. W. INGLE, J. H. TODD, and H. WEAVER, "Measurement of the Average Number of Prompt Neutrons Emitted per Fission of ^{235}U Relative to ^{252}Cf for the Energy Region 500 eV to 10 MeV," ORNL/TM-7148, ENDF-289, Oak Ridge National Laboratory (1980).

[58]M. V. SAVIN, Yu. A. KHOKHLOV, Yu. C. ZAMIATNIN, and I. N. PARAMONOVA, *Proc. Second Int. Conf. Nuclear Data for Reactors*, Helsinki, June 15-19, 1970, Vol. II, p. 157, International Atomic Energy Agency, Vienna (1970).

[59]V. G. NESTEROV, B. NURPEISOV, L. I. PROKHOROVA, G. N. SMIRENKIN, and Yu. M. TURCHIN, *Proc. Second Int. Conf. Nuclear Data for Reactors*, Helsinki, June 15-19, 1970, Vol. II, p. 167, International Atomic Energy Agency, Vienna (1970).

[60]J. W. BOLDEMAN and R. L. WALSH, *J. Nucl. Energy*, **24**, 191 (1970).

[61]M. SOLEILHAC, J. FREHAUT, and J. GAURIAU, *J. Nucl. Energy*, **23**, 257 (1969).

[62]J. W. MEADOWS and J. F. WHALEN, *Reports to the AEC Nuclear Cross Sections Advisory Group*, Washington, D.C., March 24-25, 1966, H. T. MOTZ, Secretary, WASH-1068, EANDC(US)-85U, INDC(US)-3U, p. 21, Los Alamos National Laboratory (1966).

[63]L. I. PROKHOROVA and G. N. SMIRENKIN, *Yad. Fiz.*, **7**, 961 (1968).

[64]Yu. A. BLYUMKINA, I. I. BONDARENKO, V. F. KUZNETSOV, V. G. NESTEROV, V. N. OKOLOVITCH, G. N. SMIRENKIN, and L. N. USACHEV, *Nucl. Phys.*, **52**, 648 (1964).

[65]M. V. SAVIN, Yu. A. KHOKHLOV, I. N. PARAMONOVA, and V. A. CHIRKIN, *At. Energy*, **32**, 408 (1972).

[66]K. E. BOLODIN, V. F. KUZNETSOV, V. G. NESTEROV, B. NURPEISOV, L. I. PROKHOROVA, Yu. M. TURCHIN, and G. N. SMIRENKIN, *At. Energy*, **33**, 901 (1972).

[67]R. L. WALSH and J. W. BOLDEMAN, *Ann. Nucl. Sci. Eng.*, **1**, 353 (1974).

[68]D. S. MATHER, P. F. BAMPTON, G. JAMES, and P. J. NIND, "Measurements of $\bar{\nu}_p$ for Pu-239 between 40 keV and 1.2 MeV," UKAEA, AWRE-0-42, Atomic Weapons Research Establishment (1970).

[69]H. CONDÉ, J. HANSEN, and M. HOLMBERG, *J. Nucl. Energy*, **22**, 53 (1968).

[70]M. de VROEY, A. T. G. FERGUSON, and N. STARFELT, *J. Nucl. Energy Parts A/B*, **20**, 191 (1966).

[71]J. FREHAUT, G. MOSINSKI, R. BOIS, and M. SOLEILHAC, "Mesure du Nombre Moyen $\bar{\nu}_p$ de Neutrons Prompts Emis au Cours de la Fission Induite dans ^{240}Pu et ^{241}Pu par des Neutrons d'Energie Comprise entre 1.5 et 15 MeV," CEA-R-4626, Commissariat à l'Energie Atomique, Centre d'Etudes de Bruyères-le-Châtel (1974).

[72]J. R. BOYCE, T. D. HAYWARD, R. BASS, H. W. NEWSON, E. G. BILPUCH, and F. O. PURSER, *Phys. Rev. C*, **10**, 231 (1974).

[73]V. BENZI, G. MAINO, and E. MENAPACE, *Lett. Nuovo Cimento*, **21**, 231 (1978).

[74]B. B. BACK, H. C. BRITT, O. HANSEN, B. LEROUX, and J. D. GARRETT, *Phys. Rev. C*, **10**, 1948 (1974).

[75]B. B. BACK, O. HANSEN, H. C. BRITT, and J. D. GARRETT, *Phys. Rev. C*, **9**, 1924 (1974).

[76]D. G. MADLAND and P. G. YOUNG, *Proc. Int. Conf. on Neutron Physics and Nuclear Data for Reactors and Other Applied Purposes*, Harwell, United Kingdom, September 25-29, 1978, p. 349, Organization for Economic Co-Operation and Development, Paris (1978).

[77]M. R. BHAT, "Evaluation of ^{235}U Neutron Cross Section and Gamma Ray Production Data for ENDF/B-V," BNL-NCS-51184, ENDF-248, National Nuclear Data Center, Brookhaven National Laboratory (1980).

[78]J. W. BEHRENS and G. W. CARLSON, *Nucl. Sci. Eng.*, **63**, 250 (1977).

[79]G. W. CARLSON and J. W. BEHRENS, *Nucl. Sci. Eng.*, **66**, 205 (1978).